CAPE PENINSULA UNIVERSITY OF TECHNOLOGY

IMPEDANCE MATCHING OF ELECTRICALLY SMALL PATCH ANTENNAS ON CUBESATS IN THE S-BAND

by

CAREL JACOBUS NEL
208028633

Completion Date: 31/10/2023
Supervisor: Dr. P.G. Wiid

Thesis submitted in fulfilment of CPUT guidelines

MASTER OF ENGINEERING: ELECTRICAL ENGINEERING

Declaration

I, Carel Jacobus Nel, declare that this thesis represents my own work submitted in fulfillment of the requirements for the Master of Engineering in Electrical Engineering degree at the Cape Peninsula University of Technology. It has not been submitted for any degree at this or any other academic institution before. All consulted literature has been listed comprehensively in the reference pages. All the diagrams in this thesis is my own work and were drawn in Draw.io flowchart maker.

14/02/2024

Signed **Date**

Abstract

Antennas are important components in radio frequency (RF) communication systems to convert electrical signals to electromagnetic (EM) waves, which are radiated into free space. In these modern times, electronic designers are working towards the miniaturisation of electronic hardware. CubeSat communication system components, such as patch antennas, are no exception. Electrically-small antennas are difficult to impedance match and to achieve acceptable performance characteristics.

The motivation for carrying out the research and an introduction into the communication system onboard a typical CubeSat is presented. The objectives and research methodology, which were implemented to design and impedance match an electrically-small patch antenna are then presented.

An in-depth investigation into the theory of microstrip patch antennas is presented followed by passive and non-Foster impedance matching techniques.

Then the design of electrically-small microstrip patch antennas are presented. Four patch antennas were designed and simulated in Agilent design system (ADS) and FEKO. Both internal and external impedance matching techniques were implemented.

Three patch antenna prototypes were built and tested and the measured performance parameters compared to the specifications and simulated results.

The lowering of the resonant frequency of a micostrip patch antenna by implenting miniaturisation techniques produced an input return loss of 16.678 dB, a realised gain 2.874 dBi and an axial ratio of 2.351 dB.

Acknowledgements

First and foremost, I would like to thank the dear Lord Jesus Christ for giving me the talent and strength to complete this research successfully.

Thanks to my dear parents and two brothers for their support by giving me the motivation when I needed it.

Many thanks to my supervisor Dr. Gideon Wiid for his contribution and the weekly discussions towards completing this research successfully. His kind assistance is much appreciated.

My sincere thanks goes to my mentor and friend Mr. Clive Whaits, for his guidance and motivation throughout the journey.

Thank you to CPUT and the external moderators, who were responsible for the evaluation of my work.

Thank you to my colleagues at AAC Space Africa, who supported me during the full-time work and part-time study period.

Thanks to Anneke Bester from the University of Stellenbosch, who assisted with the measurements in their anechoic chamber.

Last but not least, my sincere gratitude goes to special people like Pieter Vorster, CR Stols, Elize Maritz, the Visser family and the late Cassie Carstens who were all part of the journey. Everyone supported me in a significant way.

Contents

List of Figures

List of Tables

Acronyms & Abbreviations

***Q*-factor** quality factor.

AC alternating current.

ADS Agilent design system.

AR axial ratio.

AUT antenna under test.

BJT bipolar junction transistor.

CAD computer-aided design.

CPUT Cape Peninsula University of Technology.

CubeSat Cube-Satellite.

dB decibels.

DC direct current.

EM electromagnetic.

ESA electrically-small antenna.

EVM error vector magnitude.

F'SATI French South African Institute of Technology.

FEM finite element method.

GHz gigahertz.

ITU International Telecommunication Union.

LHCP left hand circular polarised.

LTCC low-temperature co-fired cermamic.

mm millimeters.

MoM method of moments.

MPA microstrip patch antenna.

NF noise figure.

nH nano-Henry.

NIC negative impedance converter.

op-amp operational amplifier.

OQPSK offset quadrature phase-shift keying.

PCB printed circuit board.

pF pico-Farad.

QPSK quadrature phase-shift keying.

RF radio frequency.

RHCP right hand circular polarised.

SANT S-band antenna.

SmallSat Small-Satellite.

SRX S-band receiver.

STX S-band transmitter.

TLM transmission-line model.

TM transverse magnetic.

TMTC telemetry and telecommand.

UHF ultra high frequency.

VHF very high frequency.

VNA vector network analyzer.

VSWR voltage standing wave ratio.

Chapter 1

Introduction

This introductory chapter presents the author's motivation for carrying out research on the specific topic as suggested by the French South African Institute of Technology (F'SATI), in partnership with the Cape Peninsula University of Technology (CPUT). The research objectives and the methodology used to reach final conclusions are presented, followed by recommendations. Deliniations on particular performance parameters of patch antennas are clearly stated, since the scope of this research does not cover the optimisation thereof. The thesis outline will be presented and will highlight the important aspects that will be convered within this dissertation.

1.1 Motivation

A patch antenna is designed to be resonant at a given frequency. The resonant frequency is the frequency at which the antenna is optimaly impedance matched to the RF system's characteristic impedance for maximum power transfer. Impedance matching between a source and load is a very important aspect in any RF network. In an ideal lossless network, the power transfer between a source and load will be a maximum. Any mismatches will cause unwanted reflections towards the source, resulting in standing waves (Sharma, Tripathi and Rishi, 2017: 0). Power is stored in each standing wave and maximum power can not be delivered to the load. In a typical CubeSat communication system, the source can be a radio transmitter or receiver interfaced with a patch antenna as the load.

The communication up and down-link between a CubeSat and earth ground station consists of either a very high frequency (VHF) or ultra high frequency (UHF) radio transceiver, supplemented by a S-band downlink transmitter. The S-band is the frequency band which has an upper frequency limit of 4 GHz and a lower frequency limit of 2 GHz. The S-band transmitter is utilised for high data rate transmissions and the VHF/UHF transceiver for telemetry and telecommand (TMTC) purposes. S-band uplinks are also gaining more popularity nowadays. The VHF/UHF transceiver system utilises a deployable antenna within the CubeSat structure, where a patch antenna solution is preferred for the S-band transmitter or receiver system.

The F'SATI group at CPUT developed their own S-band transmitter and receiver subsystems for their ZACUBE, MDASAT and M2MSAT CubeSats. The S-band transmitter (STX) operates within the International Telecommunication Union (ITU) Small-Satellite (SmallSat) downlink band of 2.29 to 2.3 GHz, while the S-band receiver (SRX) operates in the ITU uplink band of 2.025 GHz to 2.110 GHz. The S-band patch antenna (SANT) developed by F'SATI only covers the ITU commercial downlink band. This research presents the impedance matching techniques and the design of an electrically-small patch antenna, which will operate within the ITU's SmallSat uplink band.

Problem statement: Can miniaturisation techniques be implemented to reduce the electrical dimensions of a microstrip patch antenna (MPA), and utilising appropiate impedance matching techniques to ensure the required performance parameters for a typical CubeSat are maintained.

1.2 Objectives

The objectives of the research presented in this dissertation are as follows:

- To design and build an electrically-small S-band patch antenna which is optimally matched within the ITU frequency band of interest.
- To investigate how external impedance matching networks and miniaturisation techniques affect important antenna performance characteristics.

- To conclude if the antenna is suitable to be integrated with a CubeSat for a mission.

1.3 Research Methodology

The methodology followed to complete the research is divided into the following steps:

- Conduct a literature study on patch antenna theory, impedance matching networks and miniaturisation techniques.
- Define the performance specifications for the antenna.
- Select a suitable radiating element shape and then design a patch antenna to resonate at a frequency greater than the specified resonant frequency.
- Simulate the patch antenna in FEKO to obtain the performance characteristics for the input impedance, input return loss, voltage standing wave ratio (VSWR), gain, realised gain, axial ratio and antenna efficiency.
- Impedance match the patch antenna to the source at the specified operating frequency by implementing an external impedance matching network and miniaturisation techniques.
- Evaluate and select the optimal impedance matching approach and then design and manufacture the prototype antennas.
- Measure the performance characteristics of the constructed antennas in an anechoic chamber.
- Compare simulated and measured results.
- Evaluate whether the measured performance parameters meet the design specifications.
- Conclude on the research objectives with recommendations for future work.

This methodology is presented in the flowgraph illustrated in Figure 1.1.

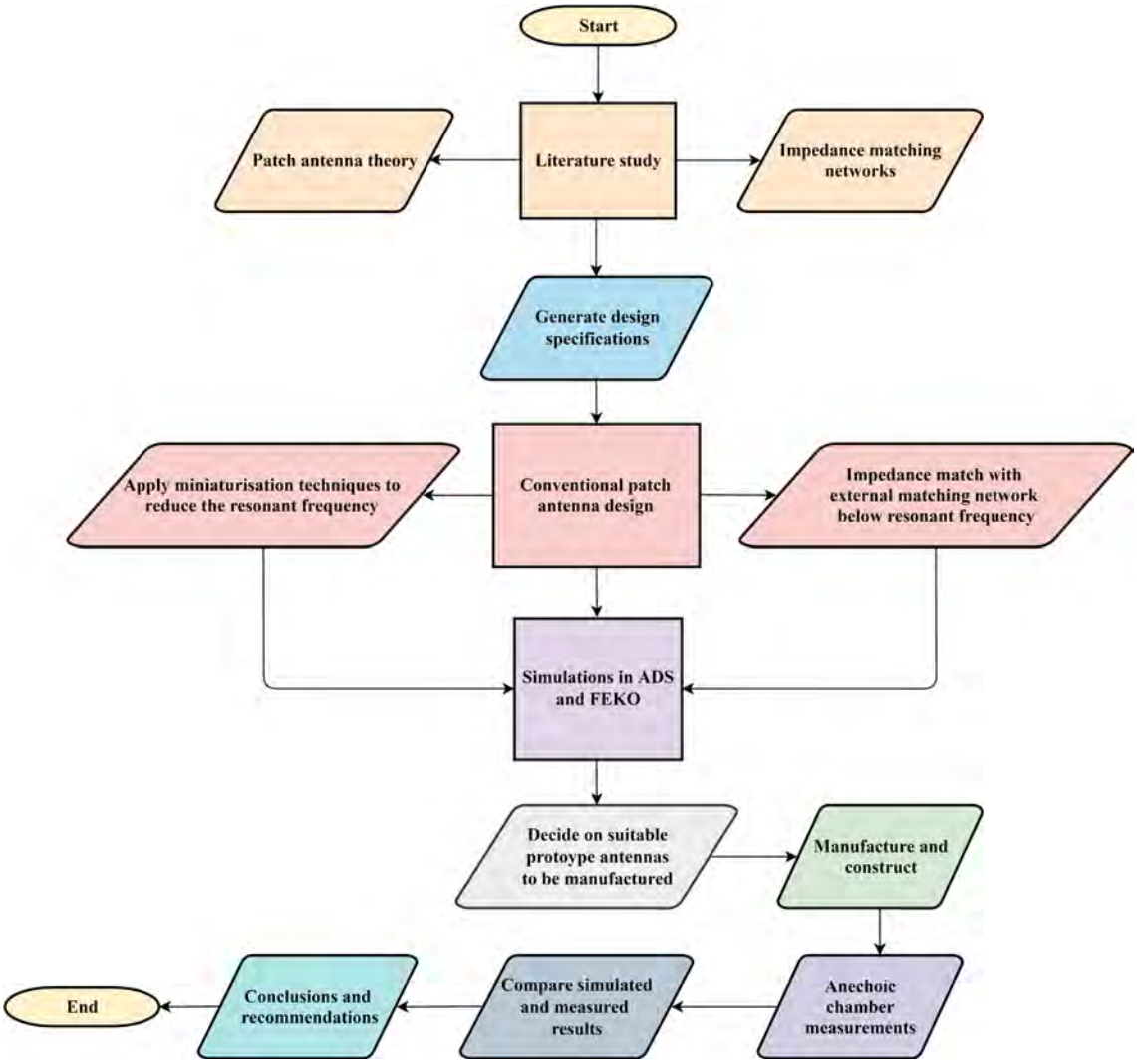

Figure 1.1: Methodology flowgraph

1.4 Deliniations

This research pertains specifically to microstrip patch antenna and matching network topology, with the following associated performance parameters: the input return loss, voltage standing wave ratio (VSWR), input impedance, gain, realised gain, axial ratio and efficiency. The methods to improve the bandwidth, antenna gain, directivity and beamwidth are not part of the scope of this research.

The electrically-small protoype antennas will operate only within the ITU up-link frequency band from 2.025 GHz to 2.110 GHz. In practice, these antennas will be inte-

grated with a quadrature phase-shift keying (QPSK) or offset quadrature phase-shift keying (OQPSK) transceiver system. The implementation of any non-linear active devices within an impedance matching network will affect the error vector magnitude (EVM) of a digitally modulated signal, hence optimisation of the EVM does not form part of the scope of this research.

1.5 Synopsis

Chapter 2 presents an introduction to microstrip patch antennas and the relevant theory thereof which includes various antenna topologies, analysis, properties, feed networks, characteristics of electrically-small antennas and miniaturisation techniques. The relevant design equations are also included. Conclusions on MPAs are then presented.

In Chapter 3, a detailed theoretical discussion on impedance matching networks is presented. The Chapter starts off with an introduction to the concept of impedance matching, followed by a discussion on series and parallel resonant circuits. The Smith chart technique is then utilised in the design of impedance matching networks. Impedance matching networks utilising passive elements is presented, followed by a discussion on non-Foster elements and a negative impedance converter (NIC) circuit. Chapter conclusions are made and a comparison between the various impedance matching networks is presented.

Chapter 4 presents the steps involved to design and impedance match electrically-small microstrip patch antennas, resulting in two approaches being implemented. Firstly, an external impedance matching network, which operates below the resonant frequency of the MPA, is implemented. Secondly, the technique of miniaturisation by lowering the resonant frequency, while maintaining similar antenna dimensions, of a MPA is implmented. This Chapter includes the design techniques, simulations and printed circuit board (PCB) layout for the prototype antennas.

In Chapter 5, the performance parameters of three prototype electrically-small MPAs are evaluated. A brief explanation on the laboratary test and measurement setup is presented. Actual laboratory measurements were performed and a comparison is then made between

the measured and simulated results.

Chapter 6 concludes the final outcomes of the research and recommendations are made for future work.

1.6 Conclusions

The miniaturisation of MPAs on a CubeSat will allow for better utilisation of the very limited available space, thus allowing more space for other systems and larger payloads to be carried. Hence, miniaturisation techniques of MPAs will be a great advantage in CubeSat missions. The design criterion need to be carefully specified and trade-offs identified, which will make the implementation of an electrically-small MPA a viable solution for future CubeSat missions.

Chapter 2

Microstrip Patch Antenna Theory

2.1 Background

Patch antennas drew the attention of antenna engineers during the early 1970s when there was a demand for high frequency communication systems. The compact and lightweight characteristics which these antennas exhibit, makes them an attractive proposition to any other antenna topology for spacecraft applications (Breed et al., 2009: 48). By observing the practical advantages which these antennas offer, their performance characteristics are not optimal, which therefore require certain design trade-offs to be made. The major performance characteristic disadvantages associated with these antennas, are the narrow input return loss bandwidth and the relatively low gain characteristics (Anisha and Enoch, 2014: 1101). The electrically-small topologies of these antennas further challenge the designer to obtain useable performance parameters. Electrically-small antennas are characterised by a low radiation resistance, which in return makes them less efficient. Individual performace parameters of MPAs can be improved by the implementation of different feed network configurations, stacked patch topologies and the arrangement of patch elements in a phased array configuration. The practical advantages versus the performance disadvantages are presented in Table 2.1. The basic topology of a MPA and how an antenna radiates will be explained within the next two subsections.

Table 2.1: MPA practical advantages versus performance disadvantages

Practical advantages	**Performance disadvantages**
Compact design	Low gain
Low profile	Low radiation efficiency
Lightweight	Limited power handling
Low manufacturing costs	Narrow bandwidth
Robust	High Q-factor
Versatile	Limited scan performance
Planar and non-planar surface compatibility	Feed network radiation spurs

2.1.1 Microstrip Patch Antenna Topology

The basic topology of a patch antenna can be represented as two metal plates, seperated some distance apart by a dielectric medium. In the case of an MPA, the patch element, which is also known as the radiating element, is etched on a dielectric substrate with a bottom ground plane as shown in Figure 2.1. The physical dimensions of the ground plane are selected to be much larger than the dimensions of the radiating element. Depending on the selection of the shape of the radiating element, this whole topology forms a circular or rectangular waveguide cavity with two metal walls. The cavity is excited by applying a signal to a selected feed-network. A discussion on the various feed-network configurations will be presented in section 2.7. The cavity has different resonant modes, which are called transverse magnetic or in short TM modes. The mode with the lowest order resonant frequency is defined as the dominant resonant TM mode (Balanis, 2005: 830). TM waves within the cavity are characterised by only having an electrical (E) component in the direction of propagation (Pozar, 2001: 95).

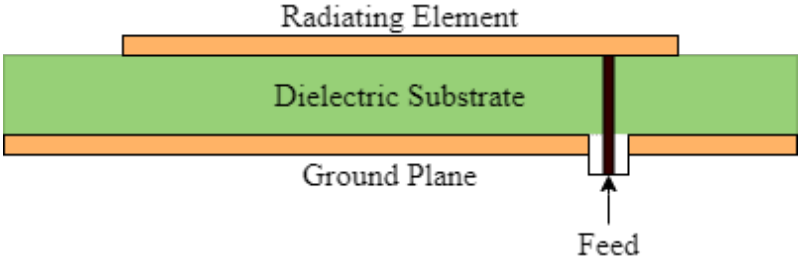

Figure 2.1: Microstrip patch antenna topology

The shape of the radiating element can be in one of the following form factors: rectangular, nearly-square, circular, ellipse, circular ring and triangle as illustrated in Figure 2.2 (Balanis, 2005: 813). The most commonly used shapes are the circular and rectangular patches, as their design equations and models for antenna analysis are well defined in the literature. More complex MPA shapes can be designed and analysed with the aid of antenna computer-aided design (CAD) software.

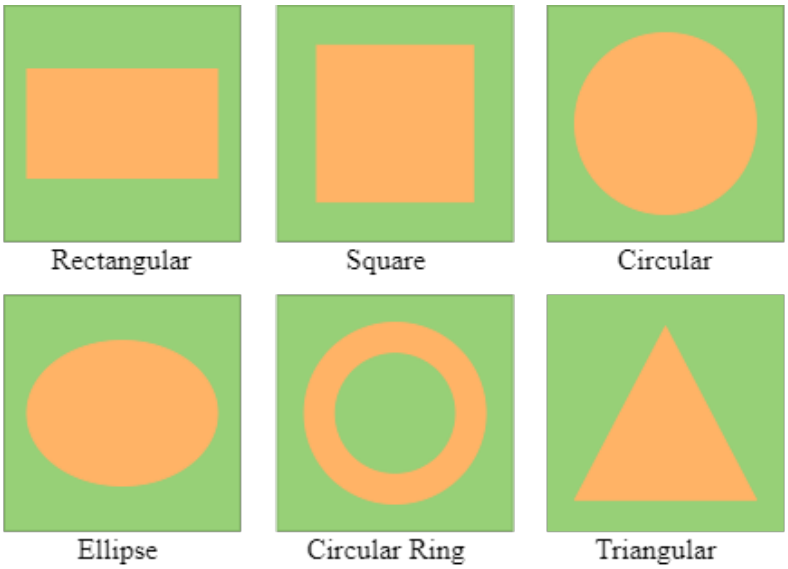

Figure 2.2: MPA radiating element form factors

2.1.2 Electromagnetic Radiation and Propagation

Electromagnetic (EM) radiation is defined as waves of electric (E) and magnetic energy (H) that propagates together in free-space. The electric and magnetic waves, as a function of the propagation distance (d), are orthogonal to each other as illustrated in Figure 2.3.

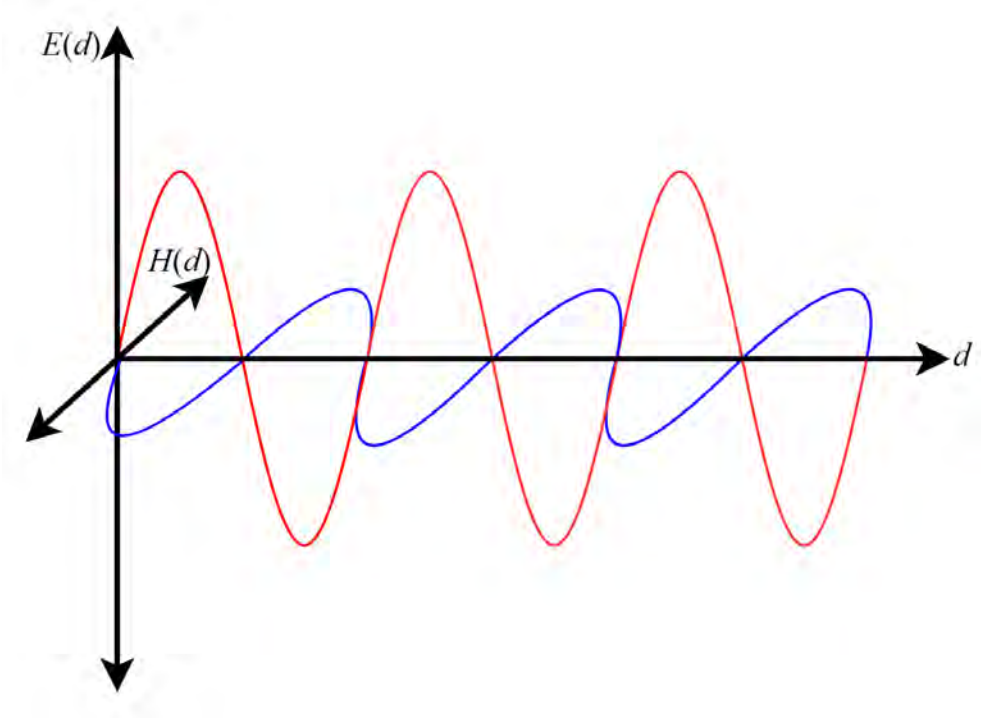

Figure 2.3: Three-dimensional representation of an EM wave

A rectangular MPA will be used as an example to explain the fringing effect and how EM radiation occurs. Radiation occurs due to the alternating electrical currents which flow along the edges of the radiating element and ground plane. The amount of radiation is controlled by the dimensions of the radiating element and the thickness of the dielectric substrate (Balanis, 2005: 816).

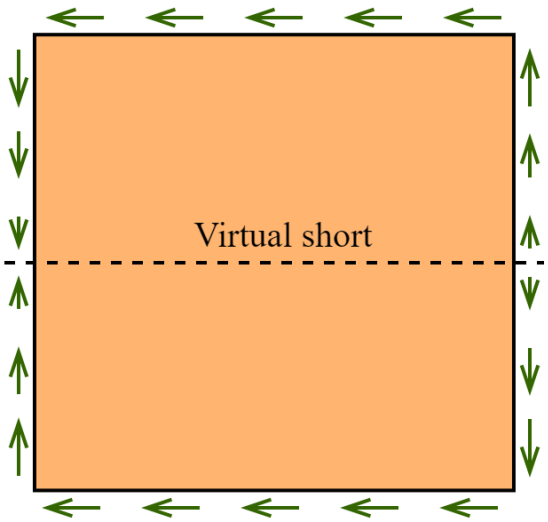

Figure 2.4: Rectangular element edge currents

The magnitude of the E-fields are uniform along two opposite edges which represent the width of the MPA. The magnitude of the E-fields on the other edges vary sinusoidaly and represents the MPAs resonant length as illustrated in Figure 2.5 (Milligan, 2005: 287).

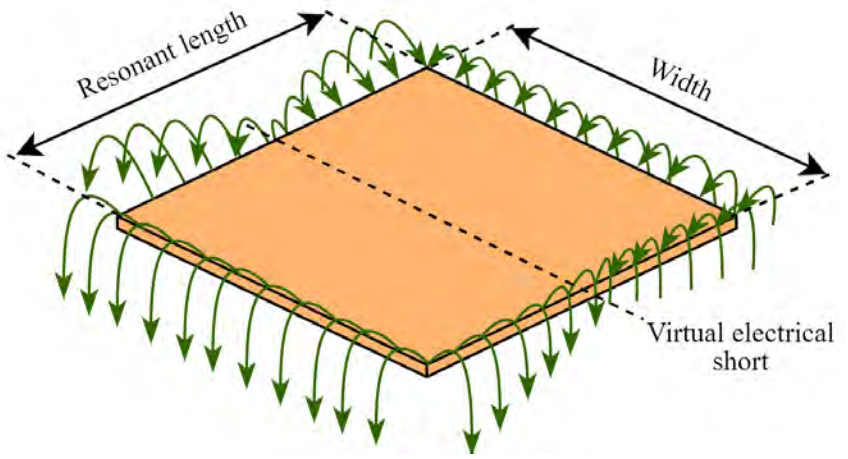

Figure 2.5: Fringing electric fields on a rectangular element

The impedance presented by the input port an MPA is of great importance throughout this research, hence the necessity to discuss the ratio of voltage to current on the surface of the radiating element. The E-field voltage to current ratio along the resonant length of the rectangular element is illustrated in Figure 2.6 (Sharma, Tripathi and Rishi, 2017: 3). The voltage $v(t)$ is a maximum with opposite polarity at the edges of the resonant length and zero in the centre. The current $i(t)$ is a maximum in the centre and a minimum at the opposite edges. The impedance is determined by the voltage to current ratio at a given point along the resonant length of the antenna. The impedance at the centre of the MPA is a minimum and presents a virtual electrical short circuit.

A graphical illustration of the above concepts is illustrated in Figure 2.6, where Z_{a} is the ratio of E-field voltage to current. The radiated field regions of an antenna will be explained in more detail in the following section.

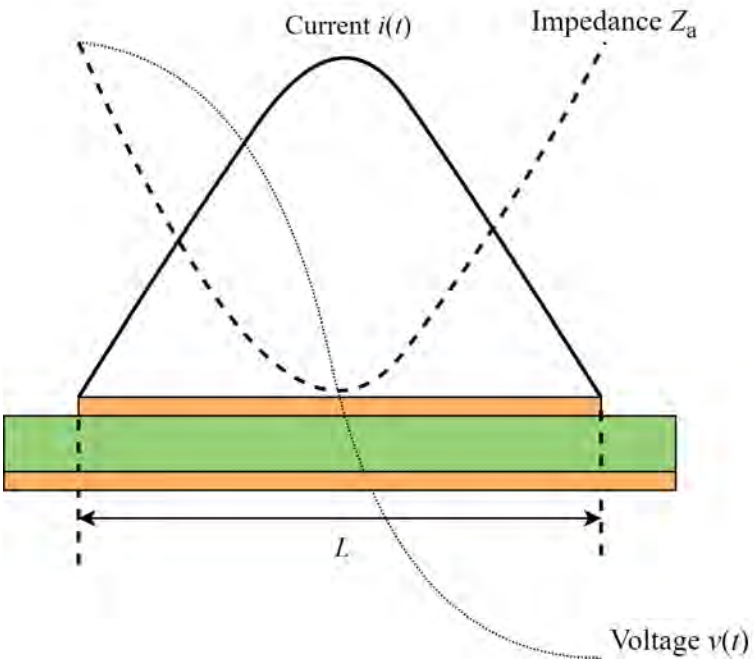

Figure 2.6: Voltage to current ratio of a rectangular MPA along its resonant length

2.2 EM Field Regions

The EM radiation of an antenna is divided into three field regions, namely the near-field region, Fresnel-region and the far-field region. A graphical illustration of the three regions are shown in Figure 2.7 (Smolders, Visser and Johannsen, 2019: 13).

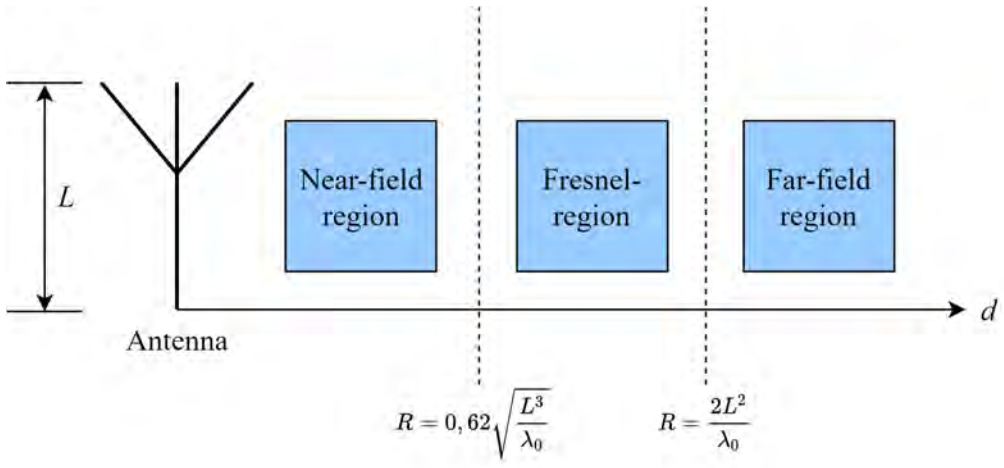

Figure 2.7: Antenna EM field regions

The near-field region is the first region next to the antenna. Within this region, the EM fields are unpredictable and not ideal for plane-wave measurements.

The region between the near- and far-fields is referred to as the Fresnel- region. Within this region, the EM field transitions from reactive to radiative fields (Everything-RF, 2018).

The far-field region is dominated by the radiating EM fields. The *E*- and *H*-fields become orthogonal in the direction of propagation. Within this region, antenna measurements are conducted under the condition that the distance from the antenna must be much greater than the largest dimension of the antenna and the wavelength of the applied signal.

With the basic concepts of antenna radiation explained, the performance parameters of antennas are presented within the next subsection.

2.3 Antenna Performance Parameters

It is important to be familiar with pertinant antenna performance parameters in order to understand the terminology used throughout this research and hence the meaniningful interpretation of both simulated and measured results. In this section, the relevant antenna performance parameters are now presented.

2.3.1 Radiation Resistance

The radiation resistance is defined as the resistance across which the radiated power of the antenna is dissipated. The radiation resistance (R_{r}) is related to the total power radiated by the antenna and is given by:

$$R_{\mathrm{r}} = \frac{p(t)}{0.5|i(t)|^2} \qquad \Omega \tag{2.1}$$

where $p(t)$ represents the total radiated power in Watts which is dissipated across the radiation resistance of the antenna when the current $i(t)$ Amperes flows through the antenna. The total radiated power is calculated by integrating the radiated power over a sphere (Smolders, Visser and Johannsen, 2019: 18).

2.3.2 Ohmic Loss

The ohmic loss within an antenna structure, is the opposition to the flow of current due to the electrical resistance within the antenna materials which is represented as the Ohmic loss resistance (R_{ohmic}). In standard patch antennas, the ohmic loss is negligible. However, in an electrically-small antenna structure ohmic loss becomes significant and increases as the antenna size is reduced below one wavelength (Stutzman and Thiele, 1998: 43).

2.3.3 Input Resistance

The input resistance of an antenna is the real part of the impedance presented by the input port, and is the sum of the radiation resistance (R_{r}) of the antenna and the ohmic loss resistance (R_{ohmic}) within the antenna structure.

2.3.4 Input Reactance

The input reactance of an antenna (X_{a}) is the imaginary part of the impedance presented by the input port, and is a function of the power stored in the near-field region of an antenna (Stutzman and Thiele, 1998: 43).

2.3.5 Input Impedance

The input impedance is the ratio of voltage and current developed across the input port of an antenna and consists of a real and an imaginary component (Sharma, Tripathi and Rishi, 2017: 2). The real part is the input resistance (R_{a}) and the imaginary part the input reactance (X_{a}). The unit of measurement is Ohms, and this impedance is given by:

$$Z_{\mathrm{in}} = R_{\mathrm{a}} \pm jX_{\mathrm{a}} \qquad \Omega \tag{2.2}$$

where $R_{\mathrm{a}} = R_{\mathrm{r}} + R_{\mathrm{ohmic}}$.

The impedance presented by the input port of a MPA coupled to a source is illustrated in Figure 2.8.

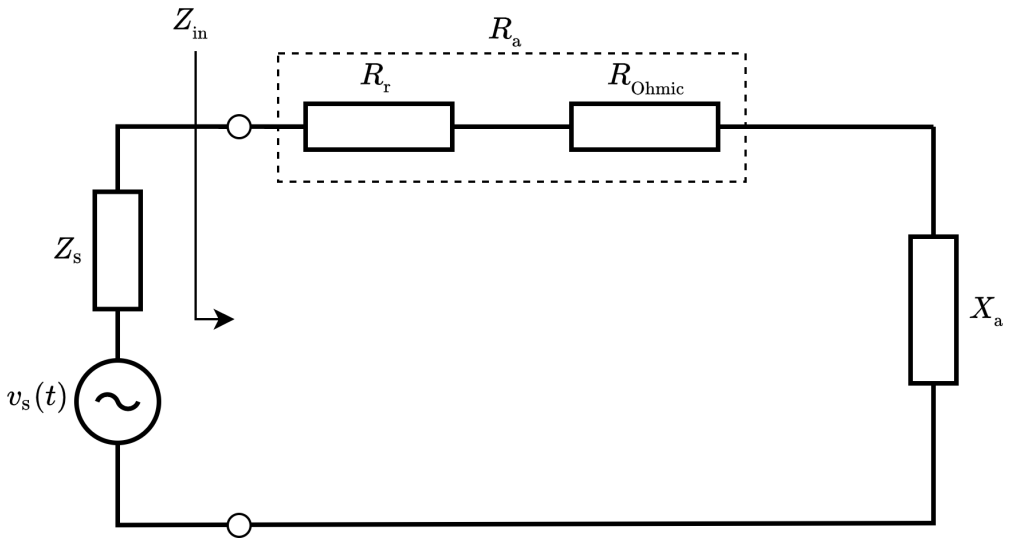

Figure 2.8: Impedance presented by input port of MPA

Figure 2.9 illustrates the variation of the impedance presented by the input port of a resonant MPA. Both the real and imaginary parts of this input impedance vary as a function of frequency and are symmetrical about the resonant frequency of 2.3 GHz (Balanis, 2005: 855).

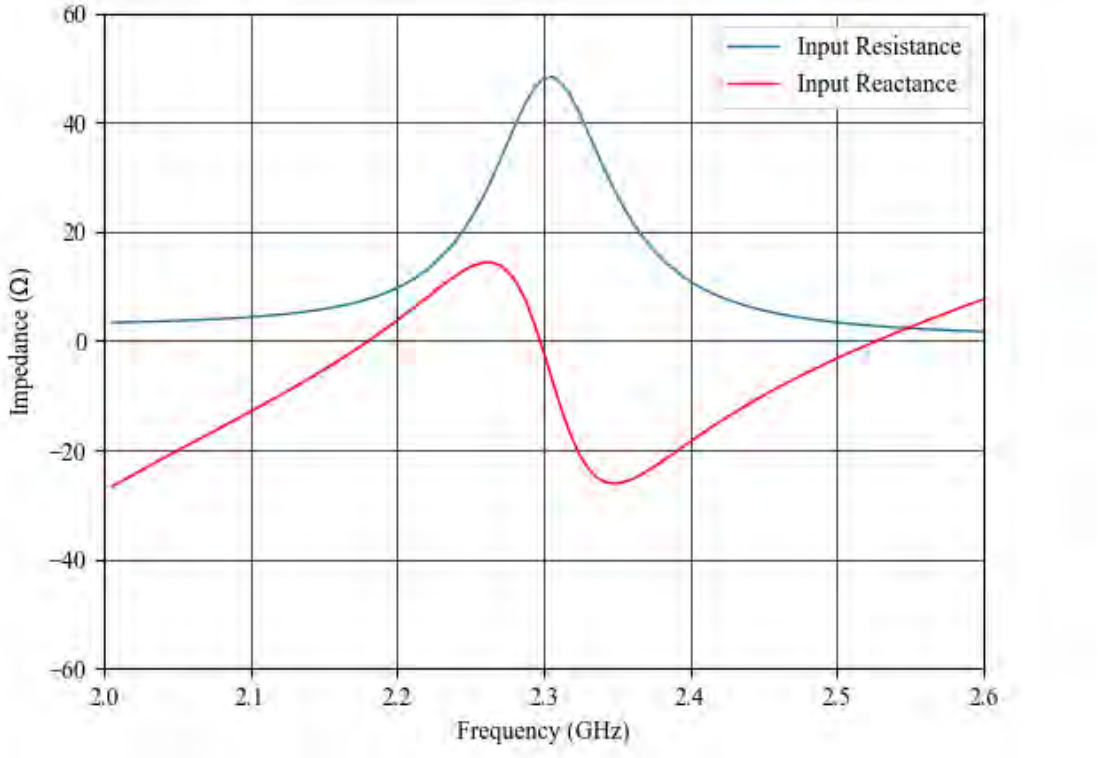

Figure 2.9: The variation of the input impedance with frequency of a MPA

At the resonant frequency, the input impedance is purely resistive and the reactance is zero Ohms. The reactance is inductive just below the resonant frequency and capacitive just above it.

2.3.6 Reflection Coefficient

The reflection coefficient is a figure of merit depicting how well a load impedance is matched to the system characteristic impedance. A load impedance of Z_{L} connected to a transmission line with a characteristic impedance of Z_0, has a reflection coefficient (Γ) which is given by:

$$\Gamma = \frac{Z_{\mathrm{L}} - Z_0}{Z_{\mathrm{L}} + Z_0} \tag{2.3}$$

A reflection coefficient of zero indicates a good impedance match, with no reflected power when the load impedance equals the system characteristic impedance (Pozar, 2001: 58). As the reflection coefficient increases, the greater the degree of mismatch. A value of one indicates that all incident power will be reflected back from the load.

2.3.7 Return loss

The return loss (RL) is defined as the loss of available power from a source, which is delivered to a mismatched load (Pozar, 2001: 59).

$$RL = -20\log|\Gamma| \qquad \mathrm{dB} \tag{2.4}$$

The input return loss of an antenna is denoted by the S_{11} S-parameter.

2.3.8 Voltage Standing Wave Ratio

The VSWR is defined as the ratio of the maximum to minimum voltage on a lossless transmission line and is a figure of merit of the degree of mismatch at the input port of an antenna (Pozar, 2001: 59).

$$\mathrm{VSWR} = \frac{1 + |\Gamma|}{1 - |\Gamma|} \tag{2.5}$$

2.3.9 Gain

The gain of an antenna is defined as the ratio of the intensity of power transmitted in a given direction to the intensity of the power radiated by an isotropic source (Balanis, 2005: 66).

2.3.10 Realised Gain

The realised gain of an antenna is the absolute gain of the antenna, which includes the impedance mismatch losses (Mathworks, 2023); (Altair, 2014: 10-17).

2.3.11 Bandwidth

The bandwidth of an antenna is defined as the range of frequencies over which power will be efficiently transmitted or received according to acceptable design criteria (Balanis, 2005: 70).

2.3.12 Quality Factor

The quality factor (Q-factor) is the ratio of the centre frequency of the antenna and the 3-dB bandwidth. An antenna with a high Q-factor, has a very narrow input return loss bandwidth. Electrically-small antennas are known to have a very high Q-factor, as the radiation resistance becomes less than the reactance below the resonant frequency (Stutzman and Thiele, 1998: 82).

2.3.13 Radiation Efficiency

The radiation efficiency is the ratio of the radiated power of an antenna to the power delivered at the input port of the antenna (Pozar, 2001: 639). Important factors that affect the efficiency of the antenna are losses within the dielectric material, conductor losses, impedance mismatches and power dissipated in any loads associated with the antenna element (Johnson, 1993: 7-11).

The radiation efficiency of an electrically-small antenna is a function of the efficiency of the matching network (η_{m}) which is given by (Sharma and Nagarkoti, 2017: 2):

$$\eta_{\mathrm{a}} = \eta_{\mathrm{m}}(1 + \frac{Q_{\mathrm{a}}}{Q_{\mathrm{m}}}) \tag{2.6}$$

where:

η_{a} = radiation efficiency of the antenna

Q_{a} = radiation Q-factor

Q_{m} = matching network Q-factor

The Q-factor of an antenna increases as the electrical size of the antenna decreases, which diminishes the radiation efficiency.

2.3.14 Radiation Pattern

The radiation pattern of an antenna is a graphical illustration of its radiation characteristics. It can be plotted in a two- or three-dimensional plane (Balanis, 2005: 27).

2.3.15 Polarisation

Antennas can either be linearly or circulary polarised. An antenna radiates a linear polarised EM wave when the E- and H-field components are confined to a given plane along the direction of propagation. A circular polarised EM wave has a constant magnitude and rotates at a constant rate perpendicular to a plane in the direction of propagation (Milligan, 2005: 19). The direction of the EM wave rotation specifies whether it is left hand circular polarised (LHCP) or right hand circular polarised (RHCP). MPAs are one of the most effective antennas to excite circular polarisation (James et al., 1989: 220). Circular polarisation in a patch antenna is achieved when two orthogonal resonant modes are excited, which have a 90 degree phase difference (Balanis, 2005: 859).

2.3.16 Axial Ratio

The axial ratio (AR) of an antenna is a figure of merit of its polarisation purity. The polarisation of an antenna can be represented as an ellipse with major and minor axis, defined

as the polarisation ellipse. The ratio of the maximum linearly polarised to minimum linearly polarised magnitudes on the ellipse represents the axial ratio (Milligan, 2005: 19). The closer the polarisation ellipse tends towards a perfect circle, the better the axial ratio. The axial ratio of the polarisation ellipse is given by:

$$\mathrm{AR} = \frac{\mathrm{Major\ axis}}{\mathrm{Minor\ axis}} \tag{2.7}$$

This implies that an antenna with perfect circular polarisation will have an AR = 1 or when expressed expressed in decibel, an AR equal to 0 dB.

The next section will explain the solver techniques used for patch antenna analysis.

2.4 Microstrip Patch Antenna Analysis

The most commonly used patch antenna shapes are the circular and rectangular patches. They can be represented and analysed by models such as the transmission-line model (TLM) and cavity model. Using these models, design equations and approximations were generated to be utilised by antenna designers. The transmission-line model is less accurate relative to the cavity model, but gives a good insight of the antenna behaviour (Chouchene, Larbi and Aguili, 2017: 646). The cavity model provides a more complex analysis, but is more accurate than the transmission-line model. Full-wave analysis is another accurate method, which utilises integral equation methods (Balanis, 2005: 816). The integral equation methods were developed by applying the method of moments (MoM) to an integral equation in the spatial domain and finite difference in the time-domain (Chen and Ney, 2007). An example of a time-domain method of analysis is the finite-element method (FEM).

The antenna simulation software package Altair FEKO has the correct solvers for MPA analysis. Table 2.2 was adapted from the Altair FEKO user manual, which lists the recommended solver types for various antenna topologies (Altair, 2014: 1-10).

Table 2.2: Recommended Altair FEKO solver techniques

Antenna type	**MoM**	**FEM, FEM-Mom**	**FDTD**	**MLFMM**	**FEM-MLFMM**
Microstrip antennas	X	X	X		
Aperture antennas	X				
Reflector antennas				X	
Windscreen antennas	X		X		
Conformal antennas	X	X	X	X	X
Broadband antennas	X	X	X	X	X
Array antennas	X	X	X	X	X
Lens antennas				X	X

The FEKO manual recommends using both the MoM and FEM solvers for microstrip antenna analysis. It was decided to use the FEM solver for the analysis of the MPAs in this thesis. The FEM solver is the most suitable for antenna geometries which have inhomogeneous dielectrics and three-dimensional anisotropic materials. This solver also uses the available memory of the computer efficiently (Reddy, 2020: 48).

2.5 The Rectangular Patch Antenna

The cavity model of a rectangular patch antenna is shown in Figure 2.10 and the corresponding design equations are provided in equation numbers 2.8 to 2.13 (Milligan, 2005: 299-301).

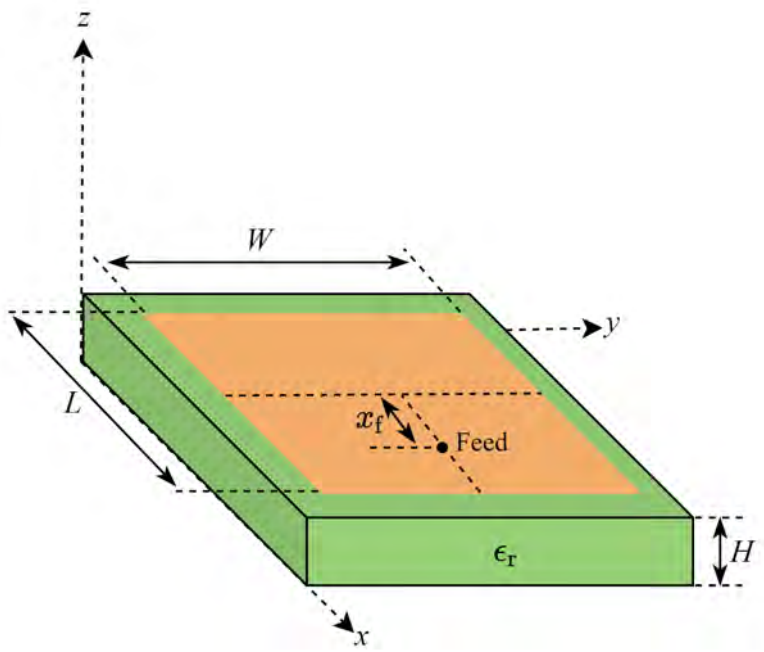

Figure 2.10: Rectangular MPA topology

The dominant resonant modes for a rectangular MPA are summarised in Table 2.3 (Balanis, 2005: 831).

Table 2.3: Rectangular MPA dominant resonant modes

Dominant Mode	**Condition**
TM_{010}	$L > W > H$
TM_{020}	$L > L/2 > W > H$
TM_{001}	$W > L > H$
TM_{002}	$W > W/2 > L > H$

The input variables which are required are the resonant frequency (f_r), dielectric constant (relative permittivity) of the substrate (ϵ_r) and the substrate height (H).

The fringing fields of the rectangular patch antenna extends the magnetic wall of the cavity to beyond the edge. The extension is given by:

$$\frac{\Delta}{H} = 0.412\frac{(\varepsilon_{\text{eff}} + 0.3)W/H + 0.262}{(\varepsilon_{\text{eff}} - 0.258)W/H + 0.813} \tag{2.8}$$

The effective dielectric constant represents the dielectric constant of a transmission line which is the same width as the rectangular radiating element and is given by:

$$\varepsilon_{\text{eff}} = \frac{\varepsilon_{\text{r}} + 1}{2} + \frac{\varepsilon_{\text{r}} - 1}{2}[1 + \frac{10H}{W}]^{-\frac{1}{2}} \tag{2.9}$$

The non-resonant width of a rectangular patch is given by:

$$W = \frac{c}{2f\sqrt{\varepsilon_{\text{eff}}}} \qquad \text{meters} \tag{2.10}$$

The resonant length of the rectangular patch is given by:

$$L = \frac{c}{2f\sqrt{\varepsilon_{\text{eff}}}} - 2\Delta \qquad \text{meters} \tag{2.11}$$

The input resistance is given by:

$$R_{\text{i}} = R_{\text{e}}\sin^2\frac{\pi x}{L} \qquad \Omega \tag{2.12}$$

The feed point x position:

$$x_{\text{f}} = \frac{L}{\pi}\sin^{-1}\sqrt{\frac{R_{\text{i}}}{R_{\text{e}}}} \qquad \text{meters} \tag{2.13}$$

The design equations for a rectangular MPA were given to determine the dimensions of the rectangular radiating element. The following subsection will present the design equations for a circular MPA.

2.6 The Circular Patch Antenna

The cavity model of a circular patch antenna topology is shown in Figure 2.11. The corresponding design equations are given by equation numbers 2.14 to 2.16 (Milligan, 2005: 314-315).

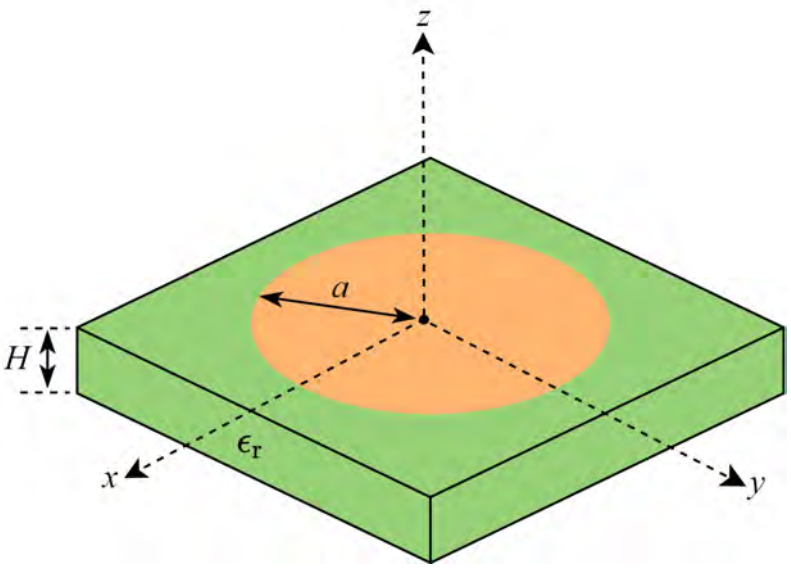

Figure 2.11: Circular MPA topology

X'_{np} represents the zeroes of the resonant TM modes and is a constant (Balanis, 2005: 845). The lowest to highest order modes are summarised in Table 2.4

Table 2.4: Circular MPA dominant modes

Resonant Mode	Condition
TM_{11}	$X'_{11} = 1.841$
TM_{21}	$X'_{21} = 3.0542$
TM_{01}	$X'_{01} = 3.8318$
TM_{31}	$X'_{31} = 4.2012$

The input variables which are required are the resonant frequency (f_r), the resonant mode (X'_{np}), the dielectric constant of the substrate (ϵ_r) and the height (H) of the substrate.

The effective radius of the circular element is given by:

$$a_{\text{eff}} = \frac{X'_{\text{np}}c}{2\pi f_{\text{np}}\sqrt{\varepsilon_{\text{r}}}} \qquad \text{meters} \tag{2.14}$$

The effective radius of the antenna is a radius which is slightly larger than the physical radius to account for the fringing fields.

Equation 2.14 is substituted into equation 2.15 to deterimine the physical radius, which is given by:

$$a = \frac{a_{eff}}{\sqrt{1 + 2H/\pi a\varepsilon_r[\ln(\pi a/2H) + 1,7726]}} \qquad \text{meters} \tag{2.15}$$

The length and width of the ground plane is a function of the substrate height and radiating element radius, which is given by:

$$LW_{\text{gnd}} = 6H + 2a \qquad \text{meters} \tag{2.16}$$

The feed location should have a start position at a distance one third of the physical radius from the centre of the radiating element when a coaxial feed is utilised (Milligan, 2005: 315). Its position relative to the centre can be optimised for an improved impedance match.

Compared to a rectangular patch antenna, the circular patch antenna is simpler to design with less equations to be dealt with. The next section presents the various feed methods that can be implemented to excite an MPA.

2.7 Patch Antenna Feed-Networks

Microstrip patch antenna designers use various techniques for antenna excitation. This section presents the feed networks which can be implemented to excite a radiating patch antenna. The selection of a feed network topology is dependent on the required performance parameters which need to be achieved. In an MPA, these parameters are controlled by the complexity and manufacturing restrictions. The most common topologies are coaxial, co-planar, proximity and aperture feeds (Balanis, 2005: 813).

2.7.1 Coaxial Feed

The coaxial feed, also known as the probe feed, is implemented from the bottom ground plane side with a coaxial centre conductor connected to the radiating element (Smolders, Visser and Johannsen, 2019: 127). The main advantage of this topology is that the feed network is not on the same electrical layer as the radiating element, which eliminates the possibility of unwanted spurious radiation. The coaxial feed position on the patch surface can be optimised to achieve a good impedance match.

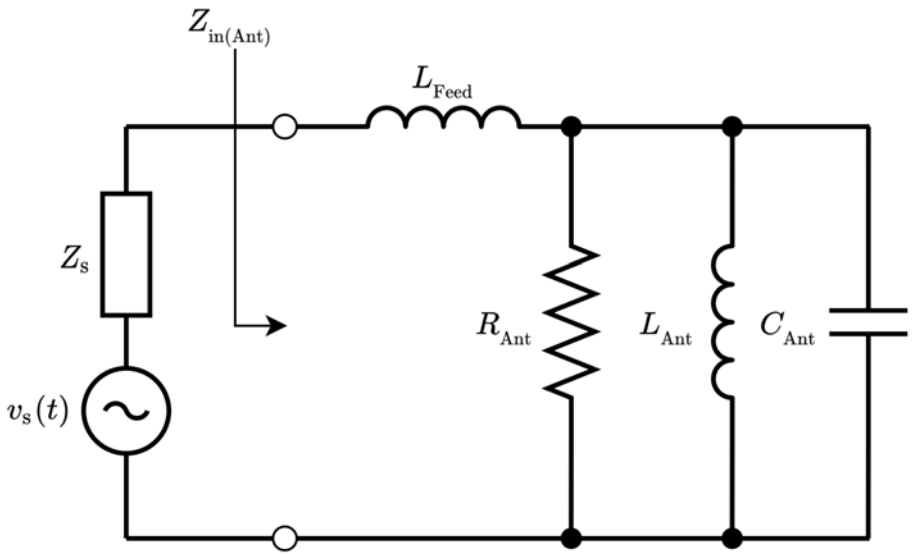

Figure 2.12: Equivalent circuit of MPA with coaxial feed

For a circular MPA, the recommended starting position is one-third of the radiating element radius from the centre (Milligan, 2005: 315). A disadvantage of this feed configuration is the additional series parasitic inductance presented by the centre conductor of the

feed. This inductance limits the VSWR bandwidth when thick substrates with low relative dielectric constants are used. The parasitic inductance can be resonated out by adding a series capacitor to form a resonant circuit at the same resonant frequency as the antenna. This capacitance can be achieved by implementing a small gap between the coaxial centre conductor and the radiating element. A small surface mount capacitor can also be used between the radiating element excitation point and the coaxial centre conductor. By using this arrangement, an impedance match bandwidth of up to 15.4% can be achieved (Milligan, 2005: 304).

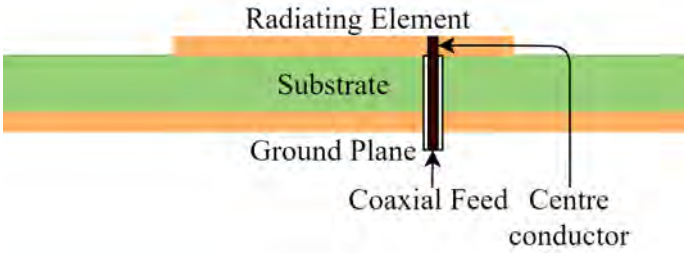

Figure 2.13: Coaxial feed topology

2.7.2 Co-planar Feeds

The co-planar feed topology utilises a transmission feed line which is either electrically connected or gap-coupled to one of the edges of the MPA. The microstrip feed line is on the same electrical layer and much smaller in width than the radiating element. This feed topology facilitates relatively simple impedance matching, analysis and fabrication. The main disadvantage of this topology is that surface waves and spurious radiation of the feed transmission line increases with an increase in the substrate thickness, which imposes a limitation on the antenna bandwidth (Balanis, 2005: 813). One of two different co-planar feed configurations can be implemented each of which have a different impedance matching characteristic.

2.7.2.1 Inset Feed

The inset feed topology utilises a microstrip transmission line which is connected to an impedance point within the radiating element surface at a distance L_{i} meters from its edge as illustrated in Figure 2.14. The gap on either side of the transmission line is chosen to be equal to its width (Milligan, 2005: 304). The input impedance of a MPA is a maximum

at its edges and decreases towards its centre. The impedance at a point L_{i} from the edge of a half-wave resonant rectangular patch antenna is given by (Bevelacqua, 2017):

$$Z_{\mathrm{in}} = \cos^2 \frac{\pi L_{\mathrm{i}}}{L} Z_{\mathrm{in}}(0) \qquad \Omega \tag{2.17}$$

where:

$Z_{\mathrm{in}}(0)$ = the input impedance at the edge of the rectangular patch antenna in Ohm

L = the length of the rectangular patch antenna in meters

L_{i} = the length of the inset in meters

The input impedance of an inset-fed MPA is dependent on the inset length and to some extent the width, W_{F} of the feed line. The inset length does not affect the resonant frequency of the MPA, but variations in the feed line width does affect the resonant frequency (Ramesh, 2003).

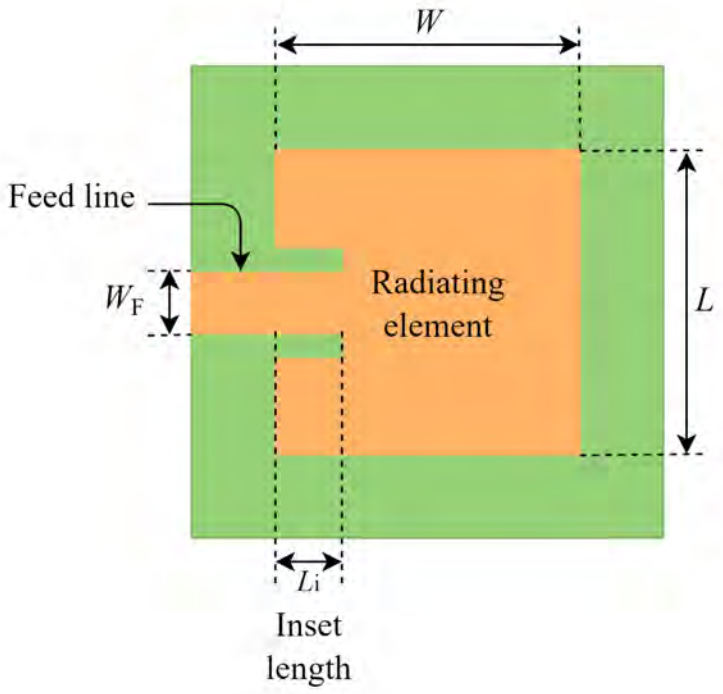

Figure 2.14: Inset feed geometry

The equivalent circuit for an inset feed MPA topology is indentical to the coaxial fed topology as illustrated in Figure 2.12 (Balanis, 2005: 815).

2.7.2.2 Gap-Coupled Feed

The gap-coupled feed topology utilises a narrow gap between the transmission feed line and the resonant radiating element. Critical coupling can be achieved by varying the width of the gap between the radiating element and the feed line until a good matching termination is achieved (James et al., 1989: 817).

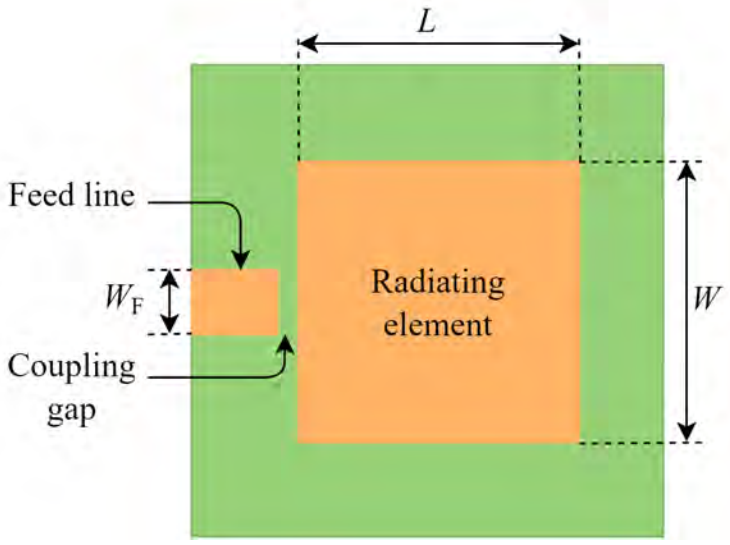

Figure 2.15: Gap-Coupled feed topology

2.7.3 Electrically Isolated Feeds

Electrically isolated or non-contact feed methods such as proximity coupling and aperture coupling, exhibit an improved input impedance bandwidth over the coaxial and inset fed co-planar microstrip feed topologies (Balanis, 2005: 815). The additional series parasitic inductance presented by a coaxial feed line or short transmission line are eliminated. These antenna topologies make it possible to select individual substrates with different dielectric constants and thicknesses for the feed and radiating element.

2.7.3.1 Proximity Feed

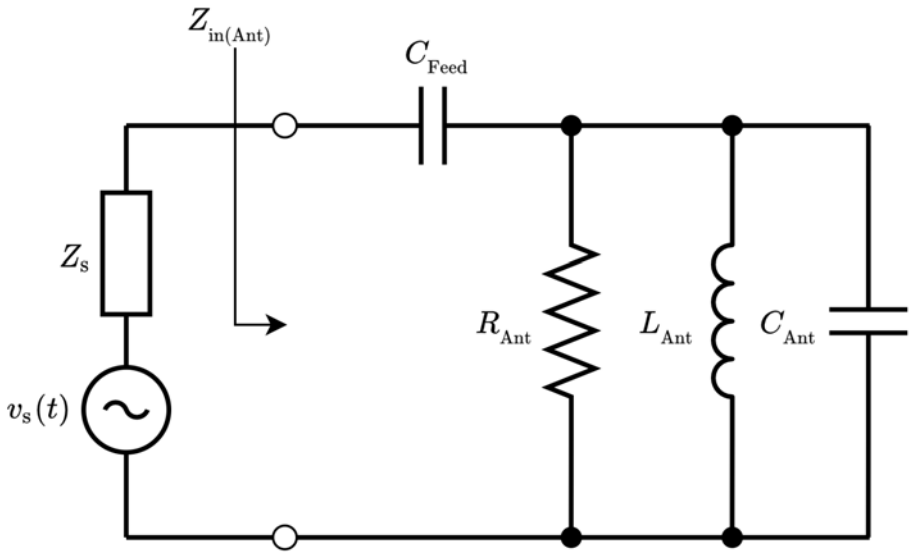

Figure 2.16: Proximity feed equivalent circuit

The antenna topology consists of two dielectric substrates with a microstrip feed line in-between. The radiating element is on top of the upper substrate. The equivalent circuit representing this configuration is a parallel *RLC* circuit in series with a capacitor as depicted in Figure 2.16 (Varma and Ghosh, 2014: 53).

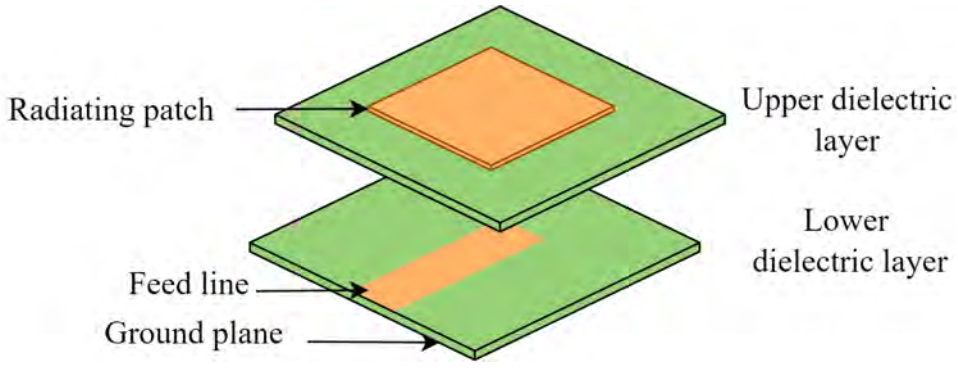

Figure 2.17: Proximity feed topology

2.7.3.2 Aperture Feed

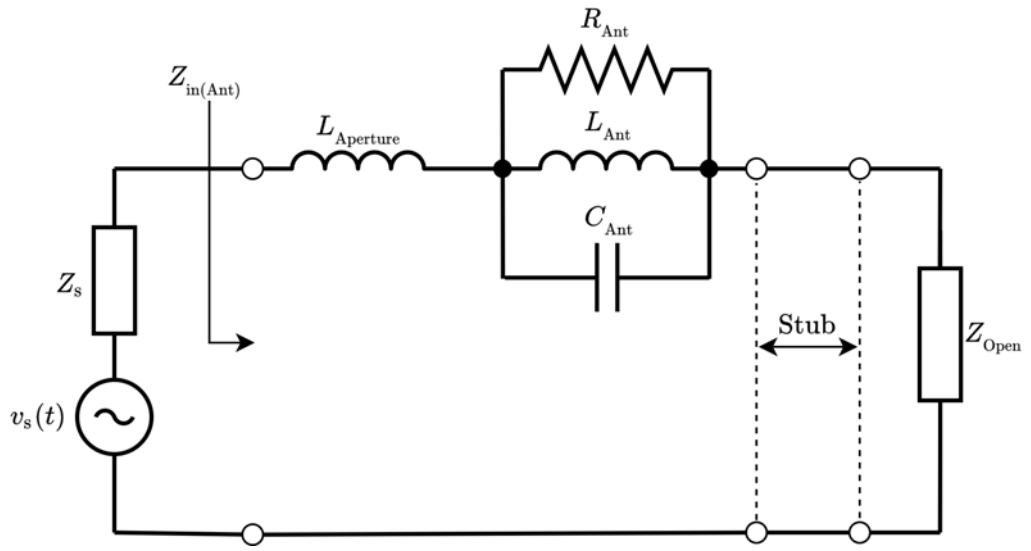

Figure 2.18: Equivalent circuit of aperture feed with open-circuited stub (James et al., 1989: 336)

An aperture coupled feed is another example of a non-contact feed method used to excite MPAs. The antenna topology consists of a common ground plane between the dielectric layers of the radiating element and open circuited microstrip feed line. Coupling between the microstrip feed line and the radiating element occurs by introducing a small aperture in the ground plane underneath the radiating element, directly above the feed line. The aperture is excited by the microstrip feed line from a standing-wave, with a current maximum at the aperture. The standing wave current is maximised by introducing a short between the microstrip feed line and the ground plane or by implementing a quarter-wave open-circuit stub (Milligan, 2005: 307).

The impedance match to the antenna can be controlled by optimising the feed line width and the length of the aperture slot (Balanis, 2005: 815).

The input impedance of the open-circuited stub is given by (Milligan, 2005: 307):

$$Z_{\mathrm{s}} = -jZ_0\cot(k_{\mathrm{eff}}L_{\mathrm{s}}) \qquad \Omega \tag{2.18}$$

where:

Z_{s} = the characteristic impedance of the microstrip feed line in Ohms

k_{eff} = the effective propagation constant of the dielectric material

L_{s} = the length of the open-circuited stub in meters

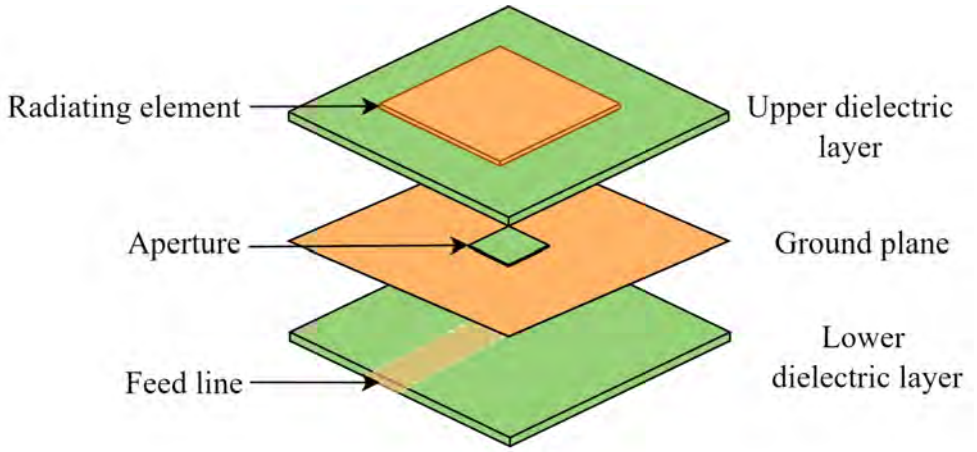

Figure 2.19: Aperture feed topology

The selection of the substrate for the upper and lower dielectric layers are based on the dielectric constant and thickness of the material. The upper dielectric layer should be a thick material with a low dielectric constant. The opposite is true for the bottom dielectric material, where a thin material with a high dielectric constant is preferred. The impedance bandwidth increases for an increase in the aperture slot dimensions and the antenna gain is inversely proportional to the slot area. The amount of coupling to the patch increases with an increase in the aperture slot size (Milligan, 2005: 307). The advantage of this feed method is that the feed topology and the radiating element can be independently optimised (Balanis, 2005: 815). Another advantage is the elimination of possible cross-polarisation experienced with the coaxial feed (Milligan, 2005: 308).

The aperture slot can be in the form of a rectangle, bowtie or H-shape. Each shape has

different coupling and bandwidth characteristics and it is up to the designer to explore which is the most suitable for the particular application.

2.7.4 Single Fed Circular Polarised MPAs

Circular polarisation with a single excitation can be achieved by either implementing truncation or perturbation segments within the radiating element surface (James et al., 1989: 221). The feed is located at an offset angle from the such a segment. The position or direction of the segment relative to the feed location determines whether the MPA is left hand circular polarised (LHCP) or right hand circular polarised (RHCP).

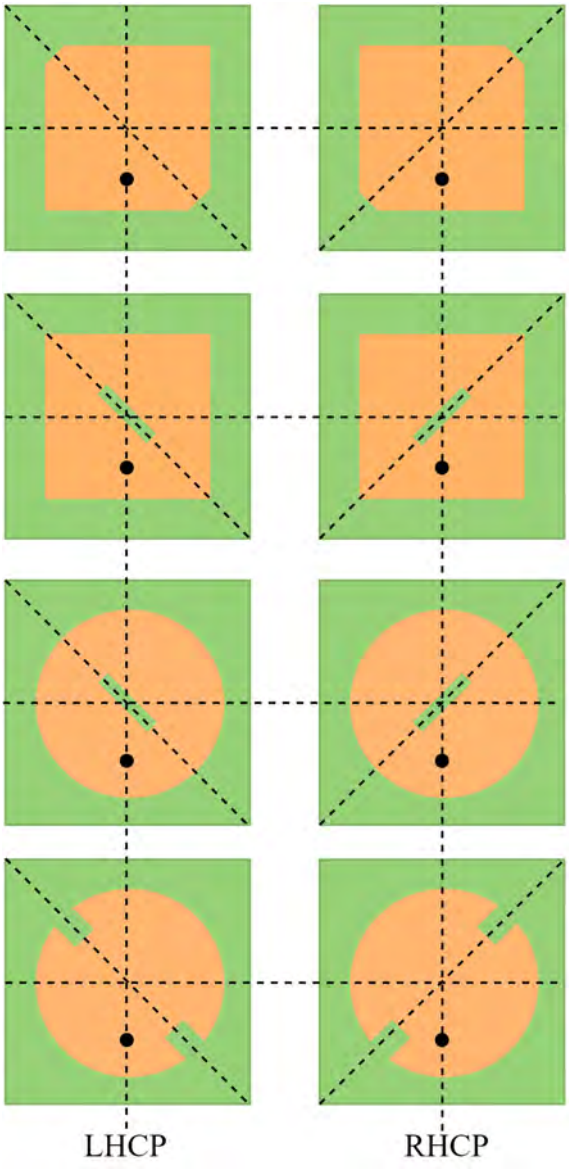

Figure 2.20: Single fed LHCP and RHCP elements

Figure 2.20 is an illustration of perturbation segments within a circular and rectangular radiating element. With a single feed, the patch antenna can be divided into two segments. Using the square patch shape as an example, the type A segment is fed along the square axis and the type B segment fed along its diagonal axis. ΔS denotes the change in the antenna's surface area which will excite two resonant modes and S is proportional to the Q-factor of the antenna. The resonant frequency of the two modes are calculated using equations 2.19 to 2.23 (Milligan, 2005: 318).

The ratio of the change in area to the area of a standard type A patch antenna is given by:

$$\frac{\Delta S}{S} = \frac{1}{2Q} \tag{2.19}$$

The ratio of the change in area to the area of a standard type B patch antenna is given by:

$$\frac{\Delta S}{S} = \frac{1}{Q} \tag{2.20}$$

The ratio of these lengths are derived from equations 2.19 and 2.20 is given by:

$$\frac{b}{a} = 1 + \frac{1}{Q} \tag{2.21}$$

The resonant frequencies of the square axis and diagonal axis lengths are given by equations 2.22 and 2.23:

$$f_1 = \frac{f_0}{\sqrt{1 + 1/Q}} \qquad \text{Hz} \tag{2.22}$$

$$f_2 = \frac{f_0}{\sqrt{1 + 1/Q}} \qquad \text{Hz} \tag{2.23}$$

The various feed-network topologies were presented. Some of the topologies can be more complex to implement due to possible manufacturing constraints. It is up to the antenna designer to decide which configuration will suit the requirements the best and what can be achieved in the manufacturing process.

2.8 Electrically-Small Antennas and the Chu-Limit

An electrically-small antenna (ESA) is defined as an antenna which has a physical size less than the radian-sphere which encloses the antenna, with a maximum dimension less than $\lambda/2\pi$ (Sharma and Nagarkoti, 2017: 2); (Wheeler, 1959: 1325).

Chu and Harold Wheeler addressed and defined the limitation on the minimum *Q*-factor of an electrically-small antenna, which is known in the literature as the Chu-limit.

The fundamental *Q*-factor limitation on the electrical size of an antenna is given by (Khan, Sharawi and Mittra, 2014: 915):

$$Q = \frac{1}{k^3a^3} + \frac{1}{ka} \tag{2.24}$$

where:
Q = the minimum Q-factor as a function of the largest linear dimension of the ESA
a = radius of the sphere enclosing the antenna
k = $2\pi/\lambda$, which is the wave-number

The radius of the radian spehere enclosing the antenna is given by:

$$r = \frac{\lambda_0}{2\pi} \qquad \text{meters} \tag{2.25}$$

The freespace wavelength is given by:

$$\lambda_0 = \frac{3\text{x}10^8\text{m/s}}{f} \qquad \text{meters} \tag{2.26}$$

An electrically-small antenna with a radius a and with a dimension less than one radian-sphere, is illustrated in Figure 2.21 (Davis et al., 2011).

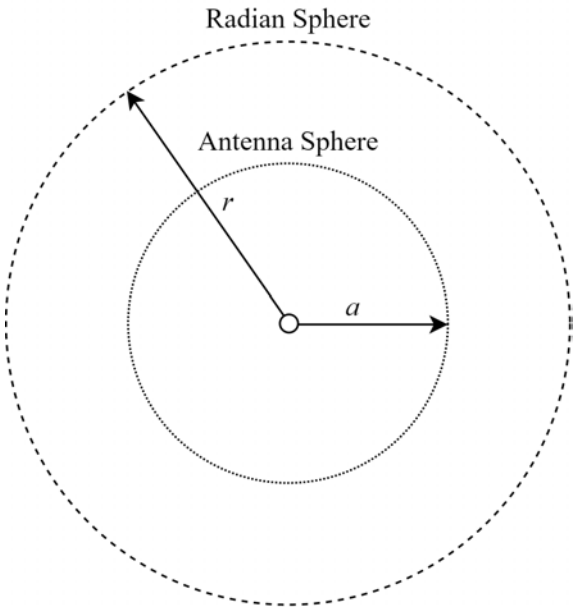

Figure 2.21: Antenna with its enclosed radian sphere

Figure 2.22 depicts the relationship between the gain and electrical size (*ka*) of the antenna.

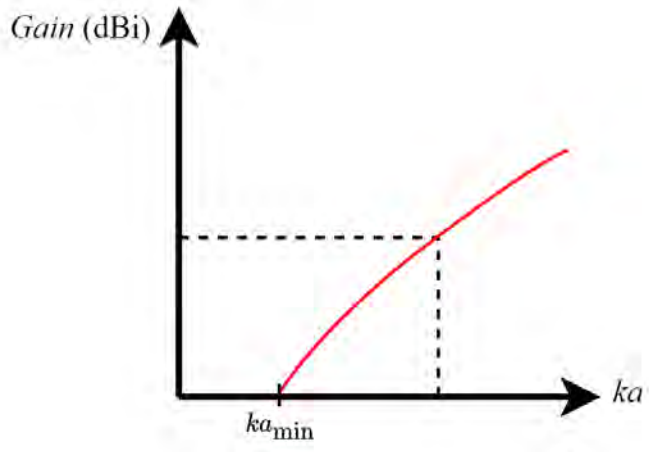

Figure 2.22: Antenna size (ka) versus gain

The gain of an electrically-small antenna is also restricted by its minimum electrical size ($ka_{\min}$) and is given by (Sharma and Nagarkoti, 2017: 3):

$$G_{\mathrm{a}} = 10\log[(ka)^2 + 2(ka)] \qquad \mathrm{dBi} \tag{2.27}$$

The minimum electrical size of an MPA must be verified and a trade-off made between the electrical size and the expected performance characteristics of the antenna.

2.9 MPA Minituarisation Techniques

Various techniques to miniaturise MPAs have been published in the literature by antenna engineers. The miniaturisation of an MPA is achieved by the lowering of the resonant frequency of the antenna, without altering the dimensions of the radiating element. A reduced resonant frequency for an MPA with a given dimension, is achieved by increasing the path length of the current at the edge of the radiating element. Miniaturisation techniques are relevant to the reduction in the physical size of the antenna which is a requirement for CubeSats. At frequencies below the resonant frequency of an MPA, the radiation resistance decreases, resulting in a decrease in the gain and radiation efficiency of the antenna.

2.9.1 Material Loading

The resonant frequency of an MPA can be reduced by using substrates with a high relative dielectric constant by an order of 10 and greater. The availability of low loss ceramic materials, such as LTCC, made it possible to achieve miniaturisation without compromising too much gain and also severely reducing the bandwidth of the antenna. Ceramic material substrates with different dielectric constants for minaturisation can be investigated for optimal antenna gain and bandwidth characteristics. The main disadvantage of using this type of material is the high purchase cost (Khan, Sharawi and Mittra, 2014: 915).

2.9.2 Shorting Pin

A shorting pin can be implemented within the MPA topology to reduce the resonant frequency of the antenna. A shorting pin positioned very close to the feed location presents an additional capacitance which forms a resonant circuit with the feed and antenna inductances. As the shorting pin is moved farther away from the feed position, its capacitance decreases and an additional parasitic inductance is introduced, which increases the total inductance of the antenna. The input impedance is determined by the locations of the feed and the shorting pins (Wong, Tang and Chen, 1998). The antenna is impedance matched

by iterating the feed location, which is recommended to be half the shorting pin diameter in the case of a coaxial feed (Milligan, 2005: 320).

The diameter of a circular patch with a shorting pin at the resonant frequency is given by:

$$d_r = \frac{0.14\lambda_0}{\sqrt{\epsilon_r}} \qquad \text{meters} \tag{2.28}$$

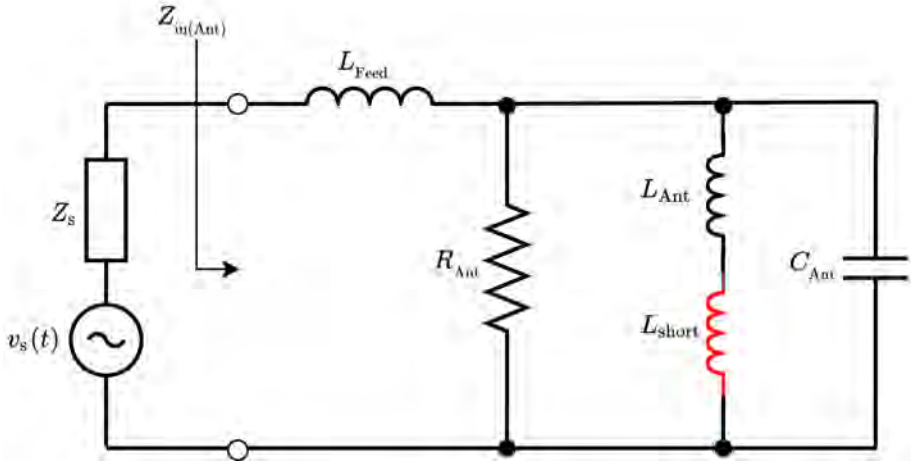

Figure 2.23: Coaxial fed MPA equivalent resonant circuit with increased inductance

To evaluate the addition of a shorting pin inductance to the equivalent parallel RLC resonant circuit of a coaxial fed MPA, an S_{11} (input return loss) simulation was completed in ADS. A resonant frequency of 2.5 GHz was selected. The equivalent circuit is shown in Figure 2.24 and the simulated input return loss in Figure 2.25.

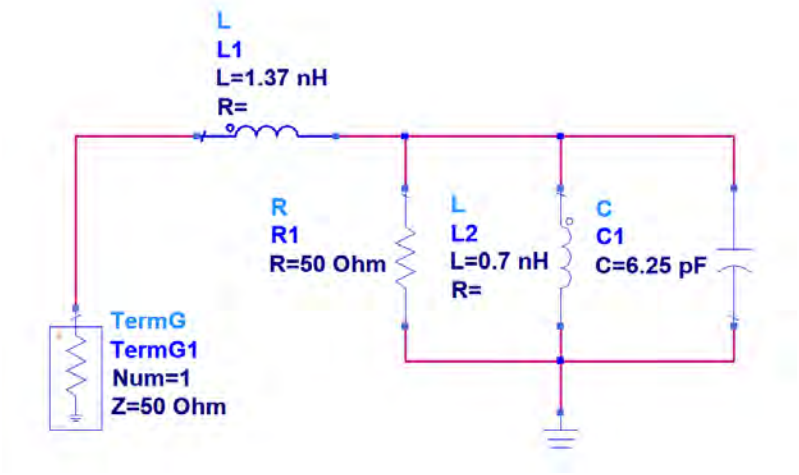

Figure 2.24: 2.5 GHz coaxial fed MPA resonant circuit

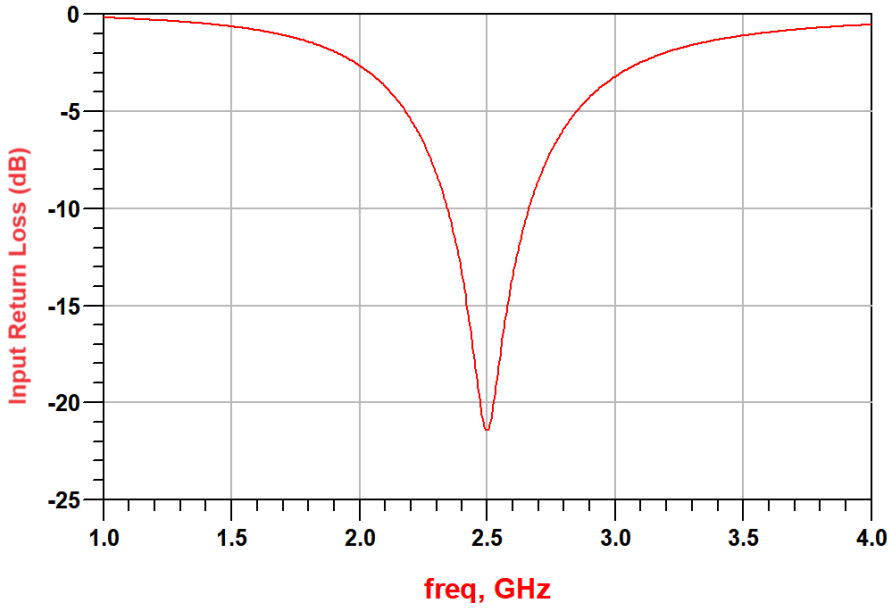

Figure 2.25: 2.5 GHz coaxial fed MPA input return loss

A 1 nH inductor was inserted in series with the parallel RLC circuit inductance to evaluate the shift in the resonant frequency of the circuit.

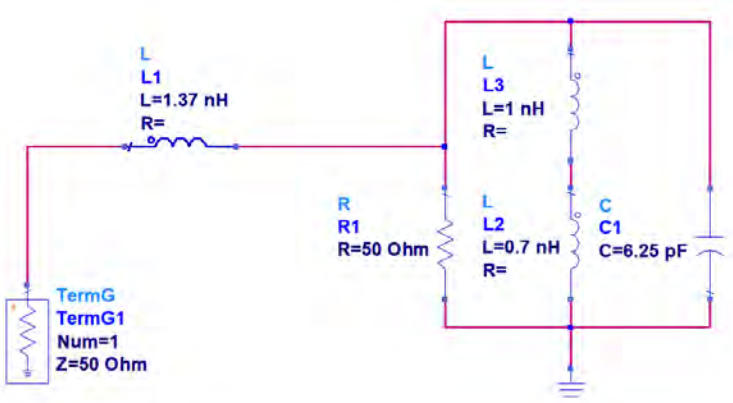

Figure 2.26: 2.5 GHz coaxial fed MPA resonant circuit with increased inductance

An increase in the total equivalent inductance of the antenna, results in a decrease of the resonant frequency from 2.5 GHz to 1.6 GHz as shown in Figure 2.27.

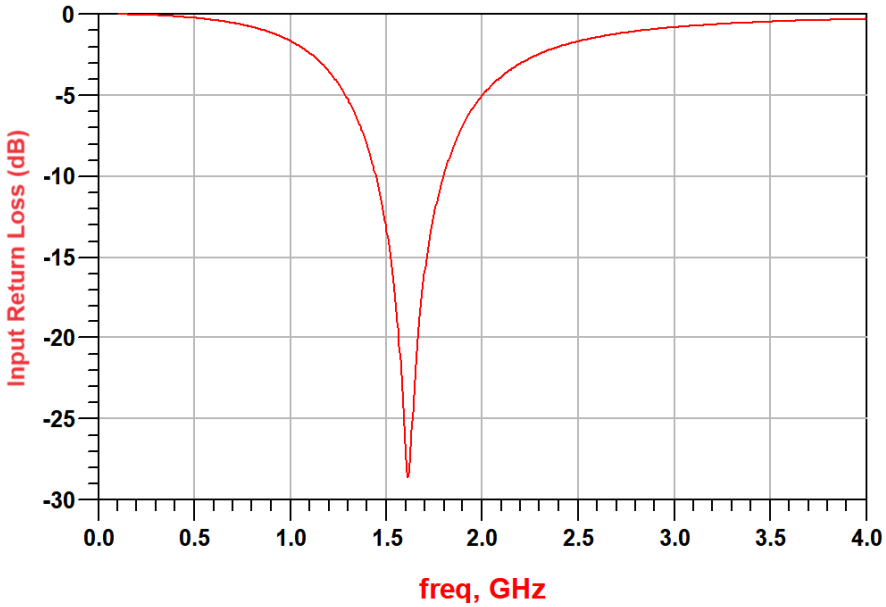

Figure 2.27: Input return loss of 2.5 GHz coaxial fed MPA with increased inductance

2.9.3 Reshaping

The shape of an MPA radiating element can be altered to obtain an increased length and thereby reduce the resonant frequency of the antenna. Notches or slits can be introduced in the perimeter of the radiating element to achieve miniaturisation by increasing the length of the current flow path. Complex radiating element shapes with spirals have been reported in the literature to meander the current path length significantly (Milligan, 2005: 320). Due to the complexity of these shapes, a genetic algorithm, which is a global opti-

misation tool in electromagnetics, can be used to optimise the performance characteristics of these antennas (Dhakshinamoorthi et al., 2020: 894). Figure 2.28 is an example of a miniaturised nearly-square patch, with four slits introduced within its perimeter (Cheng, Dong and Pan, 2019).

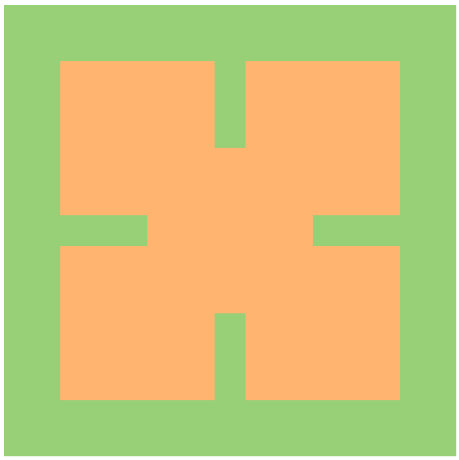

Figure 2.28: Miniaturised nearly-square MPA with slits

2.9.4 Ground Plane Modifications

The ground plane of an MPA is assumed to be of infinite size, but practically it has physical constraints. Miniaturising the ground plane can be achieved by reducing its size to be slightly larger than the radiating element itself. Reduction in the dimensions of the ground plane, reduces the polarisation purity of the antenna and also affects the input impedance. In addition, back lobe radiation increases due to edge diffraction. Adding slotted lines to the ground plane area can be used to reduce the antenna size and has been successfully implemented previously (Khan, Sharawi and Mittra, 2014: 917).

2.9.5 Metamaterials

Metamaterials are materials which are manufactured to have certain properties which are not commercially available. For example, a material could be required to have either a relative dielctric constant of approximately zero, a negative-permittivity or permeability or a combination of each. These materials are successfully used to miniaturise MPAs, but at the cost of low radiation efficiency and narrow bandwidths.

This minituarisation method is complex when the physics of metamaterial structures are not fully understood (Khan, Sharawi and Mittra, 2014: 919).

2.9.6 Non-Foster Impedances

Non-Foster impedances are useful to increase the bandwidth of the input return loss of high-Q electrically-small antennas below their resonant frequency (Ivanov et al., 2016). Examples are the impedance presented by a negative inductor or capacitor, which in this case, have inverted reactance slopes realised with an active negative impedance converter. These circuits will be covered in subsection 3.5. In the literature, these impedances are mostly utilised in impedance matching networks below microwave frequencies. The main disadvantage is the additional power consumption of the active devices required to realise these impedances. It is reported in the literature that negative impedance converters are difficult to implement in transmit antenna applications with high power requirements (Sussman-Fort and Rudish, 2009: 2239) and designers have also experienced challenges with circuit stability.

2.10 Summary and conclusion

The literature revealed that there is no definite optimal technique for miniaturisation of patch antennas. All techniques have advantages and disadvantages, some of which are frequency dependent. The techniques of material loading, shortings posts and reshaping offer relatively high degrees of miniaturisation and are the least complex and cost effective.

The different miniaturisation techniques are summarised in Table 2.5, adapted from Khan, Sharawi and Mittra (2014: 920).

Table 2.5: MPA miniaturisation techniques summary

Technique	**Miniaturisation**	**Advantages**	**Disadvantages**
Material Loading	High degree	Easy to design	Limited bandwidth Expensive
Shorting posts	Up to four times	Very cost effective	Low gain Low directivity
Reshaping	Up to eight times	Wide bandwidth	Complex geometry Affects radiation characteristics
Ground plane modifications	Up to eight times	Simple antenna geometry	Low efficiency Increased radiation back lobe
Metamaterials	High degree	Use of metamaterial inspired techniques	Limited bandwidth Low efficiency Complex geometry
Non-Foster impedances	High degree	Wide bandwidth	Additional power consumption Low efficiency for transmit applications

Chapter 3

Impedance Matching Network Theory

3.1 Introduction

A complex impedance consists of a real and an imaginary part and is given by:

$$Z = R \pm jX \qquad \Omega \tag{3.1}$$

where R = the resistive part and $\pm X$ = the reactive imaginary part which is dependent on the frequency of operation. The inverse of a complex impedance is a complex admittance which is given by:

$$Y = G \pm jB \qquad \mathrm{S} \tag{3.2}$$

where G = the conductive real part and $\pm B$ = the susceptive imaginary part, which is also dependent on the frequency of operation. Impedance matching is an important consideration in any RF system. The power transfer between a source and its load impedance is a maximum when they are matched. In order to match an arbitrary load impedance to its source impedance, which typically is the system characteristic impedance, an impedance matching network is required. The concept of impedance matching is shown in Figure 3.1. Impedance matching networks can be passive or active, depending on the power handling and circuit bandwidth requirements. In this chapter, an introduction to series and parallel resonant circuits is presented, followed by passive and active non-Foster impedance matching theory. A comparison between the behaviour of various impedance matching

circuits will be made and conclusions presented in a summary.

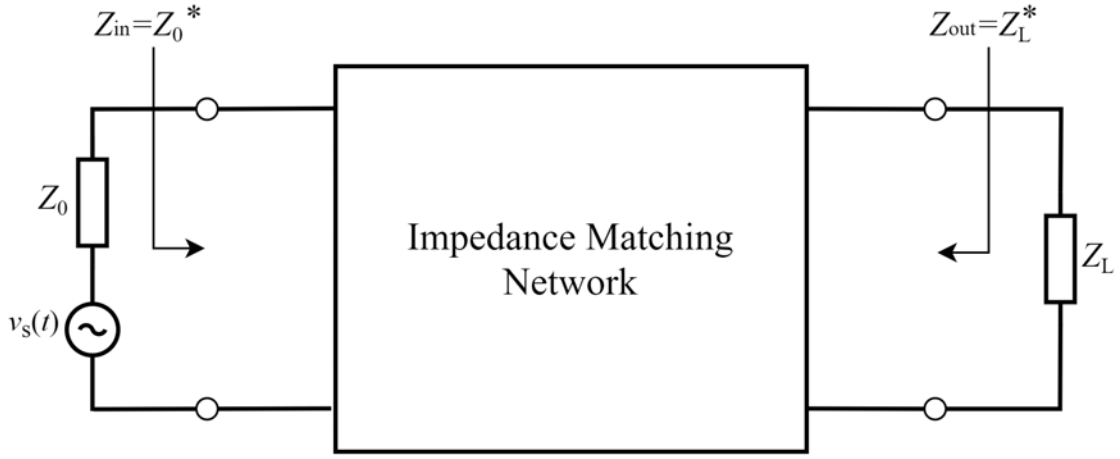

Figure 3.1: The concept of impedance matching

3.2 Resonant Circuits

The combination of an impedance matching network and an arbitrary load impedance forms a resonant circuit, resonating at a certain frequency. To understand how two opposite reactive components behave in an impedance matching network, it is necessary to understand the operation of both series and parallel resonant circuits. The term resonance is defined as the condition where the average stored magnetic energy in an inductor and the average stored electrical energy within a capacitor are equal in magnitudes (Pozar, 2001: 267). The frequency of operation at which this condition occurs is called the resonant frequency and is given by:

$$f_{\mathrm{r}} = \frac{1}{2\pi\sqrt{LC}} \qquad \mathrm{Hz} \tag{3.3}$$

The complex impedance and admittance of an inductor (L) and capacitor (C) are represented by equations 3.4 to 3.7. The impedance and admittance presented by an inductor when it is considered as a one-port network are given by:

$$Z_{\mathrm{L}} = R + j\omega L \qquad \Omega \tag{3.4}$$

and

$$Y_{\mathrm{L}} = G - j\frac{1}{\omega L} \qquad \mathrm{S} \tag{3.5}$$

The impedance and admittance presented by a capacitor when it is considered as an one-port network are given by:

$$Z_{\mathrm{C}} = R - j\frac{1}{\omega C} \qquad \Omega \tag{3.6}$$

and

$$Y_{\mathrm{C}} = G + j\omega C \qquad \mathrm{S} \tag{3.7}$$

When circuits are analysed with reactive elements connected in shunt, admittances are used rather than impedances. Equations 3.4 to 3.7 will be used for circuit analysis presented in the following sections.

3.2.1 Series Resonant Circuit

An RLC circuit consisting of a resistive component and two ideal reactive components connected in series, when considered as a one-port network and driven by an ideal source, is illustrated in Figure 3.2. At the resonant frequency, the sum of the reactances presented by the reactive components is zero ohms, making the input impedance of the circuit real. The input impedance of a series RLC circuit is given by:

$$Z_{\mathrm{in}} = R + j(\omega L - \frac{1}{\omega C}) \qquad \Omega \tag{3.8}$$

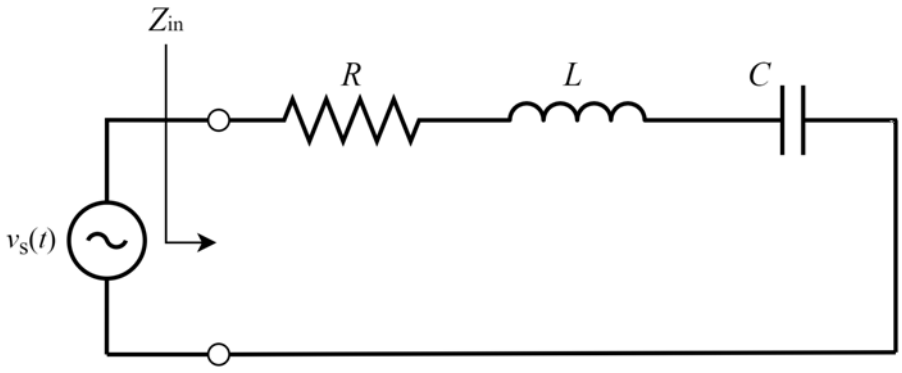

Figure 3.2: Series *RLC* resonant circuit

The magnitude and phase angle of the input impedance in polar form is given by:

$$Z_{\text{in}} = \sqrt{R^2 + X^2} \angle \tan^{-1}\left(\frac{X}{R}\right) \qquad \Omega \tag{3.9}$$

For a series resonant circuit, the magnitude of the input impedance is a minimum at the resonant frequency as illustrated in Figure 3.3.

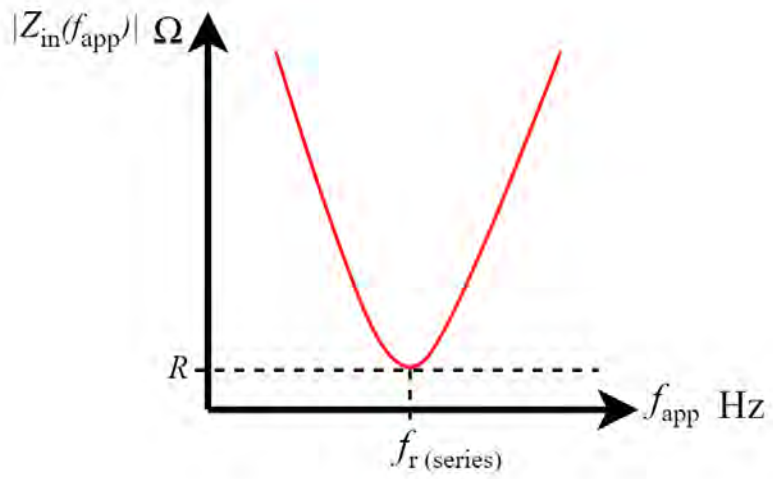

Figure 3.3: Input impedance of a series *RLC* resonant circuit

The resonant frequency for a series and parallel resonant circuit is given by:

$$f_{\text{r}} = \frac{1}{2\pi\sqrt{LC}} \qquad \text{Hz} \tag{3.10}$$

The following subsection will describe the characteristics of a parallel resonant circuit.

3.2.2 Parallel Resonant Circuit

A parallel RLC circuit consist of a resistive element and two ideal reactive components connected in shunt as illustrated in Figure 3.4.

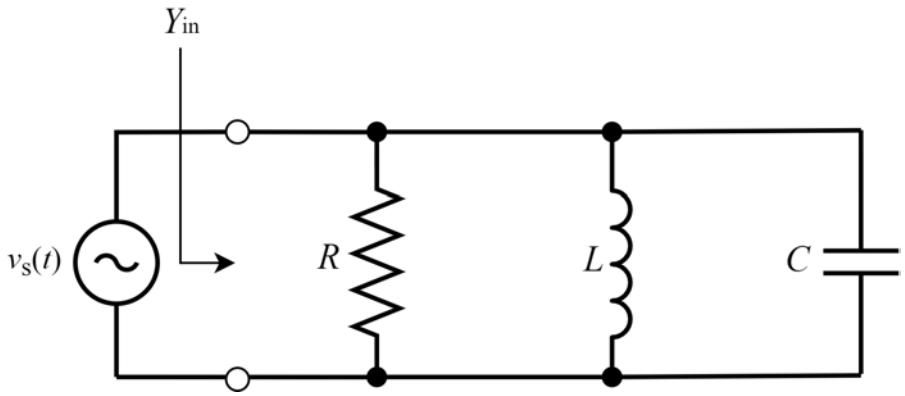

Figure 3.4: Parallel *RLC* resonant circuit

The input impedance of the circuit is calculated by converting the impedances presented by each component to their equivalent admittance. The total input admittance is calculated by summing the admittances presented by each component. The total impedance presented by the input port is the inverse of the total input admittance.

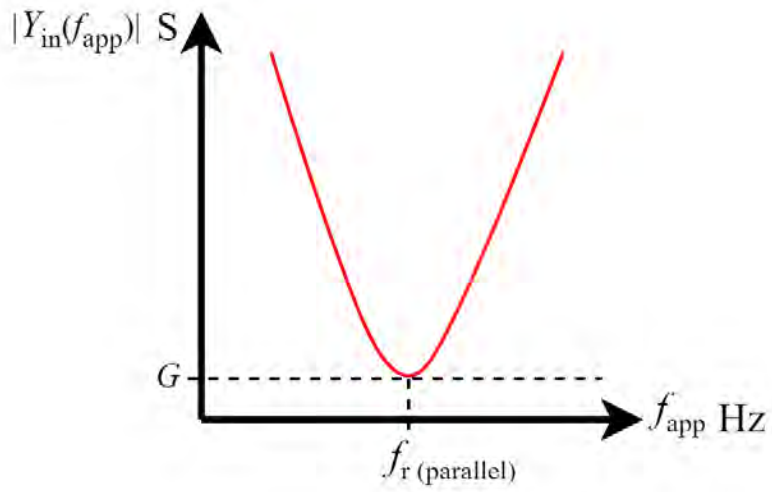

Figure 3.5: Input admittance of parallel *RLC* resonant circuit

The magnitude of the input impedance of the parallel resonant circuit shown in Figure 3.4 is a maximum at the resonant frequency. The opposite is true for the equivalent input admittance.

The input admittance of the parallel RLC circuit is given by:

$$Y_{\text{in}} = G + j(\omega C - \frac{1}{\omega L}) \qquad \text{S} \tag{3.11}$$

The characteristics of a series and parallel resonant circuit were presented. The magnitude of the input impedance and admittance presented by each resonant circuit were illustrated to indicate behavioural differences.

3.3 The Smith chart

The Smith chart is a nomogram used to graphically solve impedance matching and transmission line mathematical problems. In order the understand impedance matching theory, a brief introduction to the Smith chart shown in Figure 3.6 will be given.

The centre of the Smith chart is at point F with a normalised impedance $Z' = 1 + j0\ \Omega$. The blue circle drawn around the centre of the chart, intersecting with points A, B and C, is defined as the constant VSWR circle. The red and orange circles represents constant resistance circles. The constant resistance circle highlighted in red has a normalised impedance $Z' = 1 \pm jX\ \Omega$. The distance between points A, B and C on the constant VSWR circle is measured in guided wavelengths (λ_g). The normalised impedances within the upper region of the chart is represented as $Z' = R + jX\ \Omega$, while the normalised impedances within the bottom region as $Z' = R - jX\ \Omega$.

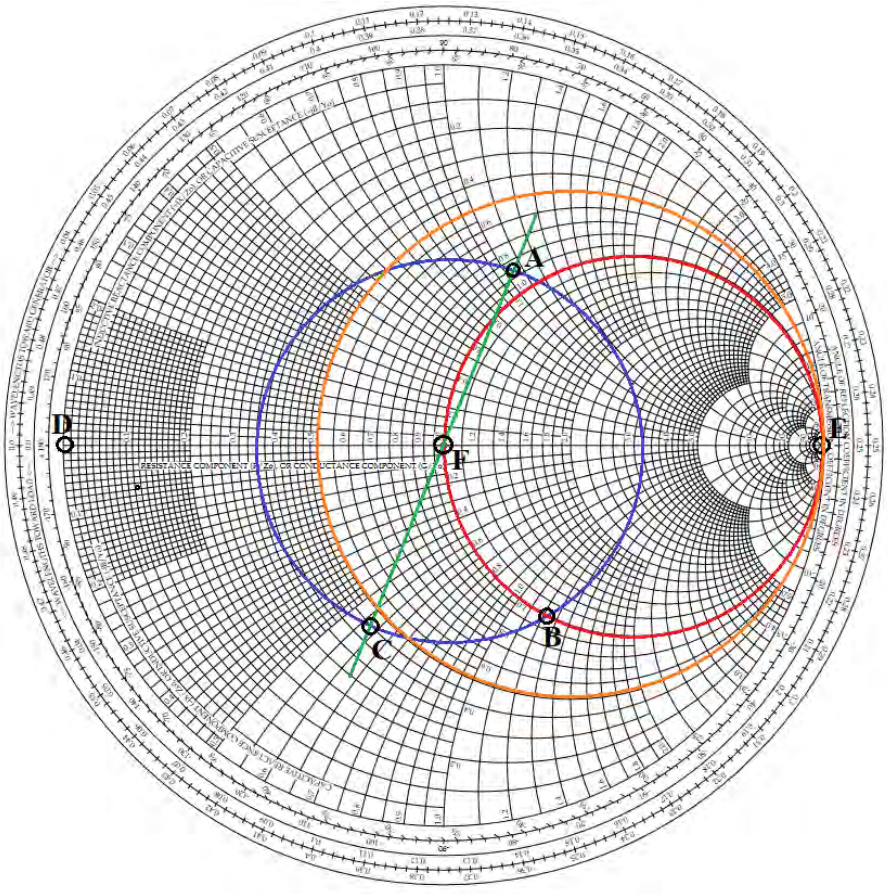

Figure 3.6: The Smith chart

When the Smith chart to design open and short-circuit stubs, it is important to know the position of the open and short-circuit impedance points on the outer edge of the chart to determine the correct stub lengths. Point D represents a short circuit with a normalised impedance $Z' = 0\ \Omega$. Point E represents an open circuit with a normalised impedance $Z' = \infty\ \Omega$. The distance between the open and short-circuit impedance points is a quarter-wavelength. When working with admittances, point D will be the open-circuit point and point E the short circuit point.

In order to find the equivalent normalised admittance of a normalised impedance point on the constant VSWR circle, a line is drawn from the impedance point through the centre of the Smith chart until it intersects with the constant VSWR circle on the opposite side. From Figure 3.6, point C represents the equivalent normalised admittance of the normalised impedance at point A. Within the next sections, the Smith chart will be referred to in the design of impedance matching networks.

3.4 Impedance matching with passive elements

In the section 3.2, resonance and the characteristics of two resonant circuit configurations were presented. Impedance matching networks and the behaviour of these circuits are based on the principles of a series resonant circuit. Working with passive elements, an inductive reactance will always be resonated out with a capacitive reactance at a selected frequency. Figure 3.7 is a graphical illustration of the reactances presented by an ideal inductor and capacitor as a function of the applied frequency.

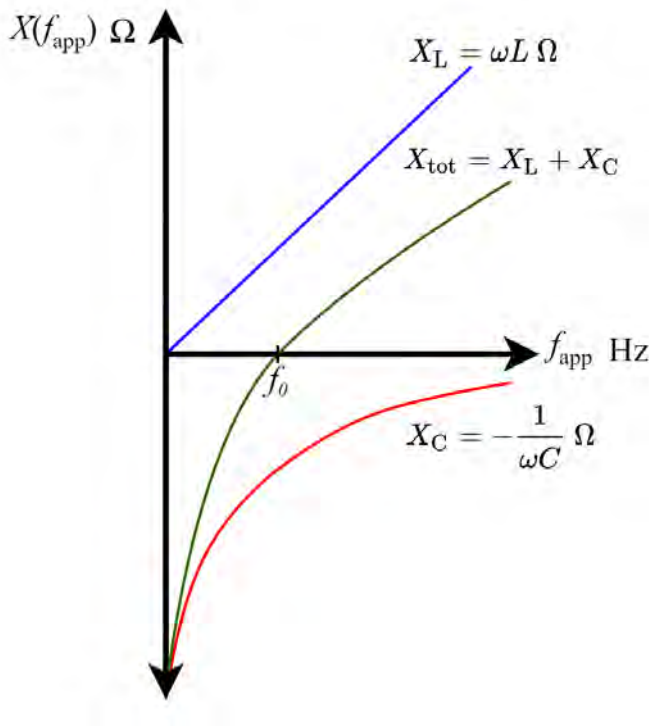

Figure 3.7: Inductor and capacitor reactances as a function of frequency

The total reactance is zero ohms at the applied frequency f_0, resulting in the complex impedance to be real. This condition only exists at one frequency when using passive elements (Sussman-Fort, 2006: 9).

3.4.1 Lumped Element Impedance Matching

Lumped elements are mostly utilised at signal frequencies up to 1 GHz, where the signal wavelength is still much greater than the physical component size (Sharma, Tripathi and Rishi, 2017: 12). Examples of lumped elements are resistors, inductors and capacitors. As the frequency of operation is increased, the operation of these components becomes less ideal due to parasitic elements within the component packages. Depending on the power handling requirements, the smallest component package must be selected as the frequency of operation is increased. Lumped components are arranged into either L, T or Pi networks to conjugately match the input impedance of a source or load to the system characteristic impedance. With the aid of the Smith chart, the values of these components can easily be determined. The bandwidth of the matching circuit is a function of its loaded Q-factor.

3.4.1.1 L-Matching Network

The L-matching network is a simple passive network which consists of two reactive elements with impedances Z_1 and Z_2 in an L-configuration. The circuit selection between the two configurations are based on the position of the normalised load impedance on the Smith chart. When the normalised load impedance lies within the $Z' = 1 + jX\ \Omega$ region, configuration 1 is selected. Configuration 2 is selected when the normalised load impedance lies within the $Z' = 1 - jX\ \Omega$ region. The L-matching network has a relatively low Q-factor and is mostly used for wider bandwidth impedance matching applications (MacPherson, 2002: 2-2).

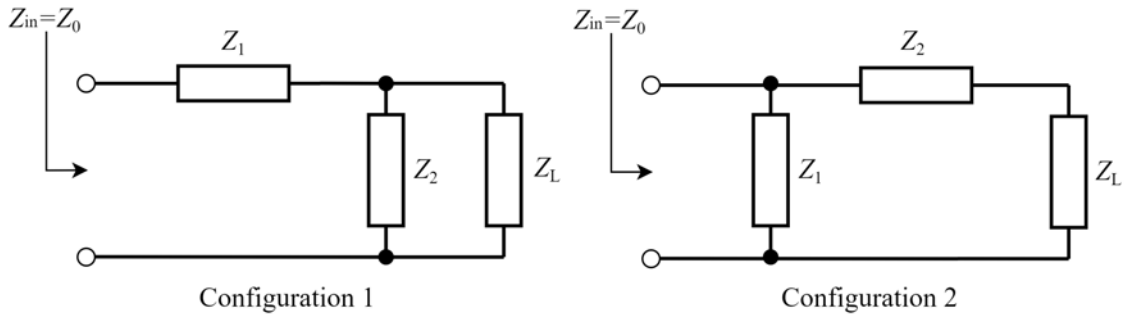

Figure 3.8: L-matching network configurations

3.4.1.2 T-matching network

The T-matching network consists of three reactive elements with impedances Z_1, Z_2 and Z_3 in a T-configuration. For circuit analysis and design, the T-network is divided into two L-networks connected back to back as illustrated in Figure 3.10. A virtual resistance R_v is in shunt with both networks. Analytical techniques or the Smith chart are used to calculate the reactive component values of each L-network. The design criterion is that the value of the virtual shunt resistor should be greater than the source and load resistances. Opposite reactive elements should be selected for each L-network (MacPherson, 2002: 2-10).

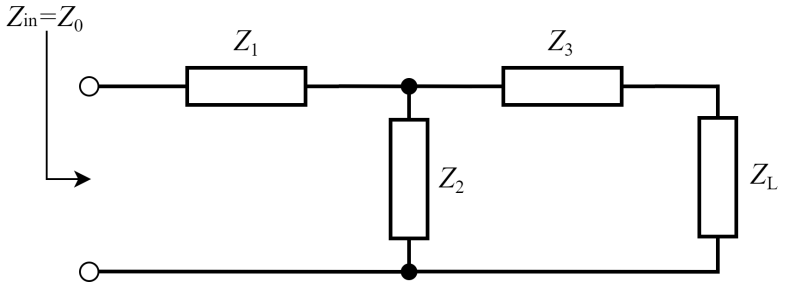

Figure 3.9: T-matching network configuration

The T-matching network is used for narrow-band impedance matching, as a relatively high *Q*-factor can be achieved with the correct component selection.

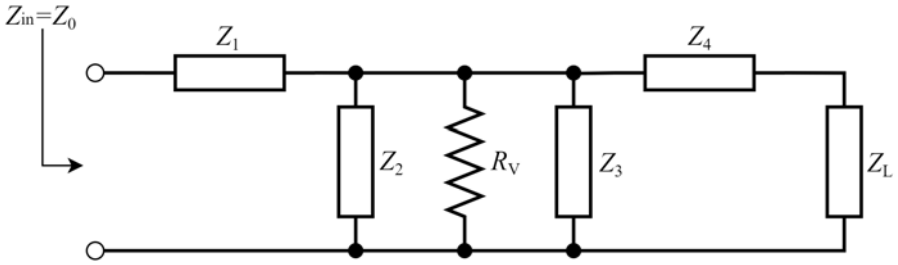

Figure 3.10: T-matching network transformed into two L-networks

3.4.1.3 Pi-matching network

The Pi-matching network consists of three reactive elements with impedances Z_1, Z_2 and Z_3 in a Pi configuration. The circuit can be divided into two L-networks, connected back

to back with a virtual resistor R_v in shunt.

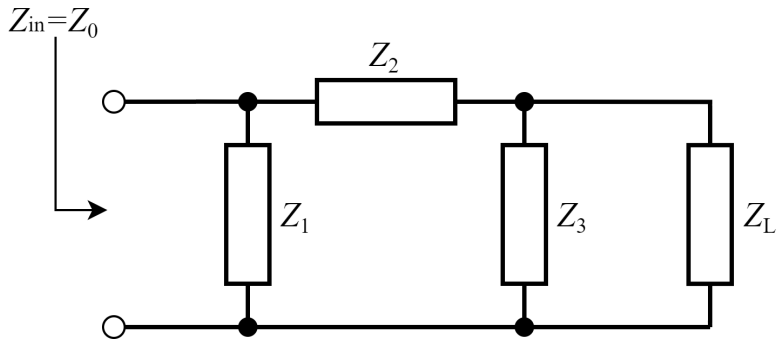

Figure 3.11: Π-matching network configuration

The design criterion is that the value of the virtual resistance R_v should be smaller than the source and load resistances and opposite reactive elements should be selected for each L-network. The circuit's loaded Q-factor is determined by the L-network with the highest Q-factor (MacPherson, 2002: 2-13).

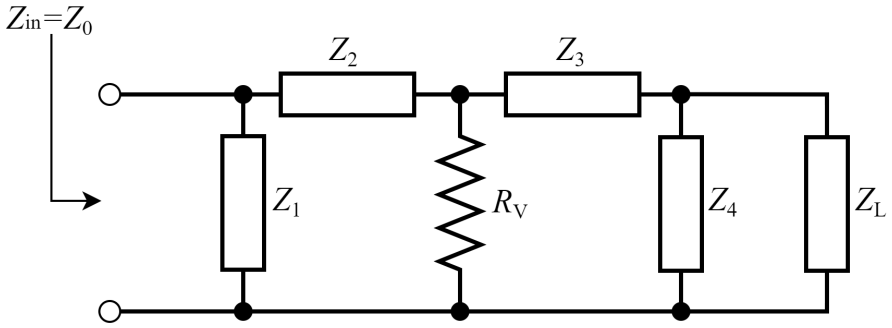

Figure 3.12: Π-matching network transformed into two L-networks

3.4.2 Distributed Element Impedance Matching

Distributed elements are designed with microstrip transmission lines. The transmission lines can be in the form of short and open-circuit stubs, quarter-wavelength impedance transformers, double stubs, radial stubs and different shapes of tapered lines. Depending on the stub selection, narrow and wider-bandwidth impedance matching can be achieved. This method of impedance matching is preferred at S-band and higher microwave frequencies, as it eliminates the problem of parasitic inductances and capacitances associated

with lumped elements at high frequencies. The disadvantage of using stubs for microstrip patch antenna (MPA) impedance matching, is the unwanted spurious radiation losses from the additional circuitry (Sharma, Tripathi and Rishi, 2017: 3).

3.4.2.1 Shunt Stub Impedance Matching

A single shunt stub is designed with a microstrip transmission line with a length l and a distance d from the load. With the aid of the Smith chart, the physical length of the stub and its distance from the load can be determined. The design procedure is to plot the normalised load impedance Z'_{L} on the Smith chart and transform it to the equivalent normalised load admittance Y'_{L}. To calculate the distance of the shunt stub from the load, draw the constant VSWR circle on the Smith chart and move along the circle from the load towards the generator until a normalised admittance of $Y' = 1 + jB$ is reached. Measure the guided wavelength λ_g between the two points to determine the variable d. The next step is to determine the length of the shunt stub, which should either be short or open-circuit at one end.

The shunt stub must have a normalised admittance of $Y' = 0 - jB$ to resonate out the $+jB$ susceptance component. Starting from the open or short circuit point on the outer edge of the Smith chart, move in a clockwise direction until a normalised input admittance point of $Y' = 0 - jB$ is reached. Measure the distance to the open or short circuit position point to get the stub length in λ_g. Using the operating frequency and dielectric constant of the substrate material, the length and width of the stub and its distance from the load can be determined in metric units.

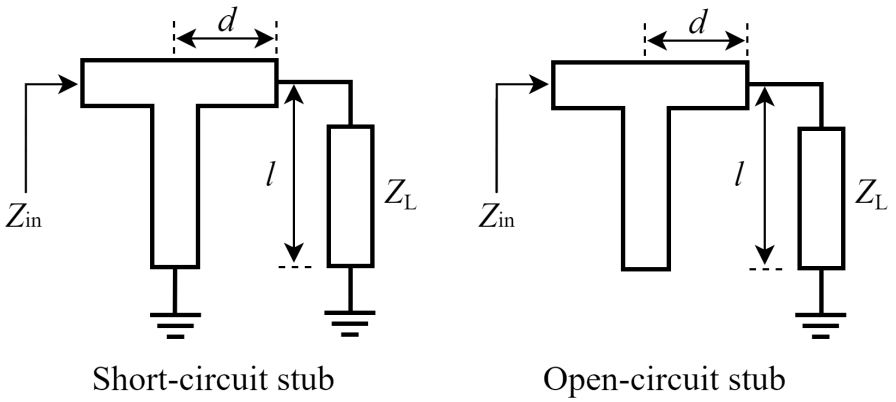

Figure 3.13: Open and short-circuited stub impedance matching

3.4.2.2 The quarter-wave Impedance Transformer

In the previous chapter, a quarter-wave ($\lambda_g/4$) impedance transformer connected in series with a MPA feed line was illustrated. The $\lambda_g/4$ transformer is a section of transmission line with a characteristic impedance Z_0' as illustrated in Figure 3.14. The characteristic impedance of the transformer is determined by the real impedance of the source connected to its input port and the load which is connected to its output port. The characteristic impedance of the transformer, connected between a source and load impedance, is given by:

$$Z_0' = \sqrt{Z_S Z_L} \qquad \Omega \tag{3.12}$$

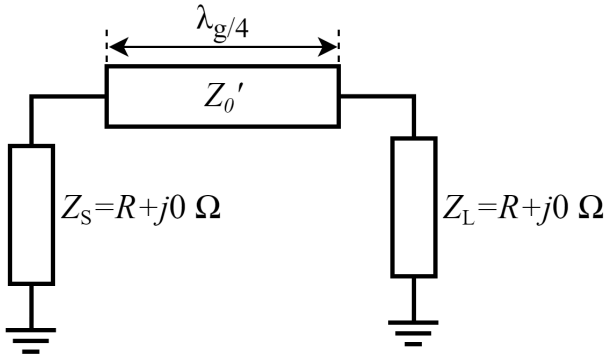

Figure 3.14: Quarter-wave impedance transformer

This section presented the implementation of passive elements in impedance matching networks. The next section will describe non-Foster reactive elements, which are realised with active devices.

3.5 Active non-Foster Impedance Circuits

Non-Foster impedances are realised with an active negative impedance converter (NIC) circuit. Active device selection can either be bipolar junction transistors or operational amplifiers. As presented in the previous chapter, the input impedance of an antenna is a function of its radiation resistance, ohmic loss resistance and reactance. The magnitude of the input reactance of the antenna becomes greater than its radiation resistance as the antenna size is reduced below its resonant frequency. This results in a very narrow input return loss bandwidth, due to the high radiation Q-factor of the antenna. High reactive energy is stored in the near-field region of the antenna and very little real power is propagated into the far-field (Oraizi and Hashemi, 2013). Non-Foster impedances are very useful to implement in wide-band input impedance matching networks for electrically-small antennas. With passive impedance matching techniques, limitations are imposed on the gain-bandwidth theories of Bode, Fano and Youla (Tade, 2014: 54); (Sussman-Fort and Rudish, 2009: 2230). By introducing non-Foster impedances in an impedance matching network, the limitations imposed by the gain-bandwidth theories are greatly reduced.

Impedance matching with non-Foster impedances requires equal reactive elements with inverse reactance slopes. Figure 3.15 is an example of two opposite capacitive reactances. The reactance with a negative slope is realised with an ideal NIC and capacitor. The summation of the positive and negative reactances are zero at all frequencies, resulting in a very wide return loss bandwidth. Practical NICs do not realise ideal negative inductances or capacitances at all frequencies. Bandwidth limitations do exist due to the parameters of the selected active devices and passive components within the NIC circuit.

NICs can be implemented to realise either a series or shunt non-Foster reactive element in an impedance matching network. These active circuits pose potential design challenges such as stability and linearity issues due to incorrect terminations and positive feedback within the circuit topology (Altuntaş, 2019: 4); (Elfrgani and Rojas, 2015: 50)

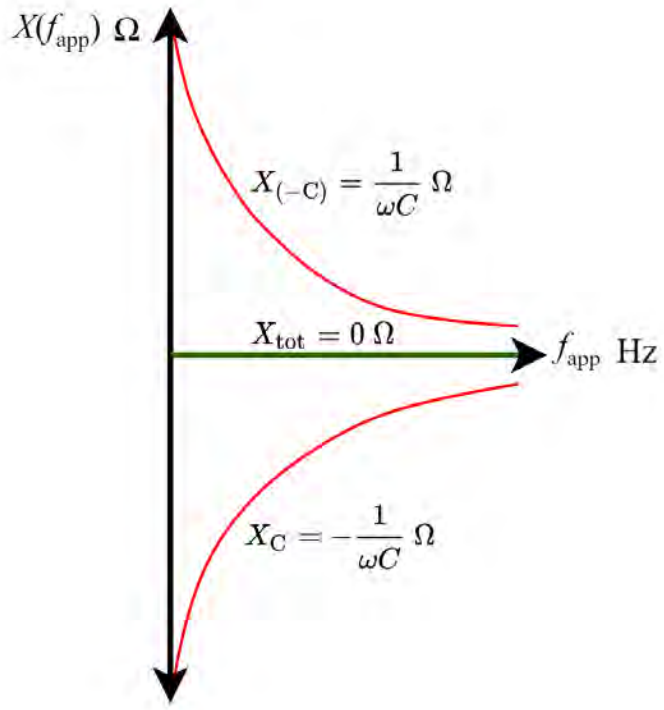

Figure 3.15: Positive versus negative capacitance reactances

The stability of these circuits are determined by the circuit topology, the internal and external load impedances, and the DC biasing of the active devices (Elfrgani and Rojas, 2015: 50).

For CubeSat applications, careful thought must be put into considering these circuits as a possible solution due to the additional power consumption. Figure 3.16 represents a coaxial fed MPA equivalent circuit, with non-Foster impedances in series and shunt to resonante out the reactive components of the antenna.

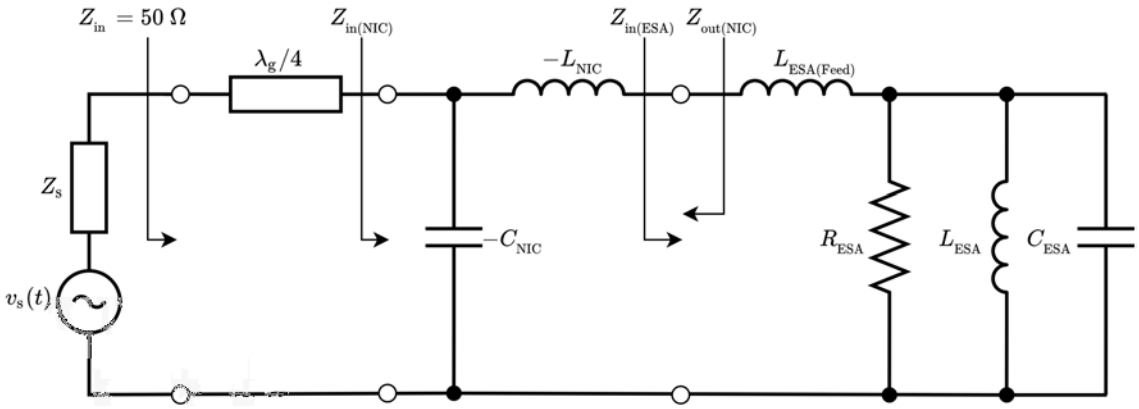

Figure 3.16: Equivalent circuit of coaxial fed antenna with negative reactive elements

3.5.1 Voltage Inversion and Negative Impedances

Transistor negative impedance converter circuits were first investigated and analysed by Linvill (1954) and Yanagisawa (1957). Figure 3.17 illustrates a NIC as a two-port network. The output port of the circuit is terminated in a passive load impedance Z_{L}. The impedance presented by the input port of the NIC will be the inverse of the passive load impedance termination, scaled by a negative transfer function coefficient k (Oraizi and Hashemi, 2013). This passive load termination is seen as the internal load of the NIC, which will be transformed to a negative impedance.

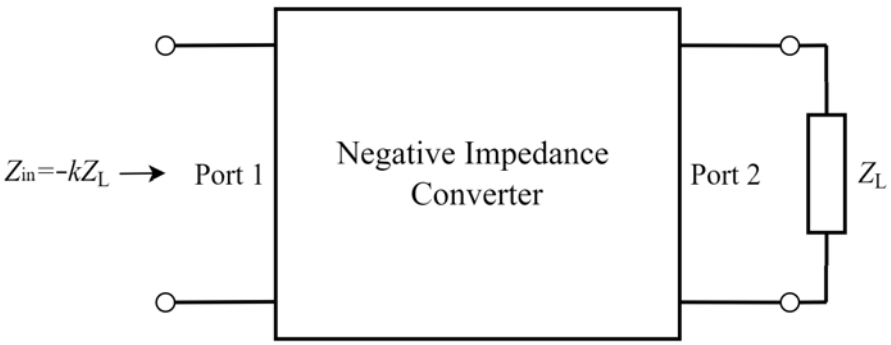

Figure 3.17: A NIC presented as a two-port network

The circuit can be either in a grounded or floating type of configuration to represent a non-Foster impedance element. The grounded NIC is implemented as a shunt element with the source impedance Z_{S} and external load impedance Z_{LEXT} as illustrated in Figure 3.18. The circuit configuration is said to be unbalanced.

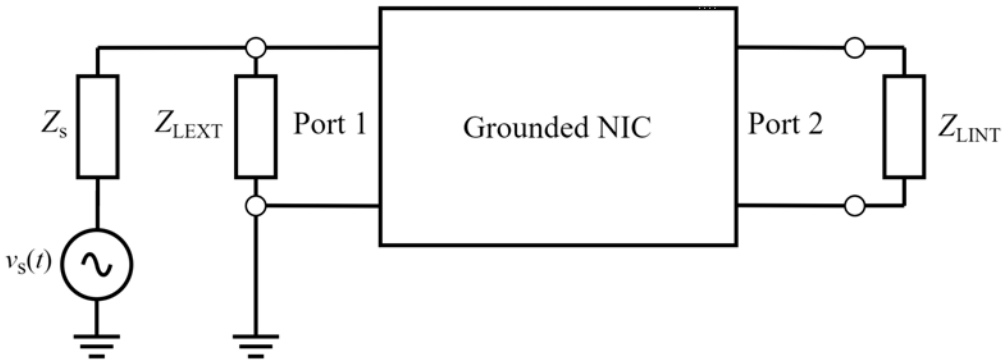

Figure 3.18: The grounded NIC as a shunt negative impedance element

The floating type NIC is implemented as a series element between the source impedance Z_{S} and the external load impedance Z_{LEXT} as illustrated in Figure 3.19. The circuit is in a balanced configuration (Jacob, 2016: 4997).

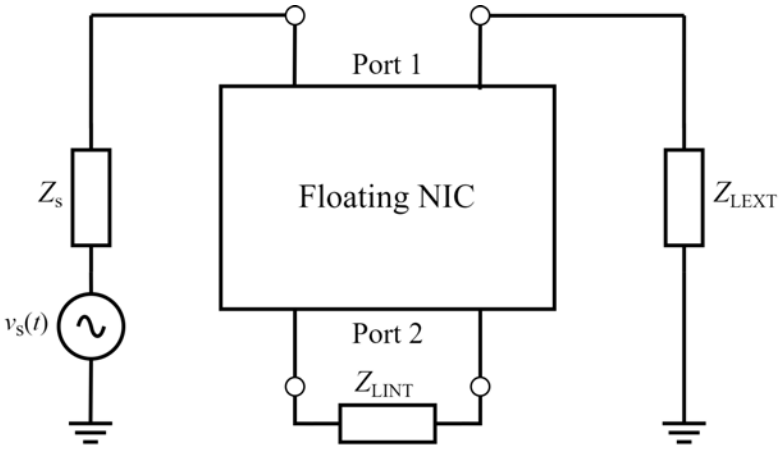

Figure 3.19: The floating NIC as a series negative impedance element

The NIC circuit realises a negative impedance at its input port by means of a voltage inversion between the signal at the input port and the signal across the internal load impedance Z_{LINT}. Figure 3.20 illustrates the voltage inversion within the grounded Linvill open-circuit stable NIC, with the assumption that ideal transistor models are used (Sussman-Fort, 2006: 12).

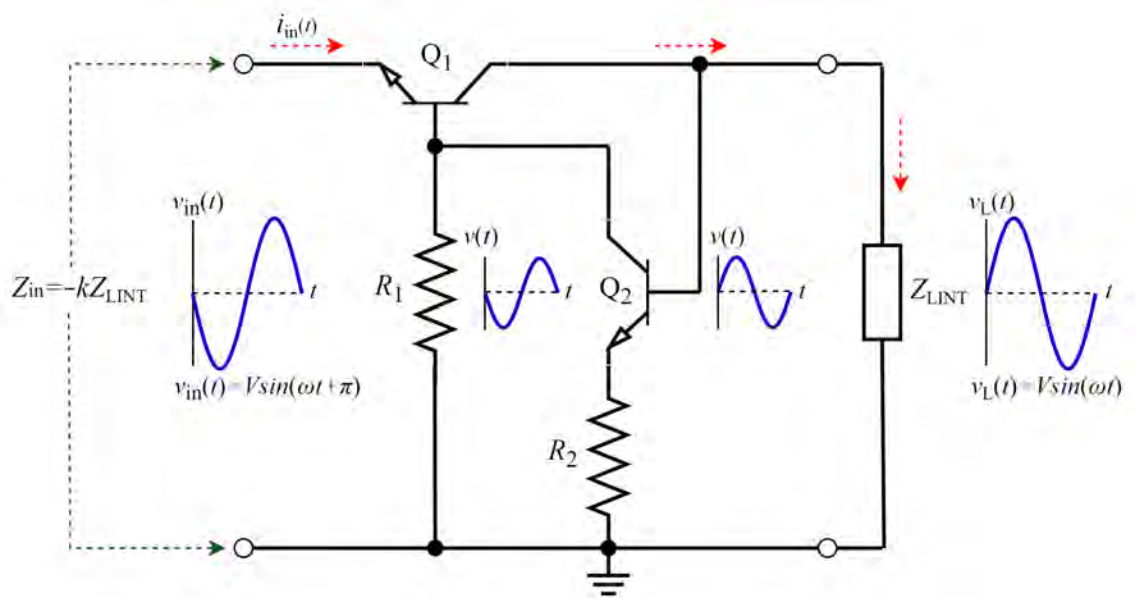

Figure 3.20: The grounded Linvill open-circuit stable NIC voltage inversion

A source is connected to the emitter of transistor Q_1. The input current from the source $i_{\mathrm{in}}(t)$ flows from the emitter to the collector and through the internal load impedance Z_{LINT}, creating a voltage drop $v_{\mathrm{L}}(t)$ across Z_{LINT}. The same signal is fed back to the base of transistor Q_2. Transistor Q_2 is in a common emitter configuration, which results in a 180° phase shift between the input signal at its base and the output signal across R_1 at its collector. The input impedance of the Linvill grounded NIC is given by:

$$Z_{\mathrm{in}} = \frac{v_{\mathrm{in}}(t)}{i_{\mathrm{in}}(t)} \qquad \Omega \tag{3.13}$$

$v_{\mathrm{in}}(t) = -v_{\mathrm{L}}(t)$ due to the 180° voltage phase shift within the circuit. Therefore:

$$Z_{\mathrm{in}} = -\frac{v_{\mathrm{L}}(t)}{i_{\mathrm{in}}(t)} = -Z_{\mathrm{LINT}} \qquad \Omega \tag{3.14}$$

The negative transfer function coefficient *k* is represented by the ratio of R_1 to R_2, which has a value greater than zero. The input impedance of the grounded Linvill NIC is given by:

$$Z_{\mathrm{in}} = -kZ_{\mathrm{LINT}} \qquad \Omega \tag{3.15}$$

where:

$$k = \frac{R_1}{R_2}\ ,\ \text{under the condition that k} > 0.$$

An NIC circuit will either be open-circuit or short-circuit stable, depending on the input and output port selection and load terminations. Brownlie and Hoskings investigated the stability of two-port NIC circuits and made the conclusion that one port must always be open-circuit stable and the other port short-circuit stable (Sussman-Fort and Rudish, 2009: 2232).

3.5.2 The Grounded Linvill Open-Circuit Stable NIC

A two-port NIC circuit is said to be open-circuit stable by terminating port 2 in a passive load impedance Z_{LINT}, while maintaining port 1 open-circuit. Figure 3.21 illustrates the grounded Linvill NIC in an open-circuit stable configuration, terminated in a passive load impedance Z_{LINT}. The emitter of transistor Q_1 represent the input port of the NIC circuit and the collector connected to the base of transistor Q_2 the output port. For the circuit to be open-circuit stable, the magnitude of the input impedance must be less than or equal to the source impedance connected to the input port.

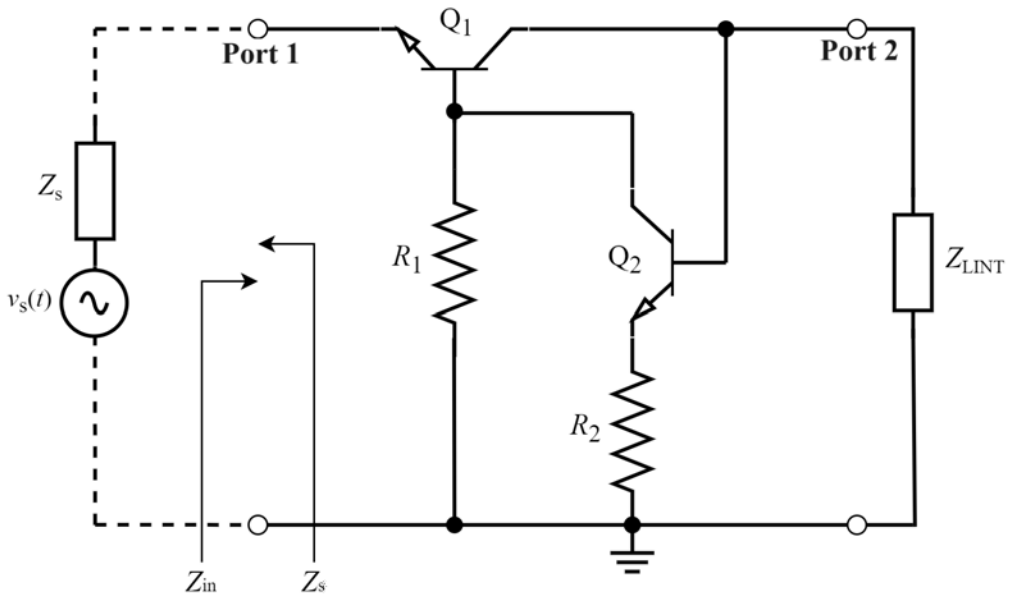

Figure 3.21: The grounded Linvill open-circuit stable NIC circuit

The input impedance of the grounded Linvill NIC in an open-circuit stable configuration is given by:

$$Z_{\text{in}} = -\frac{R_1}{R_2} Z_{\text{LINT}} \qquad \Omega \tag{3.16}$$

3.5.3 The Grounded Linvill Short-Circuit Stable NIC

The short-circuit stable NIC is a two-port network with port 1 terminated in a load impedance Z_{LINT}, with port 2 short-circuited. The collector of transistor Q_1 and base of transistor Q_2 represents the input port and the emitter of transistor Q_2 the output port. For the circuit to be short-circuit stable, the magnitude of the input impedance must be greater than or equal to the source impedance connected to the input port.

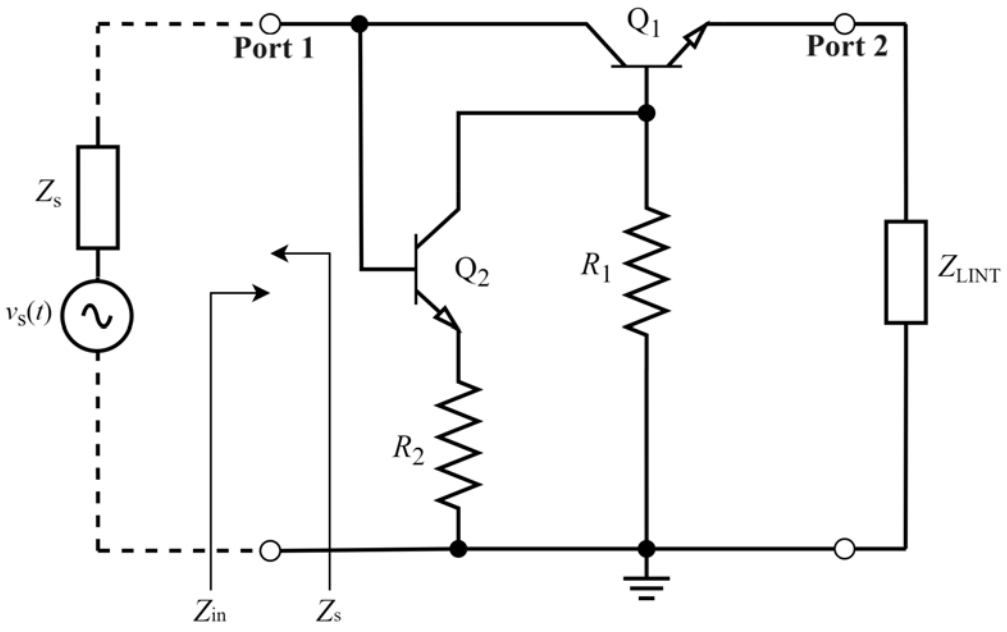

Figure 3.22: The grounded Linvill short-circuit stable NIC circuit

Figure 3.22 illustrates the short-circuit stable NIC circuit. The input impedance of the grounded Linvill NIC in a short-circuit stable configuration is given by:

$$Z_{\text{in}} = -\frac{R_2}{R_1} Z_{\text{LINT}} \qquad \Omega \tag{3.17}$$

3.5.4 The Floating Linvill Negative Impedance Converter

The floating Linvill NIC is implemented when a series negative impedance element is required. The grounded NIC configuration has one input terminal connected to the signal source and external load termination, which puts the NIC circuit in shunt, with the second input terminal connected to AC ground. The floating configuration has one input terminal connected to the source and the second input terminal connected to the external load impedance. The circuit consists of two NPN bipolar junction transistors connected to an internal load impedance Z_{LINT} (Oraizi and Hashemi, 2013). The input impedance of the NIC circuit is available between the emitters of transistors Q_1 and Q_2. This impedance is the inverse of the internal load impedance scaled by a negative transfer function coefficient of one.

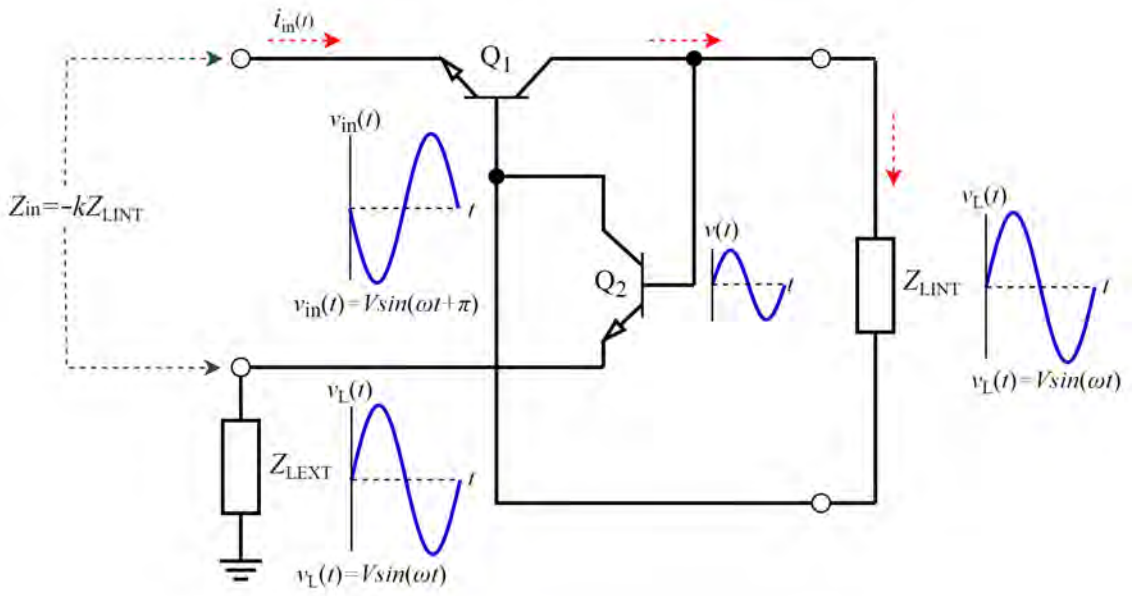

Figure 3.23: The floating Linvill open-circuit stable NIC voltage inversion

The voltage inversion within the circuit is illustrated in Figure 3.23. For this explanation, it is assumed that ideal transistor models are used. As a series negative impedance element, the emitter of transistor Q_1 is connected to a source and the emitter of transistor Q_2 to an external load impedance Z_{LEXT}. The source current $i_{\mathrm{in}}(t)$ flows from the emitter to the collector of transistor Q_1 and through the internal load impedance. A voltage drop $v_{\mathrm{L}}(t)$ is created across Z_{LINT} and this signal is fed back to the base of transistor Q_2. The signal is phase shifted by 180° at the collector of transistor Q_2 due to the common emitter configuration of the transistor, resulting in a phase inversion at the input port of

the NIC circuit. The current $i_{\text{in}}(t)$ flows through Z_{LINT} and from the collector to emitter of transistor Q_2 into Z_{LEXT}. Assuming that Z_{LINT} and Z_{LEXT} are equal impedances, the voltage drop across both impedances are the same.

The input impedance presented by the input port of the NIC circuit is the inverse of Z_{LINT} and Z_{LEXT}, which is given by:

$$Z_{\text{in}} = -kZ_{\text{LINT}} \qquad \Omega \tag{3.18}$$

where $k = 1$, under the condition that $k > 0$. Equation 3.6 transforms to:

$$Z_{\text{in}} = -Z_{\text{LINT}} \qquad \Omega \tag{3.19}$$

3.5.5 Bipolar Junction Transistors in Practical NIC Circuits

The use of NPN BJTs in a common emitter feedback configuration to perform voltage phase inversion across an interal load, was presented in the previous subsections. The circuit analysis was based on the operation of an ideal BJT, hence the effect of parasitic elements were not considered. Designing NICs to operate at microwave frequencies are challenging. The effect of parasitic capacitances and inductances within the transistor package becomes significant, which limits the linearity of the circuit's negation coefficient.

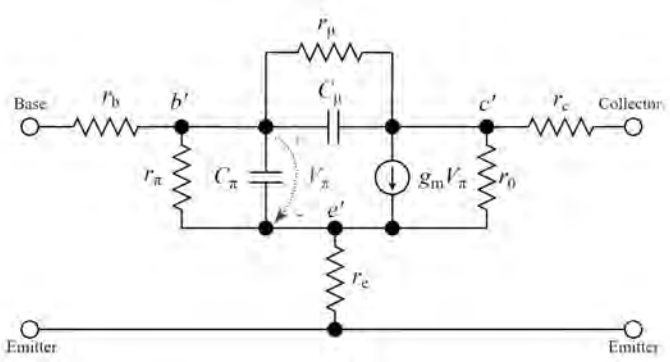

Figure 3.24: NPN BJT hybrid-Pi model

Figure 3.24 is the hybrid-Pi model of a NPN BJT (Ludwig, 2000: 376). This model is used to analyse BJT transistor circuits. The detailed analytical analysis of a NIC circuit

are not significant for the research, as the analysis and behaviour of such a circuit can be simulated in ADS.

3.5.6 Transmit Antenna Considerations

Impedance matching with NICs requires some careful thought when the circuit is implemented at the front-end of a high power transmitter. The NIC circuits presented in the previous subsections are operating in class A, which means the transistors are biased to be always on for one full cycle of the input signal. For high power transmit signals, the efficiency of these circuits operating in class A are poor. High DC bias currents are required for large input signals. Compared to a passive impedance matching network, an NIC circuit operating in class A is less efficient. NICs operating in Class B and Class C have been investigated in the literature and it was concluded that they offer a great improvement in efficiency (Sussman-Fort and Rudish, 2009: 2238).

3.5.7 Receive Antenna Considerations

A major design criterion for a radio receiver front-end is to obtain a low noise figure (NF) for optimal sensitivity. Any additional circuitry added to a receiver front-end will add to the overall NF of the receiver system (Sussman-Fort and Rudish, 2009: 2235). The NF of a two-port network is defined as the signal to noise power ratio at its output port to the signal to noise power ratio at its input port, measured in decibels (dB). Impedance matching of an electrically small MPA with an NIC, will seriously degrade the overall NF of a receiver system according to Friis' equation to an extent where optimal sensitivity can not be achieved.

3.6 Conclusions

In this chapter, an introduction to series and parallel resonant circuits was given. The Smith chart and its implementation as a tool to solve impedance matching and transmission line problems were illustrated. Narrow and wide-band impedance matching networks for electrically-small patch antennas were discussed. The conclusion is made that passive impedance matching networks produce a narrow to wider-band impedance match. NICs

with non-Foster impedances gives a great improvement in the bandwidth of the input return loss. The reliability of a NIC implemented on a CubeSat poses a potentional risk due to the stability issues, power handling capabilities, efficiency, noise characteristics and additional power consumption of this circuit. Table 3.1 is a summary of the impedance matching networks that were presented.

Table 3.1: Non-Foster and passive impedance matching networks summary

Non-Foster impedance circuits	**Passive impedance matching networks**
	L-matching network
Grounded Linvill OCS NIC	T-matching network
Grounded Linvill SCS NIC	Pi-matching network
Floating Linvill OCS NIC	Shunt stub
Floating Linvill SCS NIC	Series stub
	Quarter-wave impedance transformer

Impedance matching networks utilising passive elements are suitable to be integrated with an MPA. Negative impedance converters realising non-Foster elements are deemed to be less suitable.

Chapter 4

Electrically-Small Microstrip Patch Antenna Design and Impedance Matching

The design of four MPAs operating in the S-band are presented in this chapter. In the previous chapters, the literature was investigated to select which techniques are suitable to impedance match electrically-small MPAs. Two approaches were identified. Firstly, to impedance match the MPA with an external impedance matching network below its resonant frequency. Secondly, the implementation of minituarisation techniques in the antenna topology to lower its resonant frequency.

The first approach was implemented in the design of a coventional RHCP MPA without any miniaturisation. Then miniaturisation techniques were implemented in the design of a second, third and fourth antenna. Three antenna designs were constructed, tested and measured and a comparison was made between their performance parameters.

The radiating element radius should be less than the radius of one radian sphere, thus using equation 2.25, the circular radiating element must have a radius less than 23,291 mm at 2.05 GHz to be electrically-small.

4.1 Design Specifications

Table 4.1: MPA design specifications

Design parameters	**Requirements**
Centre frequency	2.05 GHz
System characteristic impedance	50 Ω
Input return loss	< -10 dB
VSWR	< 2
Gain	> 0 dB
Realised gain	> 0 dB
Polarisation	RHCP
Axial ratio	< 3 dB

The design specifications were obtained using the performance characteristics of the F'SATI SANT as reference. A circular radiating element was preferred to a rectangular shape. The circular shape is a more optimum fit in areas with limited space as in a CubeSat (Milligan, 2005: 313), has better performance and also enhances the concept of miniaturisation (Nkordeh, Idachaba and Oni, 2015). A coaxial feed was implemented to excite the antenna. An SMA female connector with a centre conductor diameter of 1.27 mm was utilised.

The following antenna characteristics were simulated: input return loss, the VSWR, gain, realised gain, axial ratio and efficiency. The FEKO simulation models of the various antenna designs are included in Appendixes A to D.

4.2 Substrate Properties

An FR4 substrate with a height of 3.765 mm and dielectric constant of 4.6 was selected as the base of the patch antenna topology. The selection of a thicker substrate enchances the input return loss bandwidth and also increases the miniaturisation of the radiating element to a certain degree compared to a thinner substrate. The selected layer stack-up is included in Appendix E.

4.3 Polarisation

The antenna will be utilised on an orbiting CubeSat in outer space, thus a circular polarised antenna was designed which will eliminate antenna orientation issues. A rectangular slot was embedded in the centre of each patch antenna to excite circular polarisation. The length and width of the slot was optimised in FEKO for an axial ratio below 3 dB at the frequency of operation.

4.4 Miniaturisation

Miniatursation techniques such as material loading, reshaping and the addition of a shorting pin to the antenna topology were selected as the most practical methods to be implemented. Hence, the manufacturing of the MPAs was less complex and the relatively low cost of the FR4 dielectric material resulting in a low cost MPA.

4.5 Electrically-Small Microstrip Patch Antenna Design

4.5.1 2.3 GHz Conventional RHCP MPA

This subsection presents the design of a conventional 2.3 GHz MPA with right-hand circular polarision. A design frequency of 2.3 GHz was chosen as it falls just outside the upper-frequency limit of the ITU downlink band, which can be lowered to resonate in the ITU uplink band. The antenna was matched to the source using an external impedance matching network for a lower resonant frequency as detailed in subsection 4.5.2. Miniaturisation techniques for a decreased resonant frequency were implemented on this antenna topology as detailed in subsections 4.5.3 - 4.5.5.

The MPA is designed to resonate in the lower order TM_{11} mode. In this mode, the radiating element dimension is the smallest compared to when higher resonant dominant modes are excited. Obtaining the substrate height (H), substrate relative dielectric constant (ϵ_{r}), resonant frequency (f_{r}) and X'_{11} = 1.8412, the effective radius (a_{eff}) of the radiating element was calculated using equation 2.14 as 17.821 mm.

Substituting the calculated effective radius into equation 2.15, an initial physical radius of 16.911 mm was calculated.

Figure 4.1: 2.3 GHz conventional patch antenna

An illustration of the conventional 2.3 GHz patch antenna is shown in Figure 4.1 and the calculated physical dimensions of this antenna are detailed in Table 4.2.

Table 4.2: Physical dimensions of 2.3 GHz conventional MPA

Parameter	**Value**	**Unit**
Substrate Height	3.765	mm
Substrate Length	53.942	mm
Substrate Width	53.942	mm
a	15.676	mm
L_s	13.800	mm
W_s	2.500	mm
Feed distance from centre	5.225	mm
Feed diameter	1.270	mm

A rectangular slot of 13.8 mm length was embedded into the centre of the antenna, which excited right-hand circular polarisation. The slot length was varied in FEKO, while its width was kept constant at 2.5 mm. The embedded slot was orientated at 45 degrees in an anti-clockwise direction relative to the feed position.

The radiating element radius was optimised to 15.676 mm after the slot was implemented to adjust the resonant frequency to exactly 2.3 GHz. Equations 2.19 to 2.23 were used to determine the resonant frequencies of the two orthogonal modes for a change in the surface area (ΔS) of the radiating element. The resonant frequency (f_0) of the antenna with the initial physical radius decreased slightly after the slot was implemented and the radiating element radius was optimised to counter the frequency shift. According to equations 2.22 and 2.23, the resonant frequencies of the two orthogonal modes are dependent on (f_0). The antenna was impedance-matched by positioning the feed one-third the radius of the antenna.

Using equation 2.16, the substrate length and width of the bottom ground plane was calculated as 53.942 mm.

The simulated performance parameters of this 2.3 GHz antenna are shown in Table 4.3.

Table 4.3: Simulated performance parameters of a 2.3 GHz conventional patch antenna

Parameter	**Value**	**Unit**
Input return loss	-28.807	dB
VSWR	1.1	
Gain	4.808	dBi
Realised Gain	4.797	dBi
Axial Ratio	2.98	dB
Efficiency	74.63	%
-10 dB return loss bandwidth	9.04	%

4.5.2 2.3 GHz MPA Impedance Matched to a source at an operating frequency of 2.05 GHz using a Passive L-Network

This subsection presents the design of a passive L-network to match the impedance presented by the input port of the conventioal 2.3 GHz MPA, as designed in subsection 4.5.1, to a 50 Ω source at 2.05 GHz. The L-network has a low Q-factor and is suitable when a wider input return loss bandwidth is required. ADS and FEKO were utilised to obtain simulated performance parameters.

The one-port S-parameter (.S1p) file of the input port of the antenna was obtained using a FEM simulation solver in FEKO. The .S1p file was imported into ADS and the input impedance obtained at 2.05 GHz. The normalised input impedance of the MPA was plotted on the Smith chart as shown in Figure 4.2. The normalised input impedance lies within the $Z = 1 + jX\ \Omega$ region, thus the L-matching network configuration 1 in Figure 3.8 was implemented.

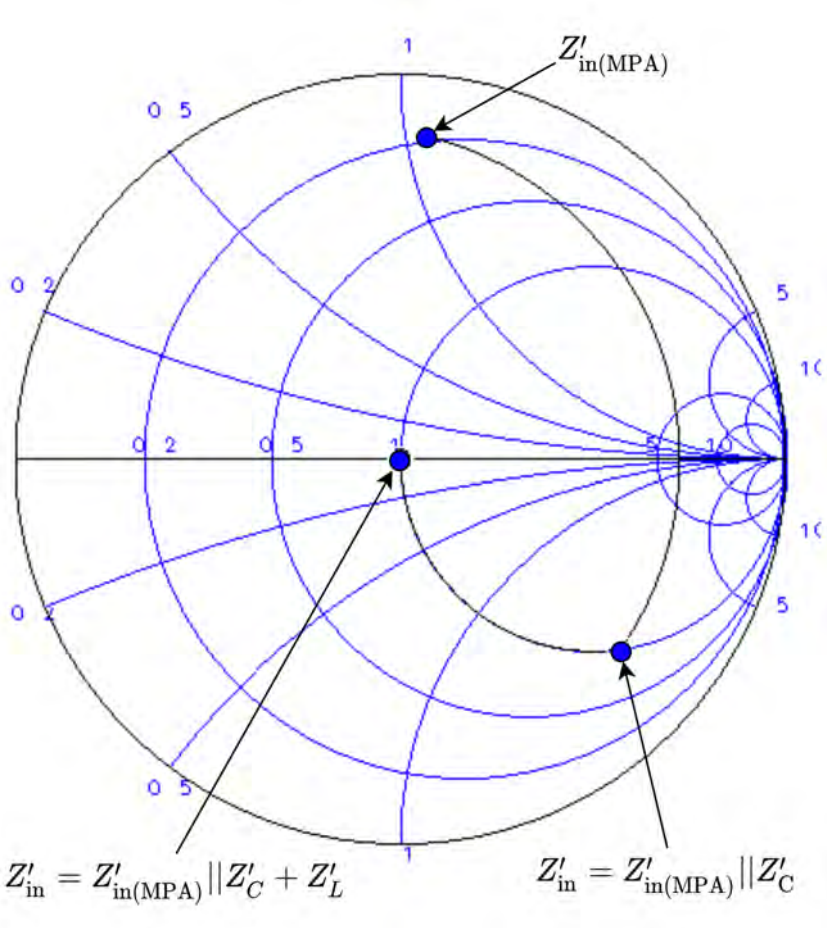

Figure 4.2: Normalised Z-plot on the Smith Chart to synthesize L-matching network

The Smith chart tool in ADS was utilised to determine the values of the series and shunt components. A shunt capacitor of 1.99 pF and a series inductor of 8.87 nH were obtained. The L-matching network is shown in Figure 4.3.

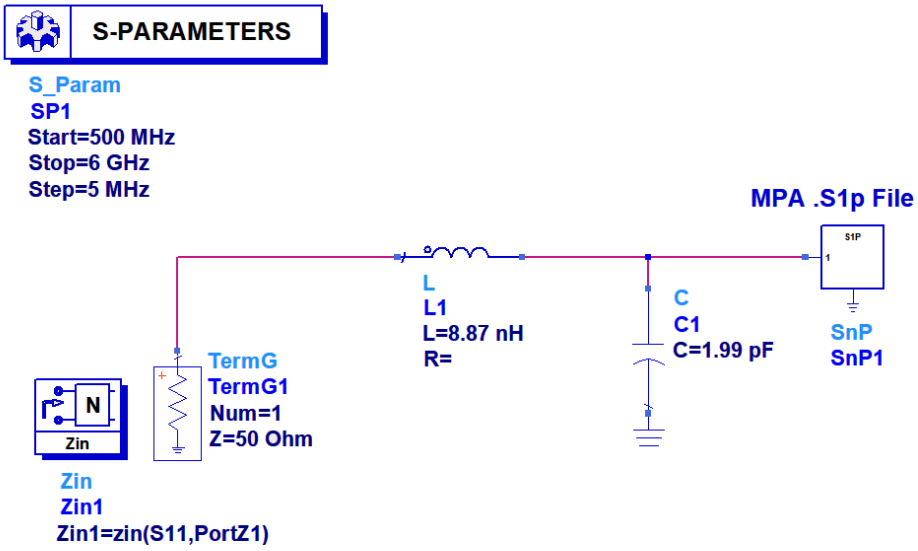

Figure 4.3: L-matching network

A two-port S-parameter simulation of the L-matching network was completed in ADS. The performance parameters were exported in a .S2p file, and which was then imported into a two-port network component generated in FEKO. This two-port component was inserted between the voltage source and the antenna input port in FEKO as illustrated in Figure 4.4. The MPA with the L-matching circuit was then simulated as a one-port network in FEKO.

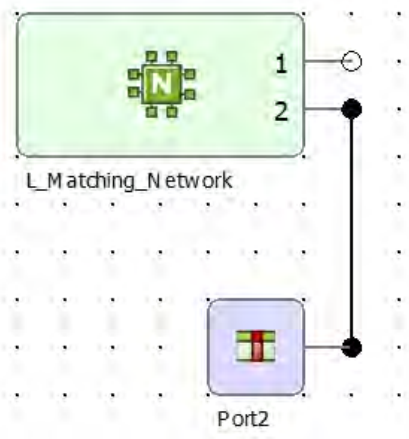

Figure 4.4: L-matching network connected to MPA in FEKO

The simulated performance parameters of the circuit illustrated in Figure 4.4 are shown in Table 4.4.

Table 4.4: Simulated performance parameters of L-matched MPA at 2.05 GHz

Parameter	**Value**	**Unit**
Return loss	-50.587	dB
VSWR	1.323	
Gain	4.047	dBi
Realised Gain	3.996	dBi
Axial Ratio	27.710	dB
Efficiency	68.93	%
$-$ 10 dB return loss bandwidth	2,43	%

4.5.3 Miniaturised 2.05 GHz MPA with Slits

The resonant frequency of the 2.3 GHz antenna designed in subsection 4.5.1 was reduced to 2.05 GHz by implementing four symmetric slits in the perimeter of the radiating element. The width of the slits was set at 2.5 mm and the length optimised to 9 mm. The radius of the radiating element were kept constant and the width and length of the slits varied to reduce the resonant frequency from 2.3 GHz to 2.05 GHz. The feed position was not altered and kept at one-third of the antenna radius. The axial ratio minimum decreased proportionally as the path length of the current was increased by implementing slits. Hence, this resulted in a reduction in the normal surface area of the radiating element. The length of the embedded slot was adjusted to 10.9 mm and its width to 1 mm to improve the axial ratio minimum at the resonant frequency. A simulated return loss of -18.646 dB indicating a very good impedance match.

The miniaturised 2.05 GHz MPA with symmetric slits is illustrated in Figure 4.5, and the calculated physical dimensions are shown in Table 4.5.

The simulated results of this miniaturised 2.05 GHz MPA are shown in Table 4.6.

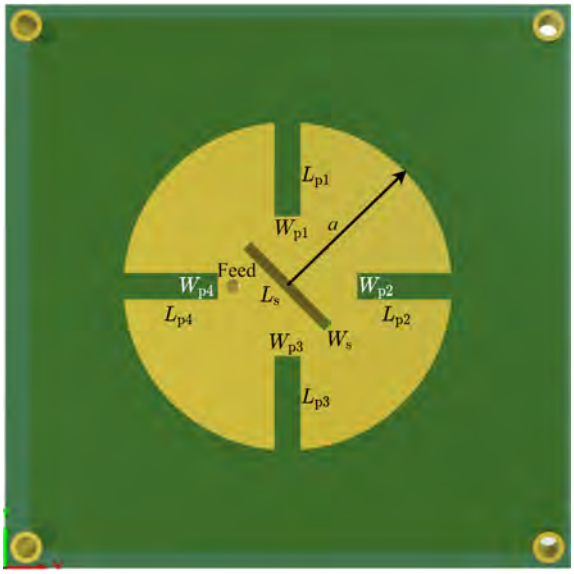

Figure 4.5: Miniaturised 2.05 GHz MPA with symmetric slits

Table 4.5: Physical dimensions of miniaturised 2.05 GHz MPA with slits

Parameter	**Value**	**Unit**
Substrate Height	3.765	mm
Substrate Length	53.942	mm
Substrate Width	53.942	mm
a	15.676	mm
L_{s}	10.9	mm
W_{s}	1.000	mm
L_{p1}	9.000	mm
W_{p1}	2.500	mm
L_{p2}	9.000	mm
W_{p2}	2.500	mm
L_{p3}	9.000	mm
W_{p3}	2.500	mm
L_{p4}	9.000	mm
W_{p4}	2.500	mm
Feed distance from centre	5.225	mm
Feed diameter	1.270	mm

Table 4.6: Simulated performance parameters of 2.05 GHz MPA with slits

Parameter	Value	Unit
Input return loss	−18.646	dB
VSWR	1.336	
Gain	3.747	dBi
Realised gain	3.588	dBi
Axial ratio	1.685	dB
Efficiency	61.87	%
−10 dB return loss bandwidth	4,43	%

4.5.4 Miniaturised 2.05 GHz MPA with Slits and Shorting Pin

A shorting pin was inserted near the feed location, between the feed point and the centre of the miniaturised antenna as designed in subsection 4.5.3. The short was implemented, with a pin of 0.9 mm diameter, and positioned at a distance of 3.575 mm from the centre of the radiating element, and 1.65 mm from the feed location. The diameter of the radiating element, the symmetrical slits, and the embedded slot dimensions were not altered. The motivation was to investigate if there is a further decrease in the resonant frequency without altering the antenna radius and to determine whether or not the input return loss and axial ratio were altered. The simulated performance parameters indicated that the antenna was resonant at 983 MHz and 2.167 GHz. The simulated input return loss was not optimal at 983 MHz and a good impedance match was not present.

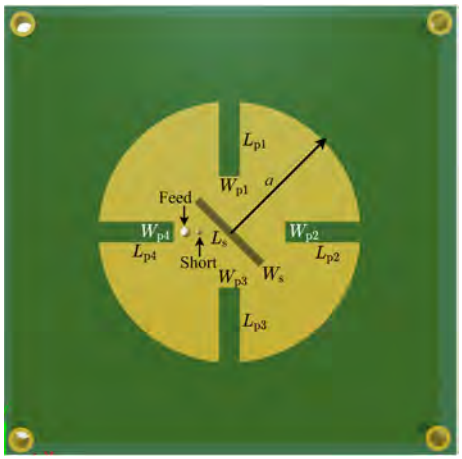

Figure 4.6: 2.05 GHz MPA with symmetric slits and shorting pin

An illustration of the miniaturised 2.05 GHz patch antenna with symmetric slits with the addition of shorting pin is shown in Figure 4.6. The calculated physical antenna dimensions are shown in Table. 4.7.

Table 4.7: Physical dimensions of 2.05 GHz MPA with slits and shorting pin

Parameter	**Value**	**Unit**
Substrate Height	3.765	mm
Substrate Length	53.942	mm
Substrate Width	53.942	mm
a	15.676	mm
L_{s}	10.9	mm
W_{s}	1.000	mm
L_{p1}	9.000	mm
W_{p1}	2.500	mm
L_{p2}	9.000	mm
W_{p2}	2.500	mm
L_{p3}	9.000	mm
W_{p3}	2.500	mm
L_{p4}	9.000	mm
W_{p4}	2.500	mm
Feed distance from centre	5.225	mm
Feed diameter	1.270	mm
Shorting pin diameter	0.900	mm
Shorting pin distance from feed	1.65	mm

The resulting simulated performance parameters at 983 MHz are shown in Table 4.8, and at 2.167 GHz in Table 4.9. The radius of the radiating element was not optimised to lower the second resonant frequency of this antenna from 2.167 GHz to 2.05 GHz. The simulations indicated that an increase in the radius was required to adjust the resonant frequency, or a shift in the position of the shorting pin relative to the feed location.

Table 4.8: 2.05 GHz MPA with slits and shorting pin simulated results at 983 MHz

Parameter	Value	Unit
Input return loss	−8.448	dB
VSWR	18.684	
Gain	−18.481	dBi
Realised gain	−19.181	dBi
Axial ratio	37.984	dB
Efficiency	40.81	%
−10 dB return loss bandwidth	0	%

Table 4.9: 2.05 GHz MPA with slits and shorting pin simulated results at 2.167 GHz

Parameter	Value	Unit
Input return loss	−12.287	dB
VSWR	1.657	
Gain	3.976	dBi
Realised gain	3.677	dBi
Axial ratio	21.161	dB
Efficiency	63.20	%
−10 dB return loss bandwidth	1,43	%

4.5.5 Miniature 2.05 GHz MPA

The miniaturised antenna designed in subsection 4.5.4 is resonant at 483 MHz and 2.167 GHz. The radius of the antenna and the dimensions of the slits were decreased to ascertain whether the lower resonant frequency of 983 MHz could be increased to 2.05 GHz. The initial embedded slot dimensions were too large for implementation in the reduced size radiating element, and therefore the width and length also had to be reduced. These interventions were investigated to ascertain whether or not an acceptable match could be achieved with the reduced size radiating element. The radius of the radiating element was reduced from 15.676 mm to 7.590 mm. This yields in a reduction in size of 51.58 %. The substrate length and width were reduced proportionally from 53.942 mm to 37.770

mm using equation 2.16. The resonant frequency increased from 983 MHz to 2.05 GHz which is exactly what was required. The position of the shorting pin was adjusted to be 1.2 mm from the feed location to ensure a good input return loss at the resonant frequency.

An illustration of the miniature 2.05 GHz MPA with slits and shorting pin is shown in Figure 4.7.

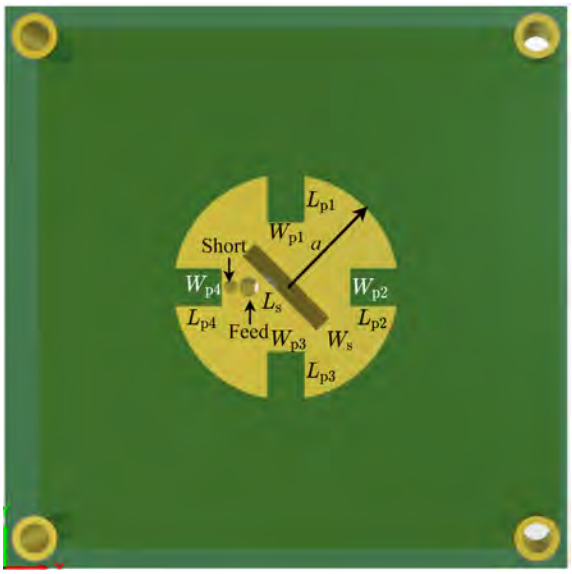

Figure 4.7: Miniature 2.05 GHz MPA with slits and shorting pin

The calculated physical dimensions are shown in Table 4.10 and the simulated performance parameters are shown in Table 4.11.

Table 4.10: Miniature 2.05 GHz MPA with slits and shorting pin dimensions

Parameter	Value	Unit
Substrate Height	3.765	mm
Substrate Length	37.770	mm
Substrate Width	37.770	mm
a	7.590	mm
L_{s}	7.000	mm
W_{s}	1.200	mm
L_{p1}	3.200	mm
W_{p1}	2.500	mm
L_{p2}	3.200	mm
W_{p2}	2.500	mm
L_{p3}	3.200	mm
W_{p3}	2.500	mm
L_{p4}	3.200	mm
W_{p4}	2.500	mm
Feed distance from centre	2.530	mm
Feed diameter	1.270	mm
Shorting pin distance from feed	1.200	mm
Shorting pin diameter	0.900	mm

Table 4.11: 2.05 GHz miniature MPA simulated results

Parameter	Value	Unit
Input return loss	-15.057	dB
VSWR	1.85	
Gain	-5.633	dBi
Realised Gain	-5.715	dBi
Axial Ratio	40	dB
Efficiency	19.00	%
-10 dB return loss bandwidth	1.17	%

4.6 Comparison of Simulated Results

The simulated input return losses of the five different antenna variants are shown in Figure 4.8. The 2.3 GHz antenna had a good input return loss at 2.3 GHz with a return loss bandwidth of 9.04 %. The same antenna impedance matched below its resonant frequency of 2.3 GHz with an external L-matching network at 2.05 GHz had an input return loss of −50.587 dB and return loss bandwidth of 2.43 %.

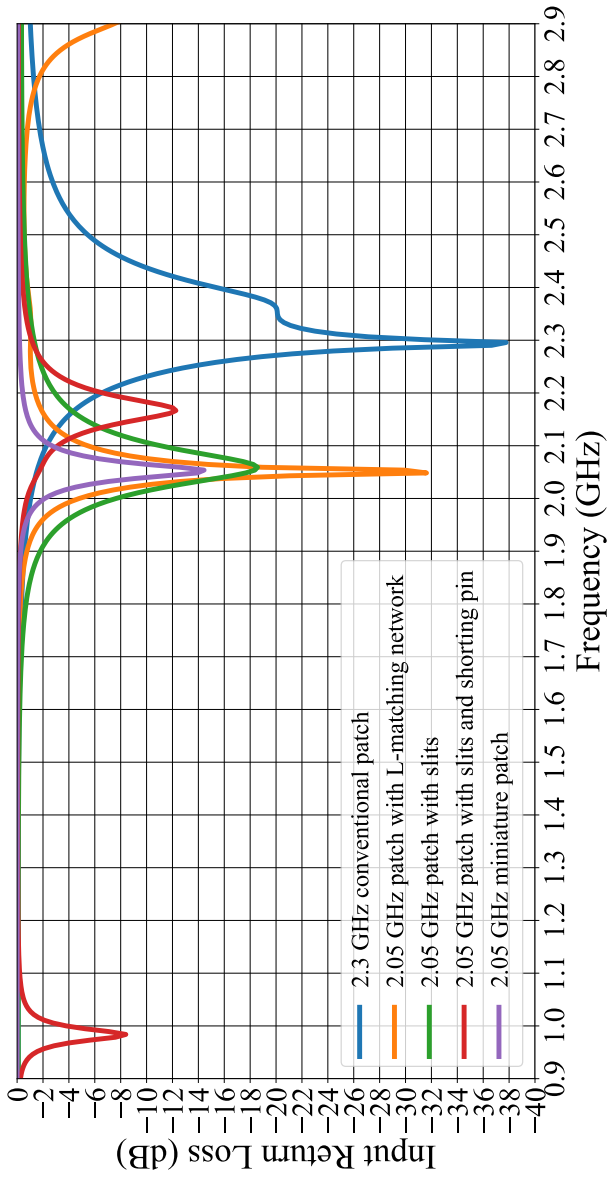

Figure 4.8: Comparison of simulated input return losses

The miniaturised antenna with slits in its perimeter had an input return loss of -18.646 dB and an increased input return loss bandwidth of 4.43 % compared to the L-matched antenna. The addition of a shorting pin resulted in resonance at 983 MHz and 2.167 GHz respectively. The miniature 2.05 GHz patch has a good impedance match with an input return loss of -15.057 dB at 2.05 GHz and return loss bandwidth of 1.17 %.

The voltage standing wave ratio of all three antennas that were impedance matched at 2.05 GHz, had a VSWR of less than 2. This indicates an acceptable impedance match between the source and the input port of the patch antennas, and which are all within specification.

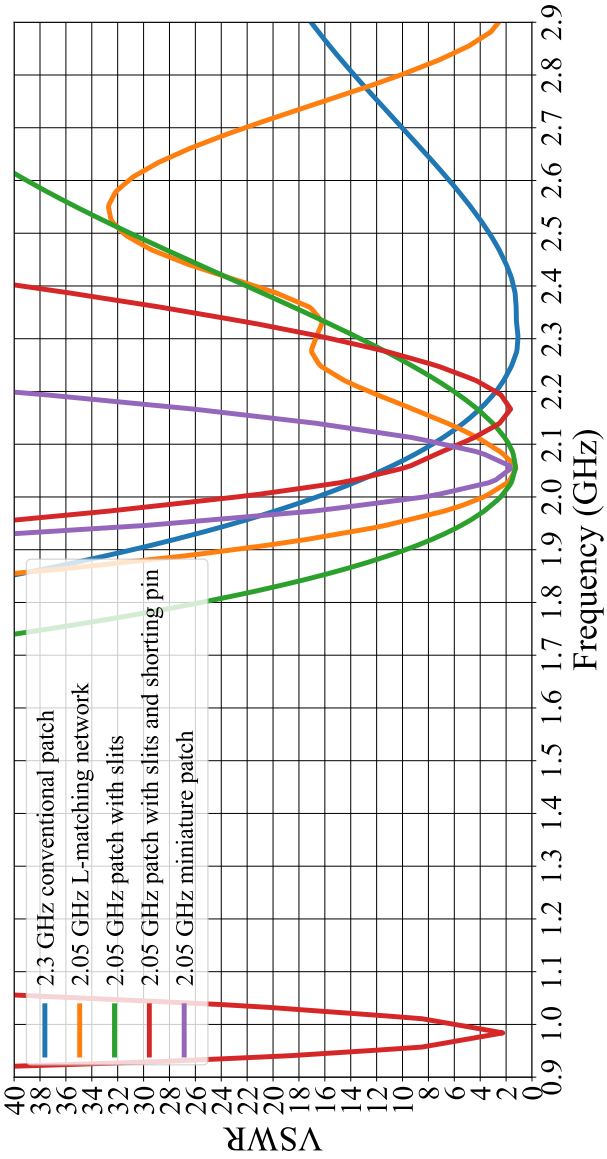

Figure 4.9: Comparison of simulated VSWRs

The simulated gain results shown in Figure 4.10 indicate that the antenna gain reduces for a decrease in the resonant frequency. The gain is also dependent on the electrical size of the antenna. The 2.05 GHz L-matched conventional antenna has exactly the same gain as

the conventional 2.3 GHz antenna without the external L-matching network. The antenna with the slits and shorting pin has more or less the same gain as the antenna which was miniaturised with the slits in its perimeter. The miniature 2.05 GHz patch antenna with a decreased radiating element size is electrically very small and has a simulated gain of less than 0 dBi at 2.05 GHz. The gain simulations proved that the electrical size of the miniature 2.05 GHz patch antenna is far below its $ka_{\min}$ value.

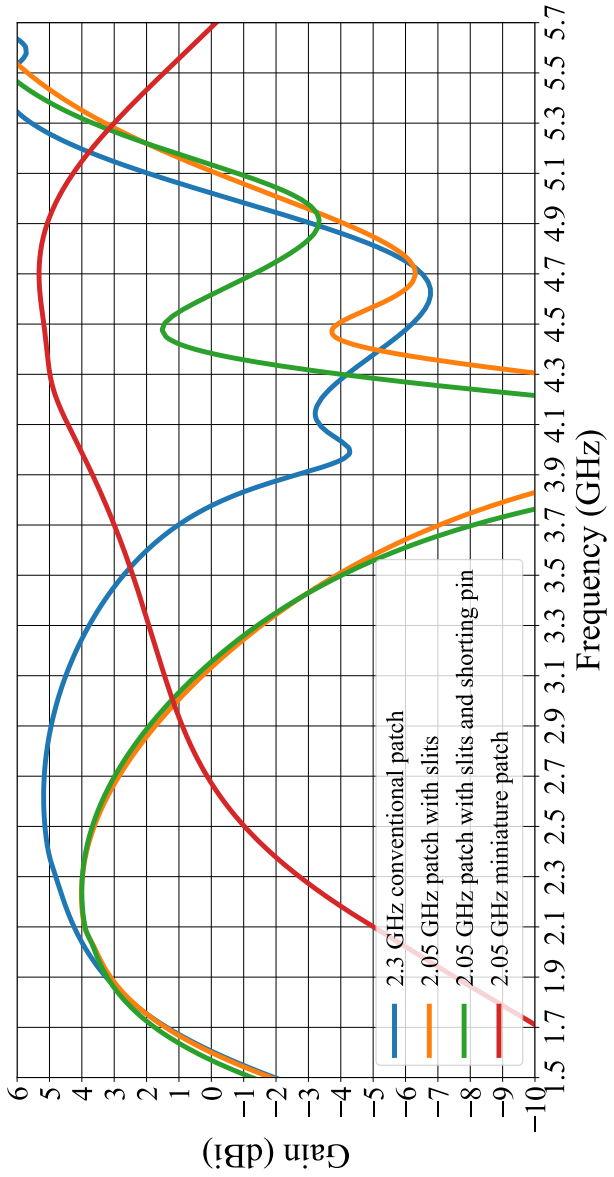

Figure 4.10: Comparison of simulated gains

The simulated realised gains of each antenna are shown in Figure 4.11. The simulated results indicates that the realised gain is dependent on the impedance match and includes the mismatch losses. The realised gain is a maximum at the frequency where the antenna has the best impedance match.

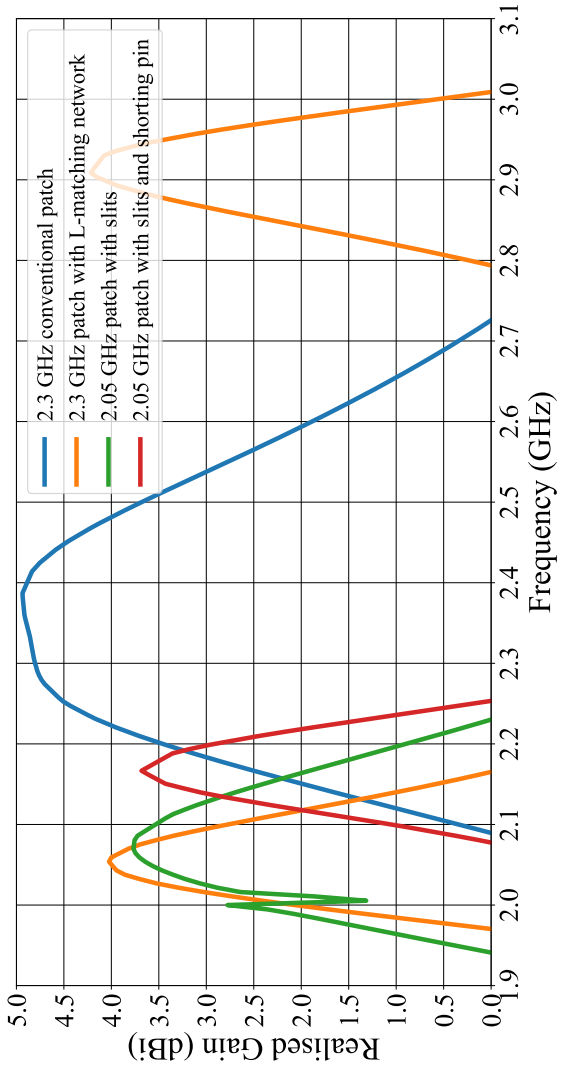

Figure 4.11: Comparison of simulated realised gains

The simulated axial ratio results of each antenna are shown in Figure 4.12. The 2.3 GHz conventional antenna has the same axial ratio with or without the external matching circuit. The axial ratio minimum changed proportionally with the resonant frequency when the antenna was miniaturised with the slits in its perimeter.

The miniature 2.05 GHz antenna with the reduced radiating element size is linearly polarised at 2.05 GHz, but is circular polarised at 4.35 GHz. The frequency of the axial ratio minimum and amplitude is a function of the dimensions of the embedded slot.

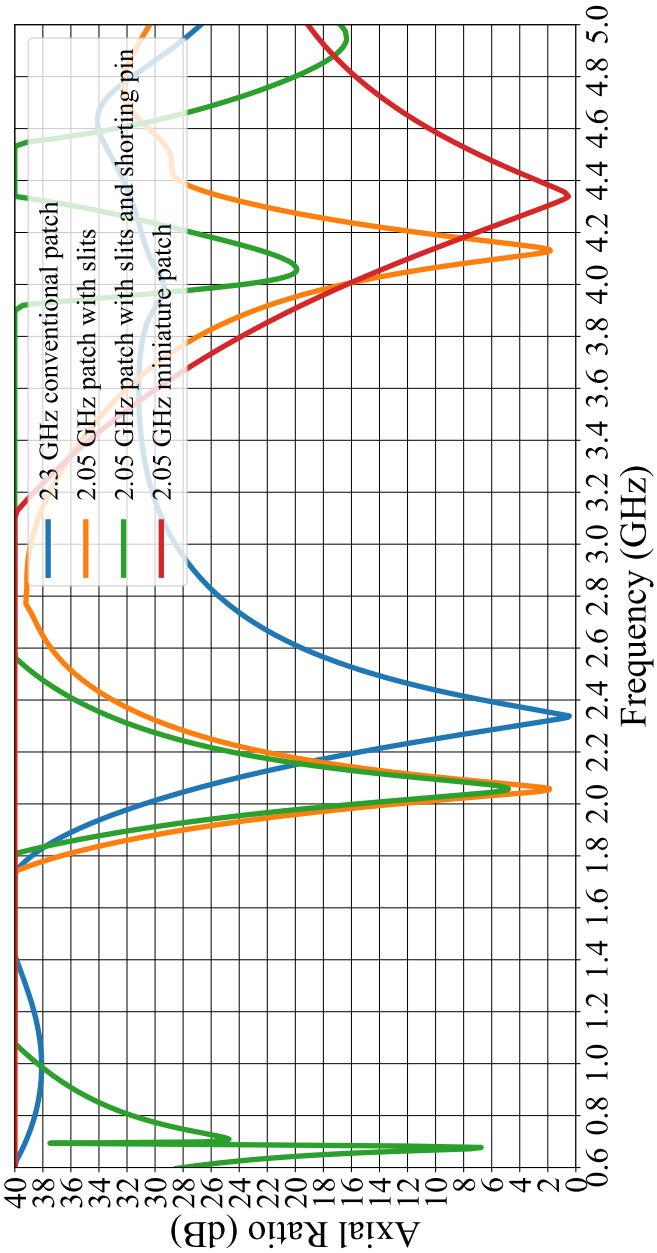

Figure 4.12: Comparison of simulated axial ratios

The simulated efficiencies of each antenna are shown in Figure 4.13. The simulated results indicate that the efficiency decreases as the electrical size of the antennas are decreased. The miniature 2.05 GHz patch has the lowest efficiency as well as the smallest electrical size when compared to the other antennas.

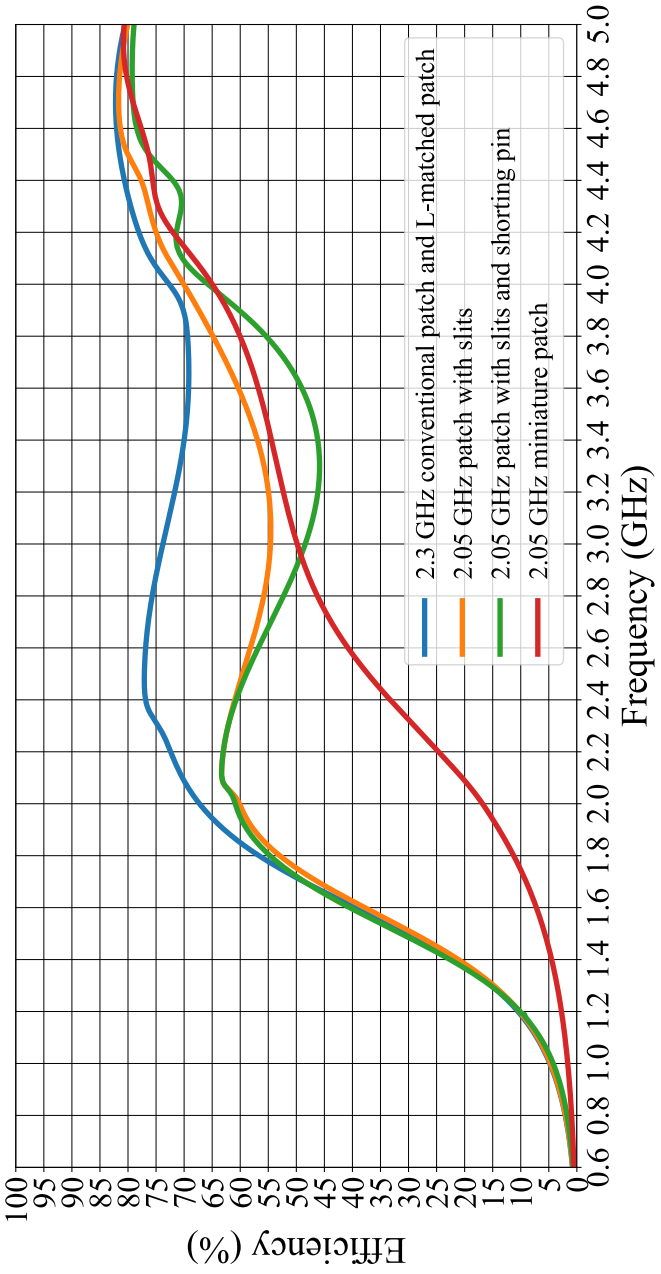

Figure 4.13: Comparison of simulated efficiencies

4.7 Conclusions

The design and simulation of three different electrically-small MPAs were presented. A L-configuration external impedance matching network was designed and implemented. Then appropiate miniaturisation techniques were applied to the antennas.

The simulations proved that as the electrical size of the MPAs was reduced, the input return loss bandwidths decreased and there was also a reduction in gain and efficiency. The axial ratio minima changed proportionally with the resonant frequency, when there was a change in the total surface area of the radiating element. The use of an external impedance matching network to match the input port of the antenna to the source at a lower resonant frequency gave a good impedance match, but had no effect on the axial ratio. The miniature antenna with symmetric slits and a shorting pin had a good impedance match at 2.05 GHz, but the efficiency was much lower and the axial ratio not at a minimum at 2.05 GHz.

The simulated results proved that a miniaturised MPA could be designed, built and tested with acceptable performance parameters. The simulated results indicated that the miniaturised patch antenna with slits gave a good trade-off between performance parameters and are suitable to be implemented on a CubeSat.

Chapter 5

The Constructed Antennas and Measured Results

5.1 Introduction

The very positive simulated results validated the actual construction of prototype antennas for testing and evaluation.

Three miniaturised protoype MPAs were designed and then manufactured by Icape Trax (PTY) LTD. Test and measurements were performed in the anechoic chamber at the University of Stellenbosch. The prototype antennas were assembled and measured to verify the success of the applied miniaturisation techniques on the antennas.

Section 5.2 presents the equipment and measurement setup used to evaluate the performance of the antennas. The measured results of each prototype antenna are presented and compared to simulated results.

5.2 Measurement Setup

An anechoic chamber is designed to have no reflections of EM waves and are also shielded from any outside EM interference.

The following equipment was used to complete the antenna measurements:

- Reference transmit antenna with a known gain value
- Agilent N5242A Vector network analyzer (VNA)
- Azimuth and elevation rotor
- Test cables
- 3U CubeSat test structure

A two-port calibration was performed on the VNA across the desired frequency range for response and transmission measurements. The correct distance (d) between the antenna under test (AUT) and the transmit antenna was measured, ensuring that the transmit antenna was in the AUT's far-field region. The fixed distance d was used in the measured gain calculations, with measurements obtained using the three antenna gain method. The azimuth and elevation rotor was used during the axial ratio measurements to rotate the AUT to a desired angle. An illustration of the measurement setup in the anechoic chamber is shown in Figure 5.1.

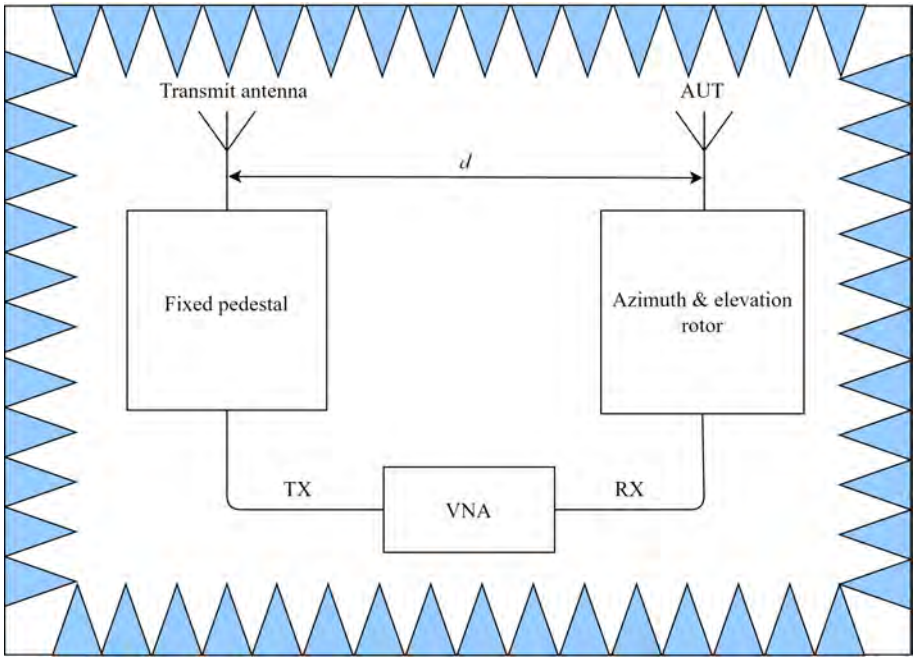

Figure 5.1: Measurement setup in the anechoic chamber

The following performance charcteristics were measured: input return loss, realised gain and the axial ratio. Figure 5.2 shows the mounting of the AUT on a 3U CubeSat test structure.

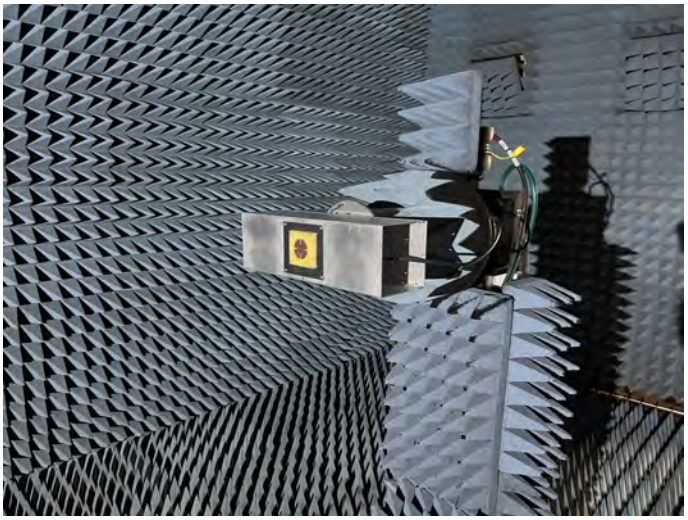

Figure 5.2: AUT mounted on a 3U CubeSat test structure

5.3 Constructed 2.05 GHz Miniaturised MPA with Slits

Figure 5.3 illustrates the constructed 2.05 GHz miniaturised MPA with slits.

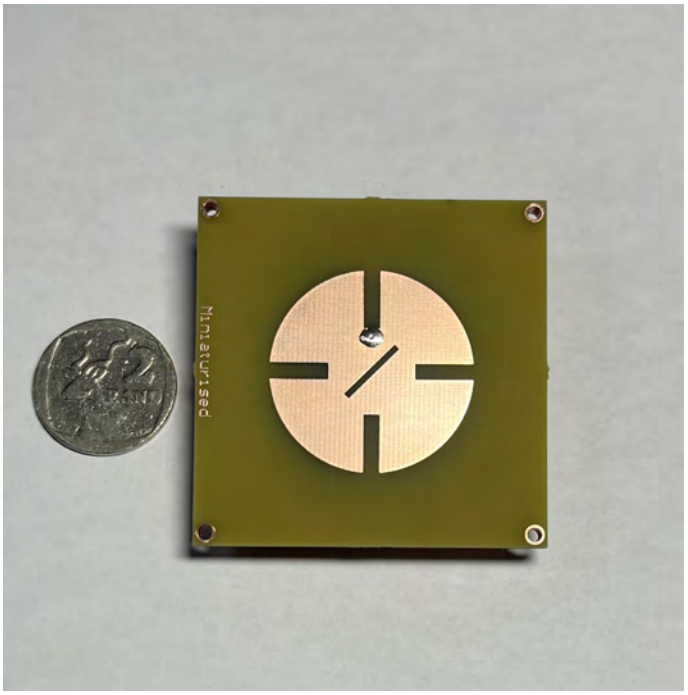

Figure 5.3: The constructed 2.05 GHz miniaturised MPA with slits

Figure 5.4 illustrates a comparison between the measured and simulated input return loss of the constructed antenna.

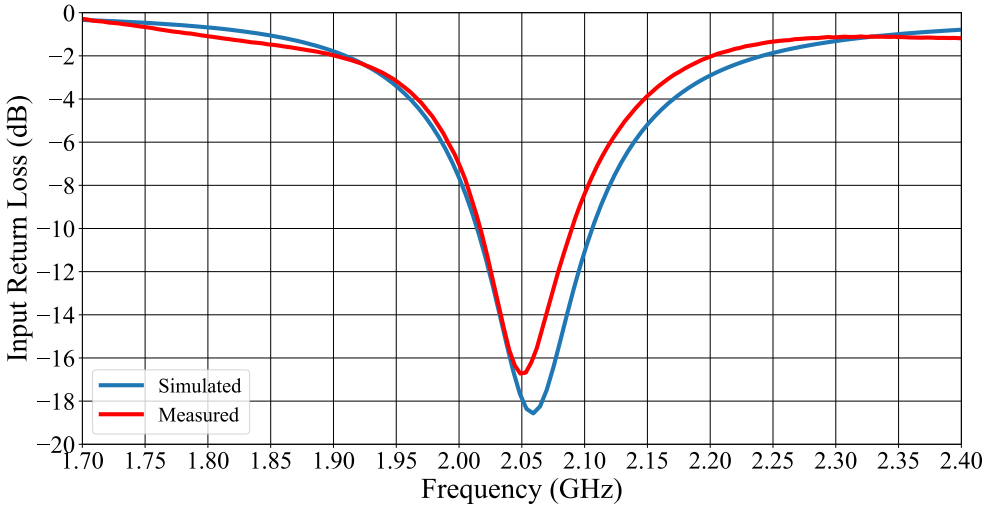

Figure 5.4: Simulated versus measured input return loss

The simulated versus measured realised gain is illustrated in Figure 5.5.

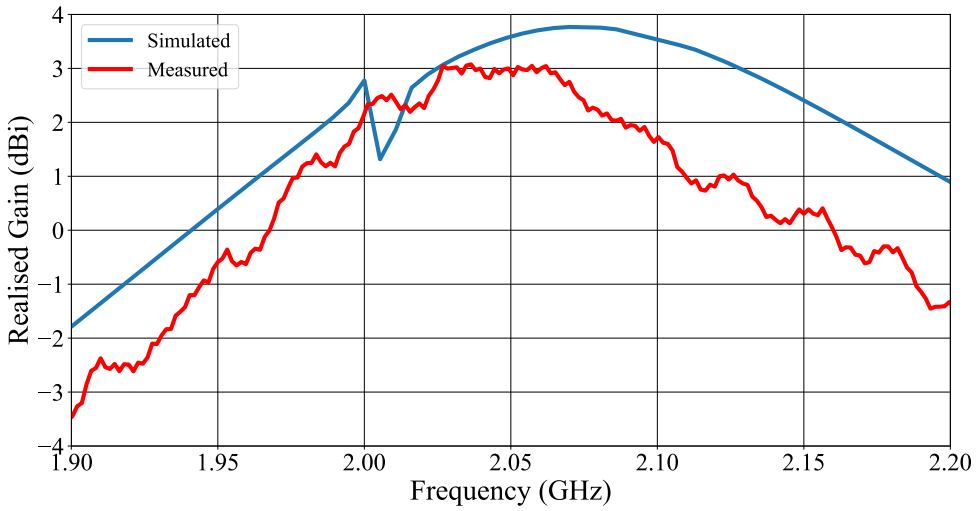

Figure 5.5: Simulated versus measured realised gain

The simulated and measured axial ratio are compared in Figure 5.6.

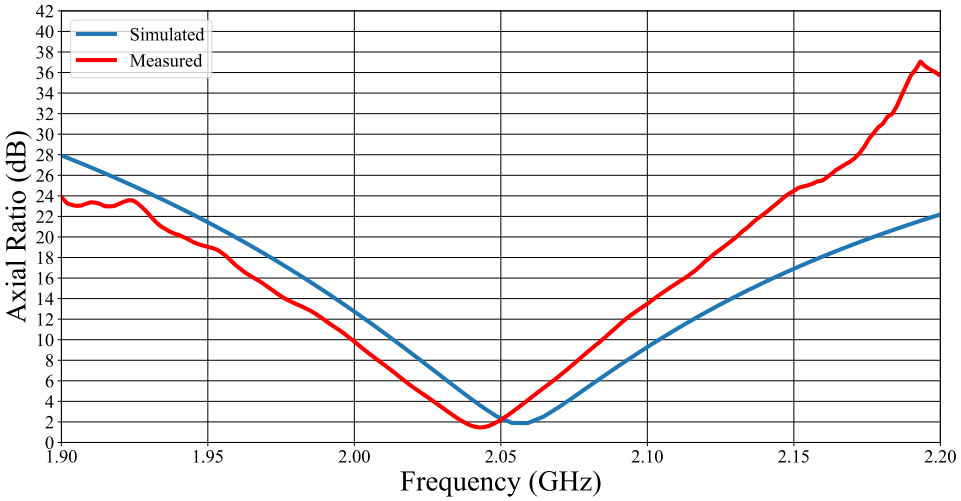

Figure 5.6: Simulated versus measured axial ratio

5.4 Constructed 2.05 GHz Miniaturised MPA with Slits and Shorting Pin

Figure 5.7 illustrates the constructed 2.05 GHz miniaturised MPA with slits and shorting pin.

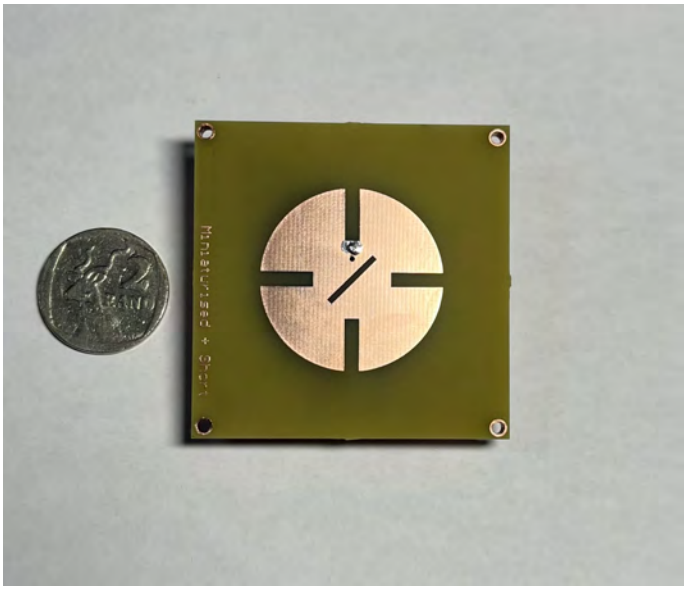

Figure 5.7: The constructed antenna

Figure 5.8 shows a comparison between the measured and simulated input return loss.

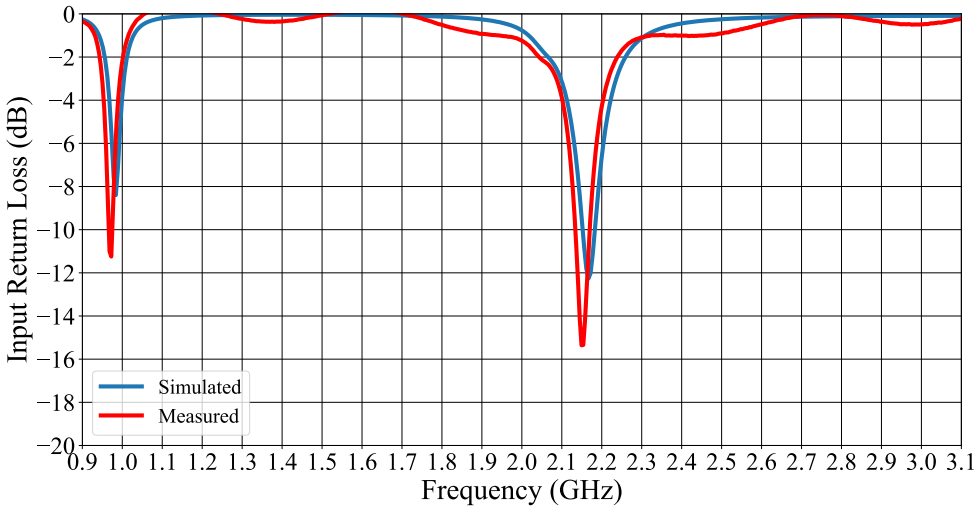

Figure 5.8: Simulated versus measured input return loss

Figure 5.9 shows a comparison between the measured and simulated realised gain.

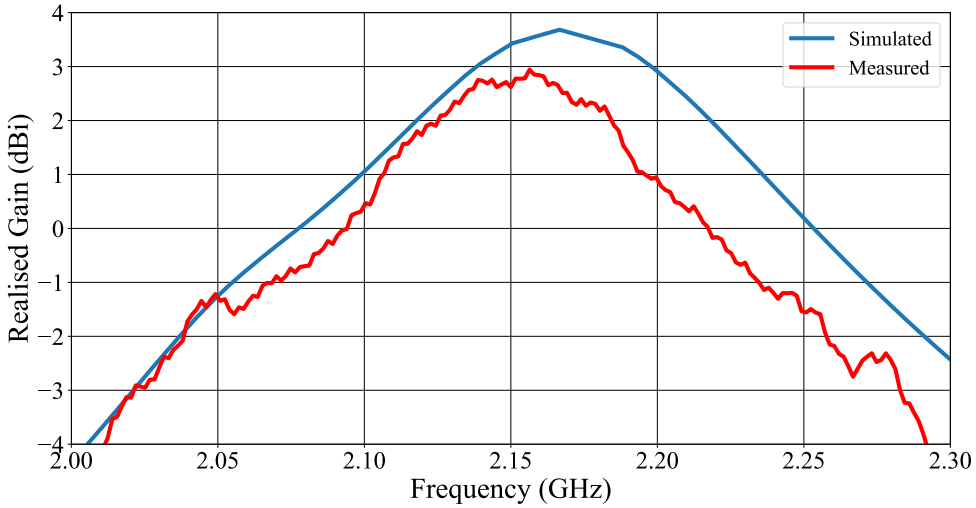

Figure 5.9: Simulated versus measured realised gain

Figure 5.10 shows a comparison between the measured and simulated axial ratio.

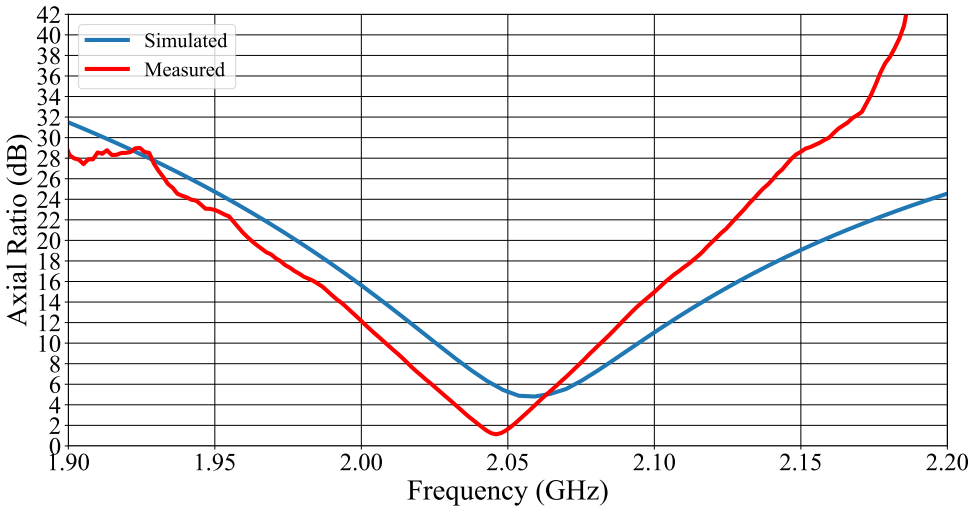

Figure 5.10: Simulated versus measured axial ratio

5.5 Constructed 2.05 GHz Miniature MPA with Slits and Shorting Pin

Figure 5.11 illustrates the constructed 2.05 GHz miniature MPA with slits and shorting pin.

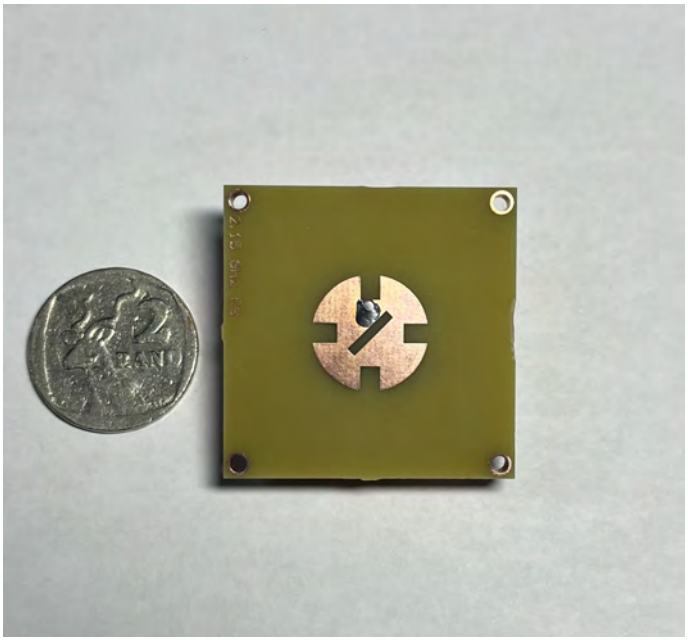

Figure 5.11: The constructed antenna

The realised gain was not measured because the simulated results indicated a loss at the

design frequency. However the input return loss could be measured indicating that a good input match was achieved. The axial ratio was not measured because the simulations indicated that the antenna was linearly polarised at the design frequency.

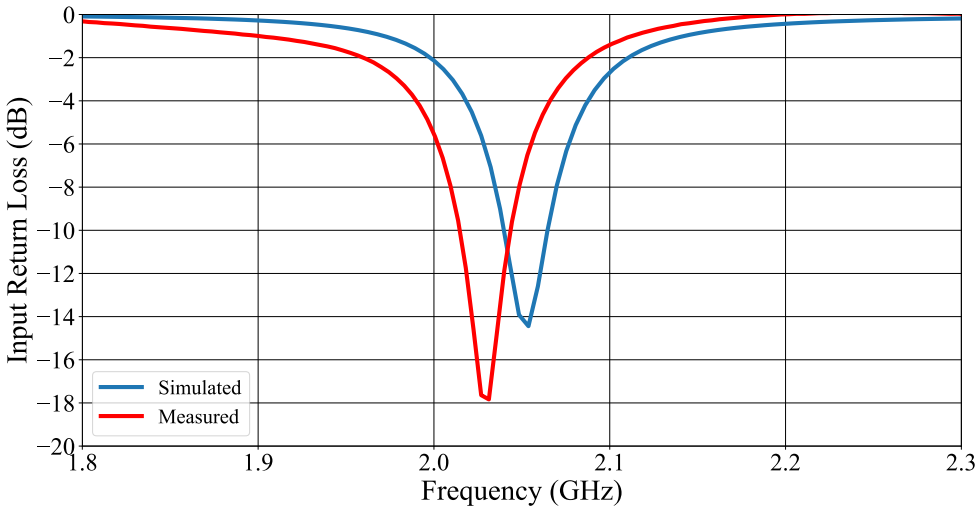

Figure 5.12: Simulated versus measured input return loss

5.6 Comparison of Performance Parameters

Table 5.1: Comparison of 2.05 GHz MPA with slits performance parameters

Design parameters	**Specified**	**Simulated**	**Measured**
Input return loss	< -10 dB	-18.646 dB	-16.678 dB
Realised gain	> 0 dBi	3.588 dBi	2.874 dBi
Axial ratio	< 3 dB	1.685 dB	2.351 dB

Table 5.2: Comparison of 2.05 GHz MPA with slits and shorting pin performance parameters at 2.167 GHz

Design parameters	**Specified**	**Simulated**	**Measured**
Input return loss	< -10 dB	-12.287 dB	-10.988 dB
Realised gain	> 0 dBi	3.677 dBi	2.5109 dBi
Axial Ratio	< 3dB	21.161 dB	31.902 dB

Table 5.3: Comparison of 2.05 GHz miniature MPA with slits and shorting pin performance parameters

Design parameters	Specified	Simulated	Measured
Input return loss	< -10 dB	-15.057 dB	-7.885 dB
Realised gain	$>$ 0 dBi	-5.715 dBi	Not measured
Axial ratio	$<$ 3 dB	40 dB	Not measured

5.7 Conclusions

The results in Table 5.1 show that all specified performance parameters were exceeded in both simulated and measured results, both of which correlated reasonably well. This miniaturised antenna with slits is suitable to be implemented on a CubeSat and a good trade-off between performance parameters were achieved.

The results in Table 5.2 clearly show the input return loss was acceptable at 2.167 GHz as was the realised gain. However, the simulated axial ratio did not correlate well with the measured result. This antenna was not optimised at 2.05 GHz with the objective to verify the effect of the shorting pin in practice.

The results in Table 5.3 show that some degree of input return loss was achieved, meaning that the antenna was slightly matched to the source. However, the realised gain and axial ratio were not measured due to the fact that the antenna had a gain of less than 0 dBi at the design frequency due to the high reduction in its electrical size. This antenna will only be suitable for a CubeSat if the electrical size of the radiating element is increased up to a point where acceptable gain can be achieved and also optimised to have a good axial ratio at the design frequency. A miniature radiating element can be well implemented in a phased array which will make it even more suitable for a CubeSat.

Chapter 6

Conclusions and recommendations

6.1 Final Conclusions

An electrically-small S-band patch antenna with a radiating element radius of 15,676 mm was designed, built and tested. The proposed topology of the patch antenna and the addition of symmetric slits in the radiating element perimeter provided acceptable miniaturisation and enabled the antenna to deliver an input return loss of -16.678 dB, a realised gain of 2.874 dBi and an axial ratio of 2.351 dB at an operating frequency of 2.05 GHz. All of the design specifications were exceeded, with the objective to achieve a good impedance match. A conventional MPA on the same substrate resonating at 2.05 GHz will have a radiating element radius of 19.051 mm without miniaturisation. Thus, a reduction in size of 17.715 % was achieved. The performance of this electrically-small antenna over the section of the S-band utilised for the communication system onboard a CubeSat makes it more than suitable for future CubeSat missions.

The implementation of an external impedance matching network with passive elements are suitable to match a conventional patch antenna below its resonant frequency. Depending on the axial ratio bandwidth, a circular polarised patch antenna with a single feed and externally matched to a lower resonant frequency will be linearly polarised at the lower resonant frequency. Non-Foster impedances realised with a NIC may be useful to achieve a wide-band input return loss. The challenges experienced with designing NIC circuits and the additional power consumption make them less suitable for a CubeSat.

The shorting pin method of miniaturisation proved to give a higher degree of miniaturisation compared to the addition of slits within the radiating element perimeter.

Miniaturisation techniques to decrease the resonant frequency and impedance match a patch antenna proved to be more effective than integrating the patch antenna with an external matching circuit. Since limited space is available on a CubeSat, it is more appealing that no additional circuitry be needed.

6.2 Recommendations

Modern communication systems use high data rate modulation schemes which generate wide bandwidth signals. It is recommended that a matching network with a wide input return loss bandwidth be used with this antenna to ensure that it can be utilised in modern communication systems.

It is also recommended that a substrate suitable for high-frequency applications be used to manufacture the antenna. This will ensure a more stable dielectric constant. Low cost FR4 substrate was just used for prototyping and the prove of concept.

6.3 Future Work

More studies need to be conducted into the implementation of more suitable feed networks which will provide optimum matching and input return loss bandwidth.

In addition methods to optimise antenna gain, directivity and beamwidth need to be investigated to enchance the overall performance of the communication system onboard a CubeSat.

Appendix A

2.3 GHz Conventional Patch Antenna FEKO Model

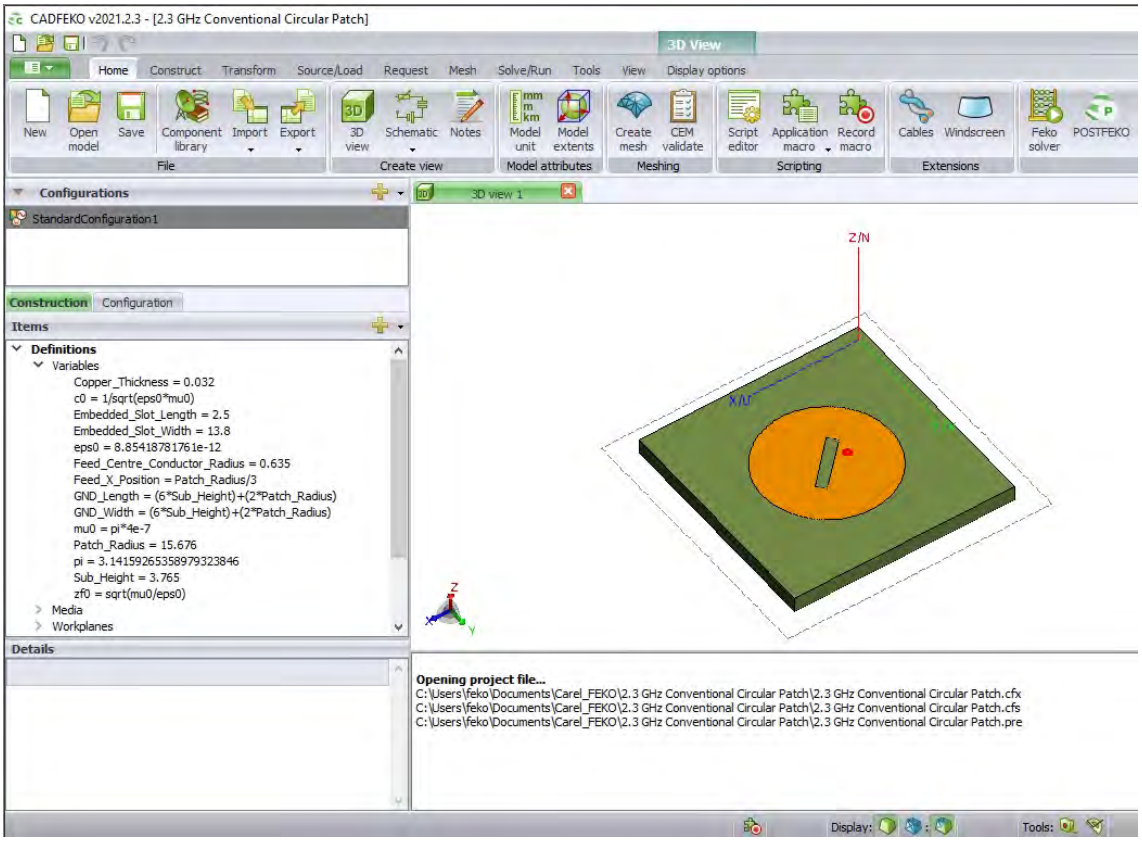

Appendix B

2.05 GHz Miniaturised Patch Antenna with Slits FEKO Model

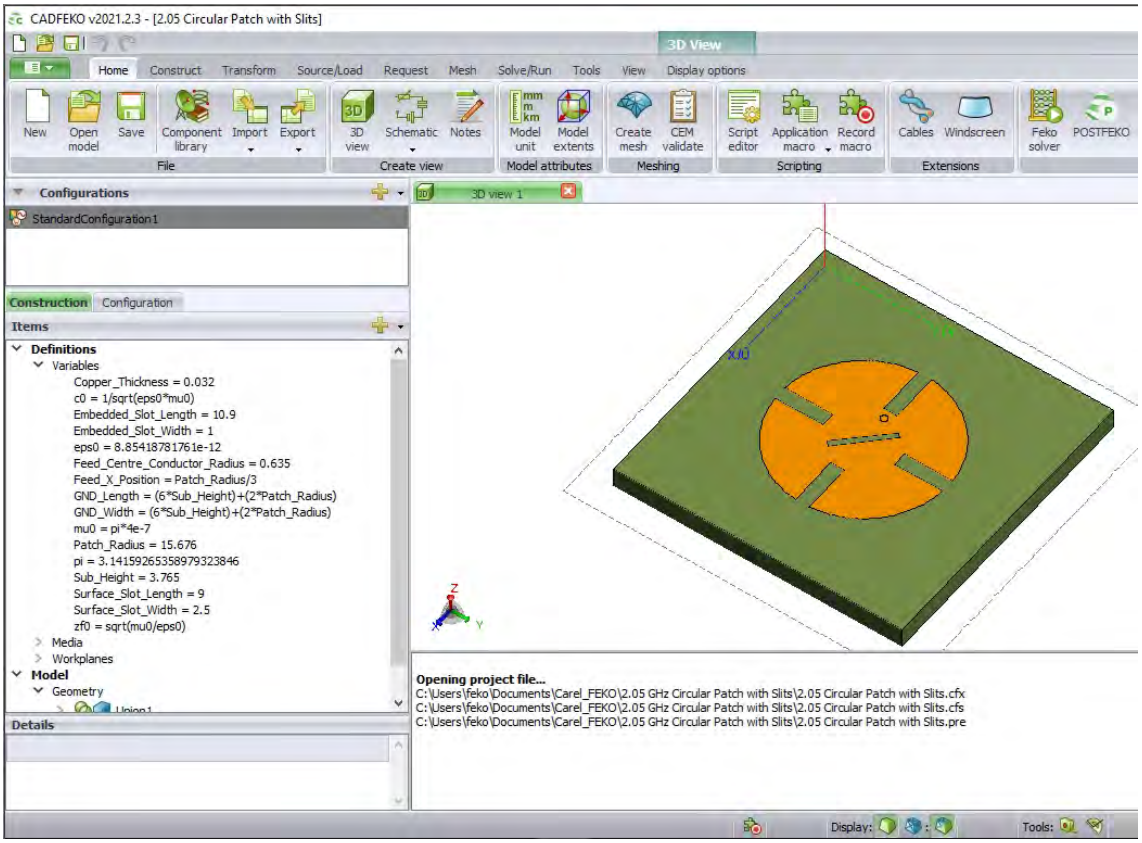

Appendix C

2.05 GHz Miniaturised Patch Antenna with Slits and Shorting Pin FEKO Model

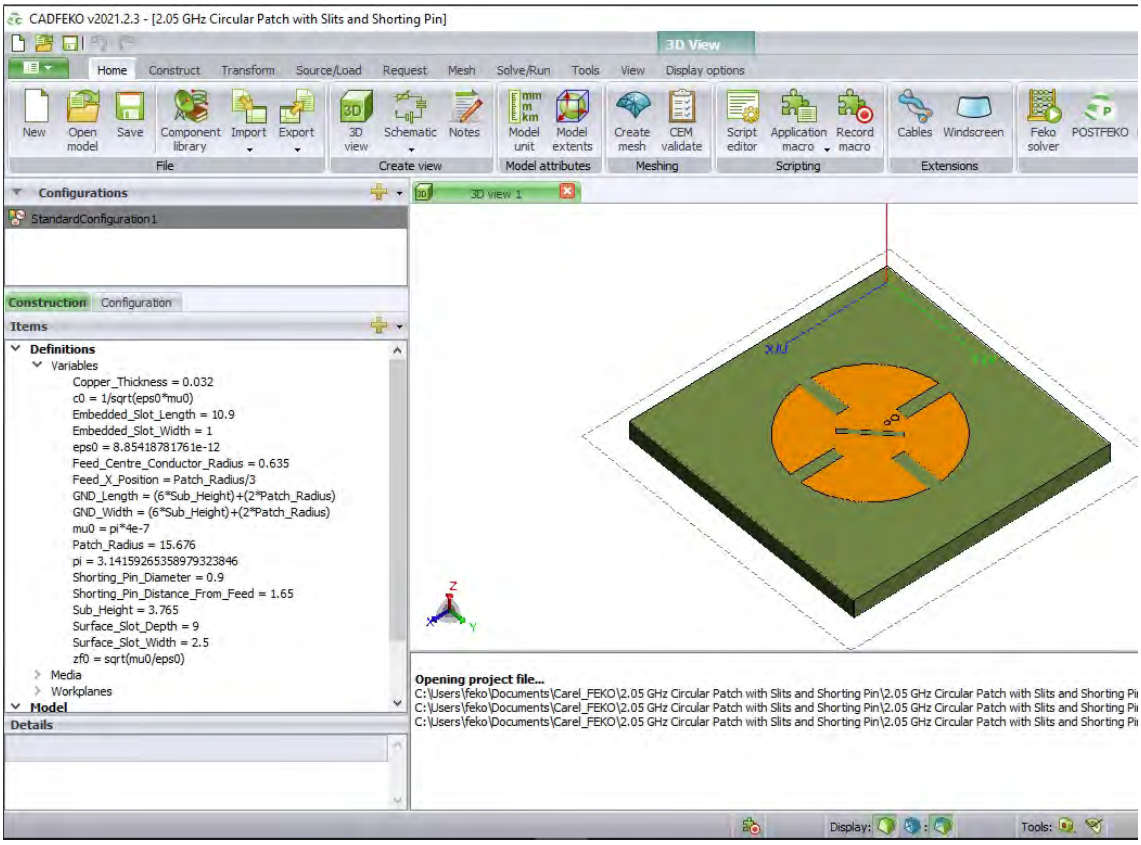

Appendix D

Miniature 2.05 GHz Patch Antenna with Slits and Shorting Pin FEKO Model

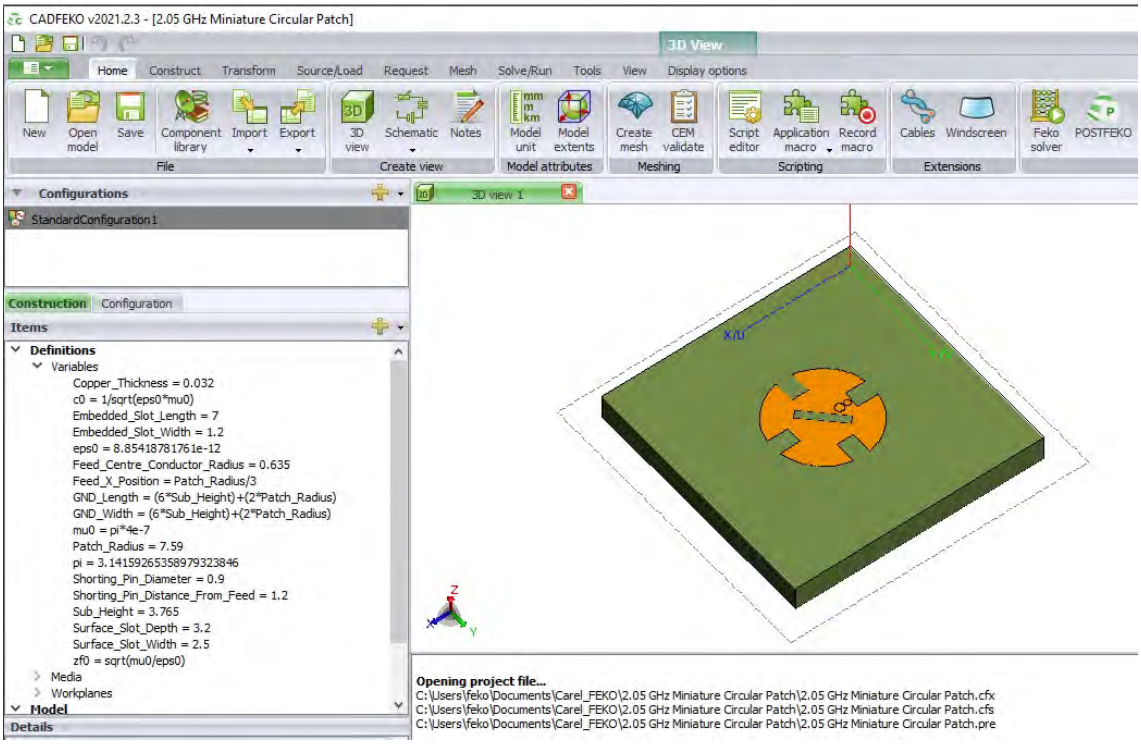

Appendix E

FR4 Layer stack-up

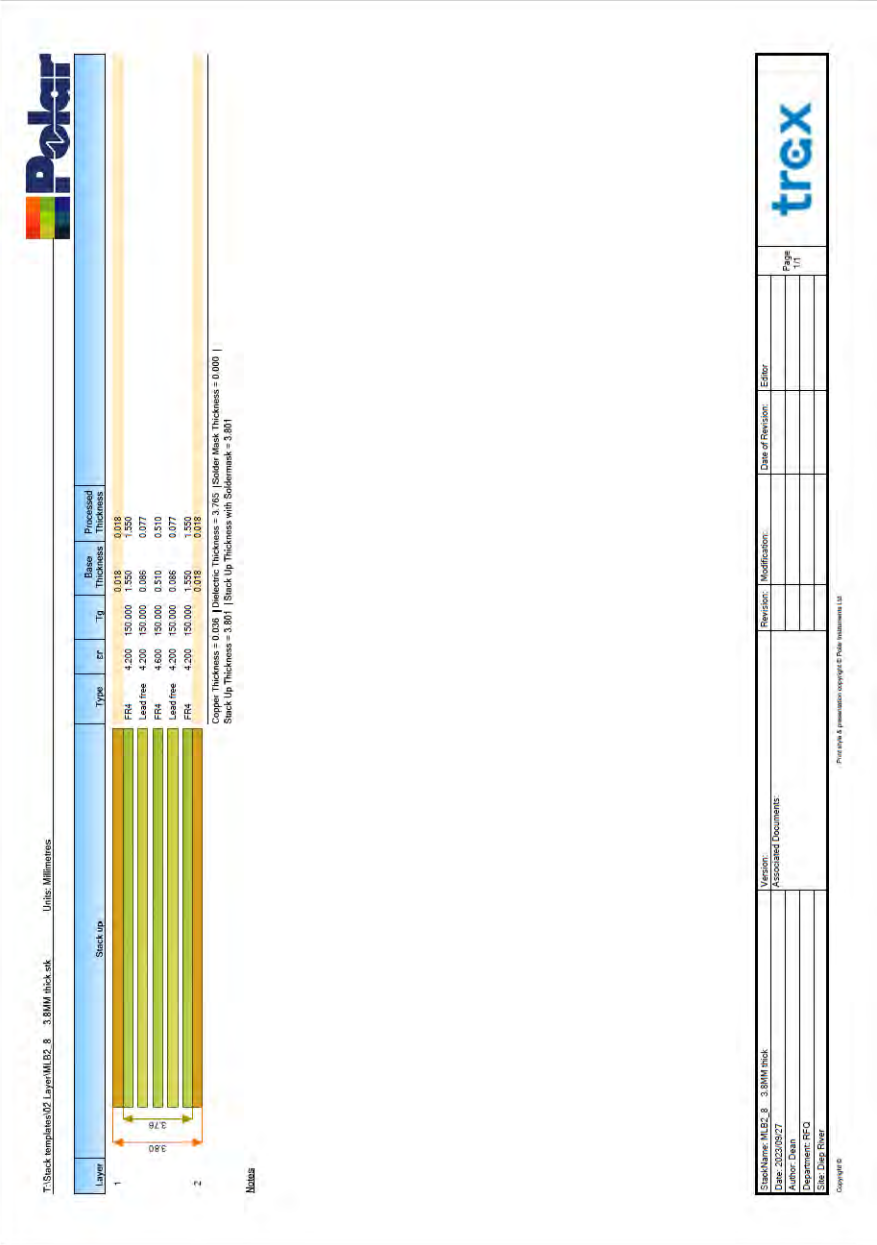

Bibliography

Altair. 2014. “FEKO User’s Manual.”.

Altuntaş, Orhun Tevfik. 2019. Non-Foster impedance matching for electrically small antennas. Master’s thesis, Middle East Technical University.

Anisha, A and Sharmini Enoch. 2014. Analysis and design of microstrip patch antenna for S-band applications. In *Proceedings of the 2014 International Conference on Control, Instrumentation, Communication and Computational Technologies (ICCICCT)*. IEEE: pp. 1101–1104.

Balanis, Constantine A. 2005. *Antenna Theory: Analysis and Design.* New Jersey: John Wiley & Sons.

Bevelacqua, P. 2017. “Antenna-theory.com.” https://www.antenna-theory.com/antennas/patches/patch3.php.
[Accessed: 4 September 2021].

Breed, Gary et al. 2009. “The fundamentals of patch antenna design and performance.” *High Frequency Electronics* 3(12): pp. 49–51, March.

Chen, Zhizhang and Michel M Ney. 2007. Method of moments: A general framework for frequency-and time-domain numerical methods. In *Proceedings of 2007 Workshop on Computational Electromagnetics in Time-Domain*. IEEE: pp. 1–4.

Cheng, Yang, Yuandan Dong and Yongsheng Pan. 2019. Miniaturized Circularly Polarized Metal Antenna with a Shorting Pin for Low Cost RFID Application. In *Proceedings of 2019 IEEE MTT-S International Wireless Symposium (IWS)*. IEEE: pp. 1–3.

Chouchene, Wissem, Chiraz Larbi and Taoufik Aguili. 2017. New electrical equivalent

circuit model of the inset fed rectangular patch antenna. In *Proceedings of 2017 Progress In Electromagnetics Research Symposium-Spring (Piers)*. IEEE: pp. 646–651.

Davis, WA, T Yang, ED Caswell and WL Stutzman. 2011. "Fundamental limits on antenna size: a new limit." *IET microwaves, antennas & propagation* 5(11): pp. 1297–1302, September.

Dhakshinamoorthi, MK, S Gokulakkrizhna, M Subha, V Mekaladevi et al. 2020. Rectangular Microstrip Patch Antenna Miniaturization using improvised Genetic Algorithm. In *Proceedings of 2020 4th International Conference on Trends in Electronics and Informatics (ICOEI)(48184)*. IEEE: pp. 894–898.

Elfrgani, Aseim M and Roberto G Rojas. 2015. Stability of non-Foster circuits for broadband impedance matching of electrically small antennas. In *Proceedings of 2015 IEEE Radio and Wireless Symposium (RWS)*. IEEE: pp. 50–52.

Everything-RF. 2018. "What are Near Field and Far Field Regions of an Antenna?" https://www.everythingrf.com/community/what-are-near-field-and-far-field-regions-of-an-antenna.
[Accessed: 25 July 2022].

Ivanov, Nikolay, Bair Buyantuev, Viacheslav Turgaliev and Dmitry Kholodnyak. 2016. Non-foster broadband matching networks for electrically-small antennas. In *Proceedings of 2016 Loughborough Antennas & Propagation Conference (LAPC)*. IEEE: pp. 1–4.

Jacob, Minu Mariam. 2016. *Non-Foster circuits for high performance antennas: advantages and practical limitations*. University of California, San Diego.

James, Jim R et al. 1989. *Handbook of Microstrip Antennas*. Vol. 1 & 2 London: Peter Peregrinus Ltd.

Johnson, Richard C. 1993. *Antenna Engineering Handbook Third Edition*. New York: Mcgraw-Hill Incorporated.

Khan, Muhammad Umar, Mohammad Said Sharawi and Raj Mittra. 2014. "Microstrip patch antenna miniaturisation techniques: a review." *IET Microwaves, Antennas & Propagation* 9(9): pp. 913–922, December.

Ludwig, Reinhold. 2000. *RF Circuit Design: Theory & Applications 2nd Edition*. New Jersey: Pearson Education Inc.

MacPherson, Stuart D. 2002. *High Frequency Small Amplifier Design*. Wandsbeck: Stuart D MacPherson.

Mathworks. 2023. "Far-field Terminologies." https://www.mathworks.com/help/antenna/ug/antenna-parameters.html.
[Accessed: 23 August 2023].

Milligan, Thomas A. 2005. *Modern Antenna Design*. New Jersey: John Wiley & Sons.

Nkordeh, Nsikan, FE Idachaba and OO Oni. 2015. "Microstrip patch antenna: comparing performance of a rectangular and a circular patch at LTE bluetooth and GSM frequencies.".

Oraizi, Homayoon and Seyyed Hamzeh Hashemi. 2013. Design of a non-Foster impedance matching network for electrically small antennas. In *Proceedings of 2013 13th Mediterranean Microwave Symposium (MMS)*. IEEE: pp. 1–4.

Pozar, David M. 2001. *Microwave and RF Design of Wireless Systems*. New Jersey: John Wiley and Sons.

Ramesh, M. 2003. "Design Inset-Fed Microstrip Patch Antennas." https://www.mwrf.com/technologies/components/article/21846562/design-inset-fed-microstrip-patch-antennas.
[Accessed: 4 September 2021].

Reddy, CJ. 2020. "Altair antenna modelling and simulation techniques.".

Sharma, Sameer Kumar and Deepak Singh Nagarkoti. 2017. "Meet the Challenge of Designing Electrically Small Antennas." *Microwaves and RF* 6(8): pp. 1–4, August.

Sharma, Sonia, CC Tripathi and Rahul Rishi. 2017. "Impedance matching techniques for microstrip patch antenna." *Indian Journal of Science and Technology* 10(28): pp. 1–16, July.

Smolders, AB, HJ Visser and Ulf Johannsen. 2019. "Modern Antennas and Microwave Circuits–A complete master-level course." *arXiv preprint arXiv:1911.08484* .

Stutzman, Warren L and Gary A Thiele. 1998. *Antenna theory and design*. New Jersey: John Wiley & Sons.

Sussman-Fort, Stephen E. 2006. "Matching network design using non-Foster impedances." *International Journal of RF and Microwave Computer-Aided Engineering: Co-sponsored by the Center for Advanced Manufacturing and Packaging of Microwave, Optical, and Digital Electronics (CAMPmode) at the University of Colorado at Boulder* 16(2): pp. 135–142.

Sussman-Fort, Stephen E and Ronald M Rudish. 2009. "Non-Foster impedance matching of electrically-small antennas." *IEEE Transactions on Antennas and Propagation* 57(8): pp. 2230–2241, August.

Tade, Oluwabunmi O. 2014. Negative impedance converter for antenna matching Phd thesis, University of Birmingham.

Varma, Ruchi and Jayanta Ghosh. 2014. "Design and Optimization of Proximity Coupled Antenna Using GA.".

Wheeler, Harold A. 1959. "The radiansphere around a small antenna." *Proceedings of the IRE* 47(8): pp. 1325–1331, April.

Wong, Kin-Lu, Chia-Luan Tang and Hong-Twu Chen. 1998. "A compact meandered circular microstrip antenna with a shorting pin." *Microwave and Optical Technology Letters* 15(3): pp. 147–149, December.